A Kinetic Perspective on DNA Base Excision Repair

By Kelly M. Schermerhorn

B.S. Quinnipiac University 2006

A Dissertation Submitted in Partial Fulfillment of the Requirements for the Degree of

Doctor of Philosophy in the Department of Chemistry at Brown University

Providence, Rhode Island May 2014

This dissertation by Kelly M. Schermerhorn is accepted in its present form by the Department of Chemistry as satisfying the dissertation requirement for the degree of Doctor of Philosophy

Recommended to the Graduate Council

Date_____ _____

Sarah Delaney, Ph.D. Advisor

Date_____ _____

Amit Basu, Ph.D. Reader

Date_____ _____

David E. Cane, Ph.D. Reader

Approved by the Graduate Council

Date_____ _____

Peter M. Weber, Ph.D.
Dean of the Graduate School

Curriculum Vitae
Kelly Schermerhorn

Education

Brown University, Providence, Rhode Island
Ph.D., Chemistry, expected May 2014

Quinnipiac University, Hamden, Connecticut
B.S., *Summa Cum Laude*, Biomedical Science, May 2006
Minor in Chemistry

Research Experience

Department of Chemistry, Brown University, Providence, Rhode Island
Graduate Student with Dr. Sarah Delaney, 2010-present
A Kinetic Perspective on DNA Base Excision Repair

- Synthesized and purified DNA oligomers
- Expressed and purified recombinant proteins
- Characterized DNA and proteins by ESI-LC/MS and MALDI-TOF MS
- Performed enzyme kinetic assay experiments using Rapid Quench Flow technology and gel electrophoresis
- Analyzed data with Kaleidagraph and KinTek Explorer Professional
- Laboratory radiation and safety officer
- Responsible for mentoring and developing projects for undergraduate and incoming graduate students

Industry Experience

Biotrove Incorporated (division now owned by Agilent), Woburn, Massachusetts
Laboratory Manager of RapidFire Division, 2006-2009

- Maintained several Rapidfire High-Throughput Mass Spectrometry (HTMS) laboratories, which included maintenance and troubleshooting of platform
- Responsible for running and analyzing pharmaceutical samples on Rapidfire-HTMS platform to identify native compounds
- Trained incoming employees on Rapidfire-HTMS platform
- Responsible for ordering and inventory of laboratory consumables
- Laboratory Safety Officer

Publications

- Schermerhorn, K.M. and Delaney, S. (2014) A Chemical and Kinetic Perspective on Base Excision Repair of DNA. *Acc. Chem. Res.*, **47**, 1238-1246
- Schermerhorn, K.M. and Delaney, S. (2013) Transient-state kinetics of apurinic/apyrimidinic (AP) endonuclease 1 acting on an authentic AP site and commonly-used substrate analogs: The effects of diverse metal ions and base mismatches. *Biochemistry,* **52**, 7669-7677
- Jarem, D.A., Wilson, N.R., Schermerhorn, K.M., and Delaney, S. (2011) Incidence and persistence of 8-oxo-7,8-dihydroguanine within a hairpin intermediate exacerbates a toxic oxidation cycle with trinucleotide repeat expansion. *DNA Repair* **10**, 887-896

Presentations, Posters

- Schermerhorn, K.M and Delaney, S. (2014) Strand Incision Kinetics of apurinic/apyrimidinic (AP) endonuclease acting on an authentic AP site

and commonly used AP site analogs (poster) *247th ACS National Meeting, Dallas, TX, March 16-20*

- Schermerhorn, K.M. and Delaney, S. (2013) Kinetics of Human Apurinic/apyrimidinic Endonuclease 1 (APE1) on an Authentic AP site or an AP site Analog (poster) *18th Conversation, Albany, NY, June 9-13*
- Schermerhorn, K.M., (2013) Base Excision Repair of Oxidative DNA Damage (presentation) *Providence Area Aging Research Forum, Providence, RI, Brown University, February 26*
- Schermerhorn, K.M. and Delaney, S. (2012) Kinetics of the Human Base Excision Repair Enzyme APE1 (poster) *Gordon Research Conference: Mutagenesis, Newport, RI, August 19-24*
- Schermerhorn, K.M., (2012) Kinetics of the Human Base Excision Repair Enzyme APE1 (presentation) *Boston DNA Repair and Mutagenesis (DRAM) Group Meeting, MIT, Cambridge, MA April 18*
- Schermerhorn, K.M, and Delaney, S., (2011) Base Excision Repair of Triplet Repeat DNA (poster) *17th Conversation, Albany, NY, June 14-18*
- Schermerhorn, K.M., Wilson N.R., Jarem, D., and Delaney, S. (2010) Implication of Base Excision Repair on onset of Huntington's Disease (poster) *240th ACS National Meeting, Boston, MA, August 22-26*

Teaching Experience

- High School Science and Math Tutor, Lincoln, RI, 2012-present
  -*Tutor 9th/10th grade student in Biology, Chemistry and Geometry*
- Teaching Assistant, Brown University, Department of Chemistry, Providence, RI, 2009-2010
  -*Taught laboratory course for first and second semester organic chemistry*
- Organic Chemistry Tutor, The Learning Center at Quinnipiac University, Hamden, CT, 2004-2006
  -*Tutored undergraduate students in first and second semester organic chemistry*

Awards

- Graduate Dissertation Fellowship, Brown University, Providence, RI, 2013
- National Institute of Health/Mars Incorporated Young Research Fellow at 63rd Lindau Nobel Laureate Meeting, Lindau, Germany, *June 28-July 7 2013*
- Horace Goldsmith Fellowship Award, Brown University, Providence, RI, Spring 2013
- Best Poster Award, Chemistry Department Poster Session, Brown University, Providence, RI, Fall 2011

Extracurricular Involvement

- Chemistry Department Events Committee, Brown University, Providence, RI, 2010-present
- Graduate Student Council Departmental Representative, Brown University, Providence, RI, 2010-2012 (four semesters)

Preface and Acknowledgements

To my advisor, labmates, family, friends, B, and Willie,

I thank you for your support, love, and sense of humor.

Table of Contents

List of Tables

List of Figures

Chapter 1: Introduction[†]

[†]**Adapted From:**

Schermerhorn, K.M. and Delaney, S. (2014) A Chemical and Kinetic Perspective on Base Excision Repair in DNA. *Acc. Chem. Res. 47*, 1238-1246.

1.1 Formation and Toxicity of DNA Lesions

DNA nucleobases are chemically reactive; this reactivity leads to a wide variety of nucleobase modifications that can occur by oxidation, alkylation, deamination, or hydrolysis. Indeed, more than 70 modified nucleobases have been identified *in vitro*, of which ~15 have been found in cellular DNA (*1,2*). Examples of several modified nucleobases are shown in Figure 1.1. Oxidation of DNA nucleobases results from exposure to reactive oxygen species generated during normal cellular metabolism or an inflammatory response, ionizing radiation, or other oxidizing species. Oxidatively damaged DNA nucleobases commonly detected in cellular DNA are 8-oxo-7,8-dihydroguanine (8oxoG) and thymine glycol (Tg). DNA alkylation, often at the electron rich heteroatoms, occurs upon reaction with endogenous methyl donors, environmental toxins, or chemotherapeutic agents. The alkylated DNA lesions 3-methyladenine (3meA) and 7-methylguanine (7meG) are frequently observed in cellular DNA. Hydrolysis of the exocyclic amine of cytosine (C), adenine (A), or guanine (G) leads to deamination and formation of uracil, xanthine, and hypoxanthine, respectively. Finally, hydrolysis of the carbon-nitrogen bond that adjoins the nucleobase to the deoxyribose sugar, the glycosidic bond, results in loss of the nucleobase and formation of an abasic site, also referred to as an apurinic/apyrimidinic (AP) site.

Many of these DNA lesions are highly mutagenic when formed in cellular DNA, meaning they are mispaired by DNA polymerases during replication. For example 8oxoG, which should be paired with C during replication, as it is a lesion derived from G, can also be paired with A to form a Hoogsteen base pair (*3*). In addition, DNA lesions can

be cytotoxic meaning that they cause a polymerase to stall and halt DNA replication, leading to cellular apoptosis.

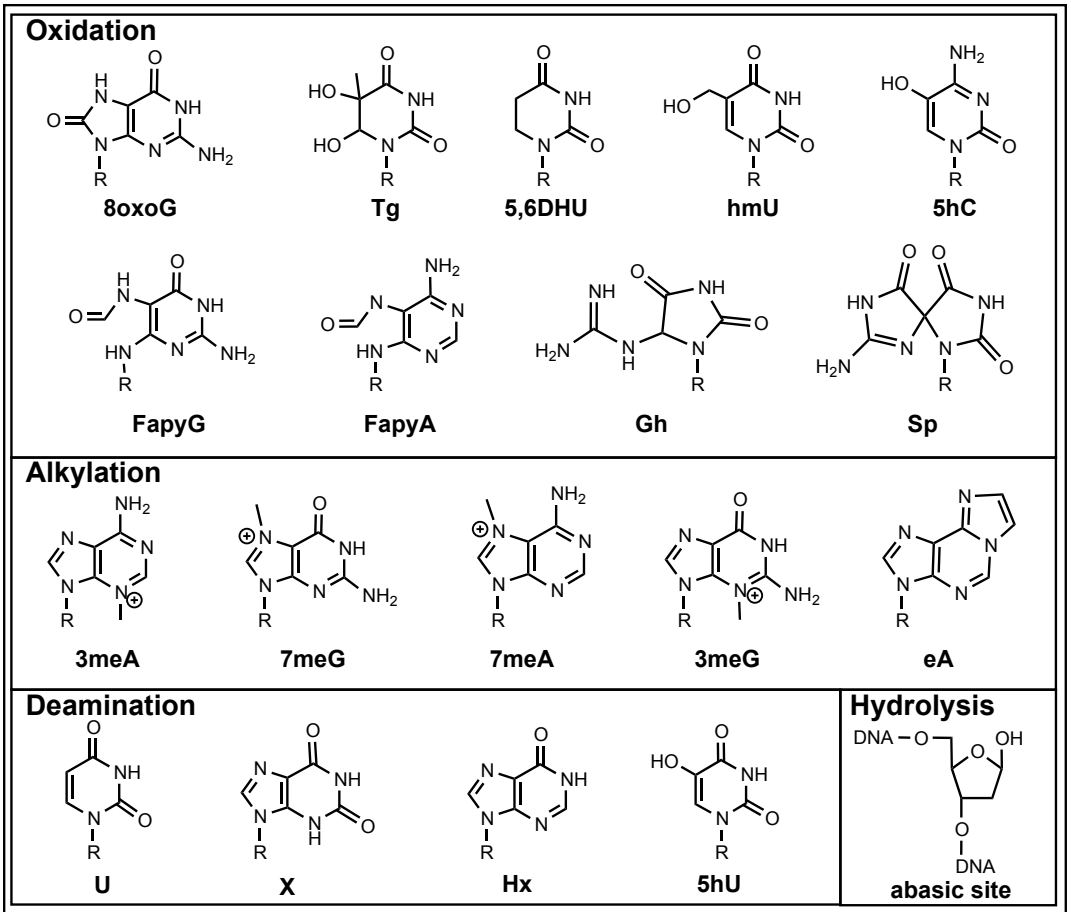

Figure 1.1. Examples of DNA lesions formed by oxidation, alkylation, deamination, and hydrolysis of canonical nucleobases. 5hU is a product of deamination and oxidation. Shown are 8oxoG (8-oxo-7,8-dihydroguanine), Tg (thymine glycol), 5,6DHU (5,6-dihydrouracil), hmU (hydroxymethyluracil), 5hC (5-hydroxycytosine), FapyG (4,6-diamino-5-formamidopyrimidine G), FapyA (4,6-diamino-5-formamidopyrimidine A), Gh (guanidinohydantoin), Sp (spiroiminodihydantoin), 3meA (3-methyladenine), 7meG (7-methylguanine), 7meA (7-methyladenine), 3meG (3-methylguanine), eA (1, N^6-ethenoadenine), U (uracil), X (xanthine), Hx (hypoxanthine), 5hU (5-hydroxyuracil), and an abasic site.

Due to the extensive range of lesions formed, and the deleterious effects they can have, the ability to repair the damaged DNA is integral to genomic stability and cell viability. Cells have evolved a whole host of DNA repair pathways, including base excision repair (BER), nucleotide excision repair (NER), and non-homologous end joining (NHEJ). Each

DNA repair pathway relies upon the activity and coordination of several DNA repair enzymes to initiate and complete repair. The BER pathway, comprised of enzymes including a DNA glycosylase, AP endonuclease 1 (APE1), DNA polymerase, and DNA ligase, along with several accessory proteins, is responsible for recognizing and repairing modified nucleobases and abasic sites. The proceeding sections describe the role(s) of each of the BER enzymes. Although focus is placed on human BER enzymes, homologous repair enzymes are present in bacteria and yeast.

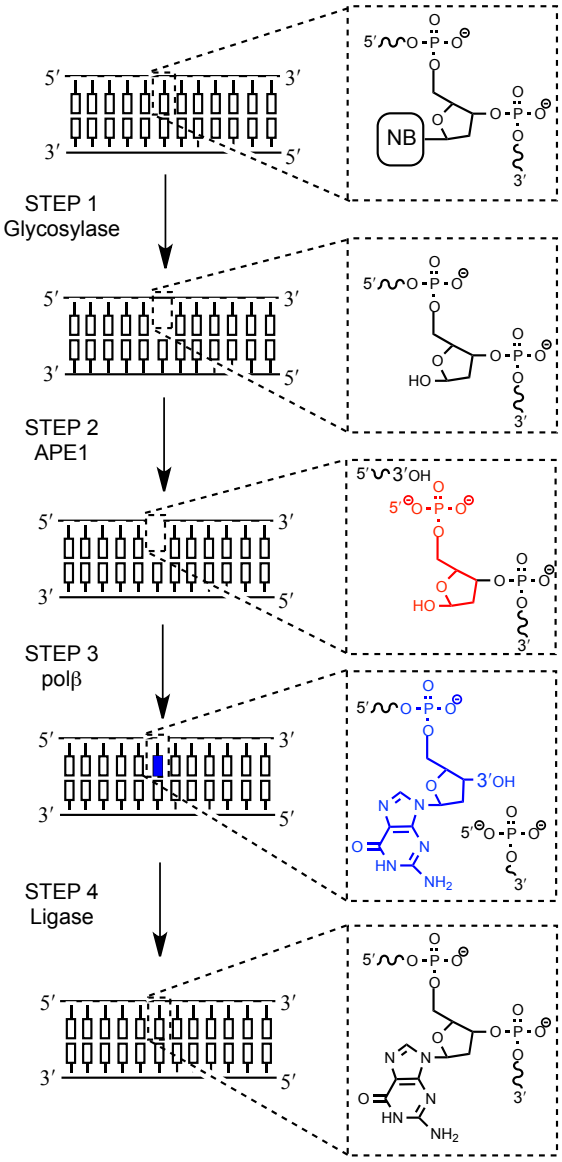

Figure 1.2. A modified DNA nucleobase lesion (NB) is recognized and removed by a glycosylase creating an abasic site (STEP 1). APE1 cleaves the DNA backbone 5' to the abasic site, creating a nick with 3'-OH and 5'-dRP (red) termini (STEP 2). Polβ removes the 5'-dRP and inserts an unmodified nucleotide (blue) at the 3'-OH (STEP 3). Finally, a ligase seals the nick between the 3'-OH of the newly incorporated nucleotide and 5'-phosphate in the backbone (STEP 4).

1.2. DNA Glycosylases

A DNA glycosylase initiates the BER pathway, and is responsible for recognizing and binding specific nucleobase lesions, and flipping the targeted nucleobase into the active site to

catalyze cleavage of the glycosidic bond (Figure 1.2, Step 1). There are at least 11 known human DNA glycosylases; some have activity on a variety of nucleobase lesions, others are specific for just one or two DNA lesions. Preferred substrate lesion(s) for each glycosylase are listed in Table 1.1.

The ability of a DNA glycosylase to find its substrate amongst the excess of unmodified nucleobases present in the genome has been likened to finding a needle in a haystack; much research has been dedicated to understanding this process. Most models include short-range sliding along DNA, with the glycosylase probing and extruding individual nucleobases; in doing so, the glycosylase can identify its substrate(s) and catalzye cleavage of the glycosidic bond (*4*). Subsequent BER enzymes are also thought to employ a sliding mechanism, which allows for enzyme processivity; indeed, several DNA glycosylases have been shown to remove multiple DNA lesions during a single binding event (*5-7*).

Table 1.1. Human DNA glycosylases and their preferred lesion substrates (*E. Coli* homolog provided in parenthesis)

Monofunctional DNA Glycosylases	**Substrate(s)**
UNG1/2 (UDG)[a,d]	U
MBD4[b]	**T**:G; **U**:G; **hmU**:G[c]
TDG[b]	**T**:G; **U**:G; **T**:C; **T**:T[c]
SMUG1[a] (MUG)	U; hmU
MUTYH[b] (MutY)	**A**:8oxoG[b]
AAG[b] (AlkA)	3meA; 7meG; eA; Hx; X
Bifunctional DNA Glycosylases	
OGG1[b] (Fpg)	8oxoG; FapyG
NTH1[b] (Nth)	FapyG; Tg; 5,6DHU, 5hC; 5hU
NEIL1[a] (Nei)	Sp; Gh; FapyG; FapyA; 5,6DHT, 5,6DHU
NEIL2[d] (Nei)	Sp; Gh; 5hU; 5,6DHT, 5,6DHU; 5hC
NEIL3[d] (Nei)	Sp; Gh; FapyG; FapyA

[a] Activity on single-stranded and double-stranded DNA
[b] Activity on double-stranded DNA
[c] N:N represents a mispair where nucleobase removed is in bold
[d] Prefers lesions in single-stranded DNA

Some glycosylases work on lesions in both single- and double-stranded DNA, others only work on double-stranded DNA (*8-10*). Interestingly, some glycosylases have a preference for lesions in single-stranded bulged or bubble structures (*11,12*). It is also noteworthy that not all DNA glycosylases remove modified nucleobases; MUTYH removes the A from a 8oxoG:A mispair (*13*). This activity prevents the point mutation that would result if 8oxoG were removed instead. Furthermore, several glycosylases work on canonical DNA nucleobases that are mispaired, for example TDG, which removes T from T:G mispairs (*14*).

DNA glycosylases can be divided into two categories: monofunctional and bifunctional (Table 1.1). Monofunctional DNA glycosylases use an activated water molecule to hydrolyze the glycosidic bond, affording an abasic site product. Bifunctional DNA glycosylases utilize an amino group of the enzyme for nucleophilic attack on the 1´-carbon of the deoxyribose ring, and in addition to glycosidic bond cleavage, bifunctional glycosylases also have AP lyase activity; such activity catalyzes β-elimination of the DNA backbone 3' to the abasic site via formation of a Schiff base, creating a single-stranded break with 3'-α,β-unsaturated aldehyde and 5'-phosphate termini. Some bifunctional DNA glycosylases can also perform δ-elimination to yield a 3'-phosphate. Notably, it has been proposed that for some bifunctional glycosylases, β-elimination strand cleavage may be bypassed *in vivo*, with the subsequent BER enzyme, APE1, acting directly on the abasic site (*15,16*).

Figure 1.3 shows a proposed S_N1 (D_N*A_N) mechanism for DNA glycosylases, in which nucleobase removal progresses through two oxocarbenium ion-like transition states (TS) (Figure 1.3 A,C) and a distinct oxocarbenium intermediate (Figure 3B). TS

analysis of the *E. coli* homologs of UNG and MUTYH, UDG and MutY, respectively, has been performed using kinetic isotope effect (KIE) measurements. Examination of primary ^{13}C and ^{15}N KIEs along with secondary deuterium and ^{15}N KIEs suggests a strongly dissociative TS with extensive oxocarbenium character for both UDG and MutY (*17,18*). KIE measurements for other glycosylases remain to be performed.

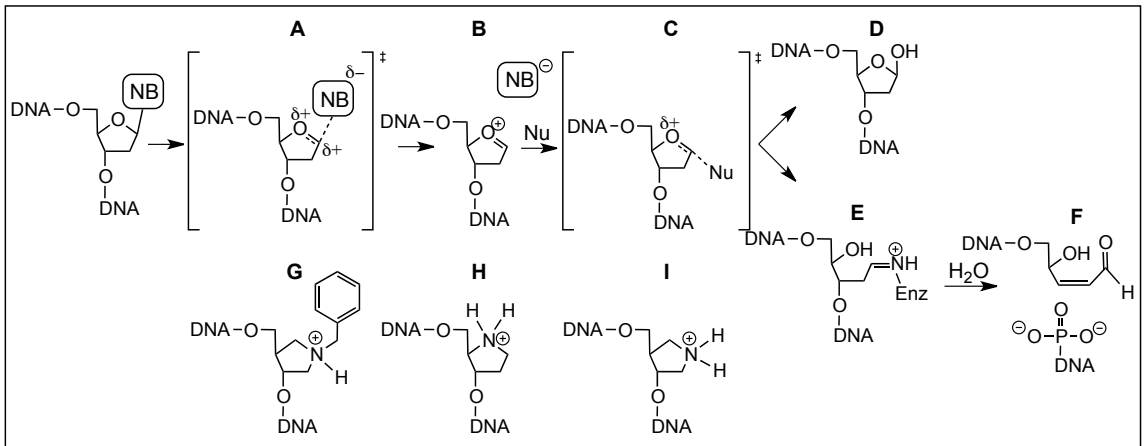

Figure 1.3. Proposed S_N1 (D_N*A_N) mechanism for DNA glycosylases which proceeds through two oxocarbenium ion-like transition states (A, C) and a distinct oxocarbenium intermediate (B). Monofunctional DNA glycosylases use H_2O as the nucleophile (Nu) yielding an abasic site product (D), while bifunctional DNA glycosylases use an active site amine with formation of a Schiff base (E) prior to β-elimination and hydrolysis to yield a nick in the DNA backbone with 3'α-,β-unsaturated aldehyde and 5'-phosphate termini (F). The corresponding transition state and intermediate pyrrolidine analogs are shown in G, H, and I. Chu et al reports use of both H and I as analogs of the transition state C.

In addition to TS analysis by KIE measurements, electrophoretic mobility shift assays (EMSA) also support a D_N*A_N mechanism. Using several *E. coli* monofunctional (AlkA, MutY) and bifunctional (Fpg, Nth) and human monofunctional (AAG, TDG) glycosylases, tight binding between a pyrrolidine abasic site analog, which mimics the oxocarbenium intermediate, (Figure 3H) and the glycosylase was revealed (*19,20*). Interestingly, this binding event is strong enough to inhibit activity of many of the glycosylases on their prototypic substrate lesion(s). A more recent EMSA study using pyrrolidine abasic site analogs that mimic the two oxocarbenium TS (Figure 3 G,I),

demonstrated binding of bifunctional glycosylases Fpg, Nei, OGG1, and NEIL1 to mimics of both TS (*21*). Interestingly, OGG1 and NEIL1 displayed different binding for the two TS mimics, suggesting alternate modes of recognition and catalysis for these bifunctional glycosylases.

1.3. AP Endonuclease 1

The enzyme following a DNA glycosylase in the BER pathway is AP endonuclease 1 (APE1). APE1, a Mg^{2+}-dependent enzyme, is responsible for incising the DNA backbone at abasic sites, creating a nick with 3'-OH and 5'-deoxyribose phosphate (dRP) termini (Figure 1.2, Step 2). Abasic sites are highly mutagenic and cytotoxic, and can also form protein-DNA and DNA-DNA crosslinks (*22*). Therefore, repair of abasic sites by APE1 is critical in maintaining genomic integrity. For APE1, an activated water molecule has been implicated as the nucleophile for strand incision. A Mg^{2+} ion is also required; the divalent metal ion coordinates an oxygen of the 5'-phosphate, increasing its electrophilicty and also orienting the DNA backbone within the APE1 active site (*23,24*). Interestingly, *in vitro*, the authentic abasic site is highly labile leading to a strand break; therefore, the use of stable abasic site analogs, such as the tetrahydrofuran (THF) site which lacks the C1'-OH group, are commonly used to understand the molecular mechanism and kinetics of APE1.

1.4. Polymerase β

Polymerase β (pol β) follows APE1 in the BER pathway and has two catalytic functions: (1) it converts the 5'-dRP to a 5'-phosphate using its dRP lyase activity and (2)

in a Mg^{2+}-dependent reaction, catalyzes incorporation of a single nucleotide to the 3'-OH of the nick (Figure 2, Step 3) (*25*). Nucleotide incorporation and dRP lyase chemistry of pol β occur at separate active sites, although evidence suggests that both catalytic events occur during a single pol β/DNA binding event. Notably, rate of dRP removal by pol β is 20-fold faster than incorporation, and therefore it is postulated that dRP removal occurs prior to nucleotide incorporation (*26*).

1.5. DNA Ligase

The final step of the BER pathway is sealing of the nick in the backbone by a DNA ligase (Figure 2, Step 4). Both DNA ligase I (Lig1) and DNA ligase III (Lig3) have been implicated in nick sealing by catalyzing formation of a phosphodiester bond between the 3'-OH of the newly incorporated nucleotide and the 5'-phosphate of its neighbor. Human ligases require ATP and Mg^{2+} for activity, and their mechanism involves three distinct steps: (1) enzyme adenylation at an active site lysine, (2) adenylyl transfer to the 5'-phosphate of the nick, and (3) nucleophilic attack of the 3'-OH to seal the nick and release AMP (*27*).

For activity *in vivo*, Lig3 requires the presence of x-ray repair cross-complementing protein 1 (XRCC1); this protein, described later in this chapter, has no known catalytic function, but rather acts as a scaffold (*28*). While it has traditionally been thought that Lig3 is the major ligase in short-patch BER (*vide infra*) in the nucleus, it was recently reported that Lig1 is the major ligase in nuclear short-patch BER while Lig3 is essential for mitochondrial short-patch BER (*29,30*).

1.6. Long-Patch BER

The pathway described above is typically referred to as short-patch BER (SP-BER), in which pol β removes the 5'-dRP group at the gap site and inserts a *single* nucleotide. Under conditions where the 5'-dRP group is modified such that the dRP lyase activity of pol β is blocked, an alternate pathway, long-patch BER (LP-BER), is utilized (Figure 1.4) (*31,32*). In LP-BER, *multiple* nucleotides are incorporated at the gap site by polymerase β, δ,

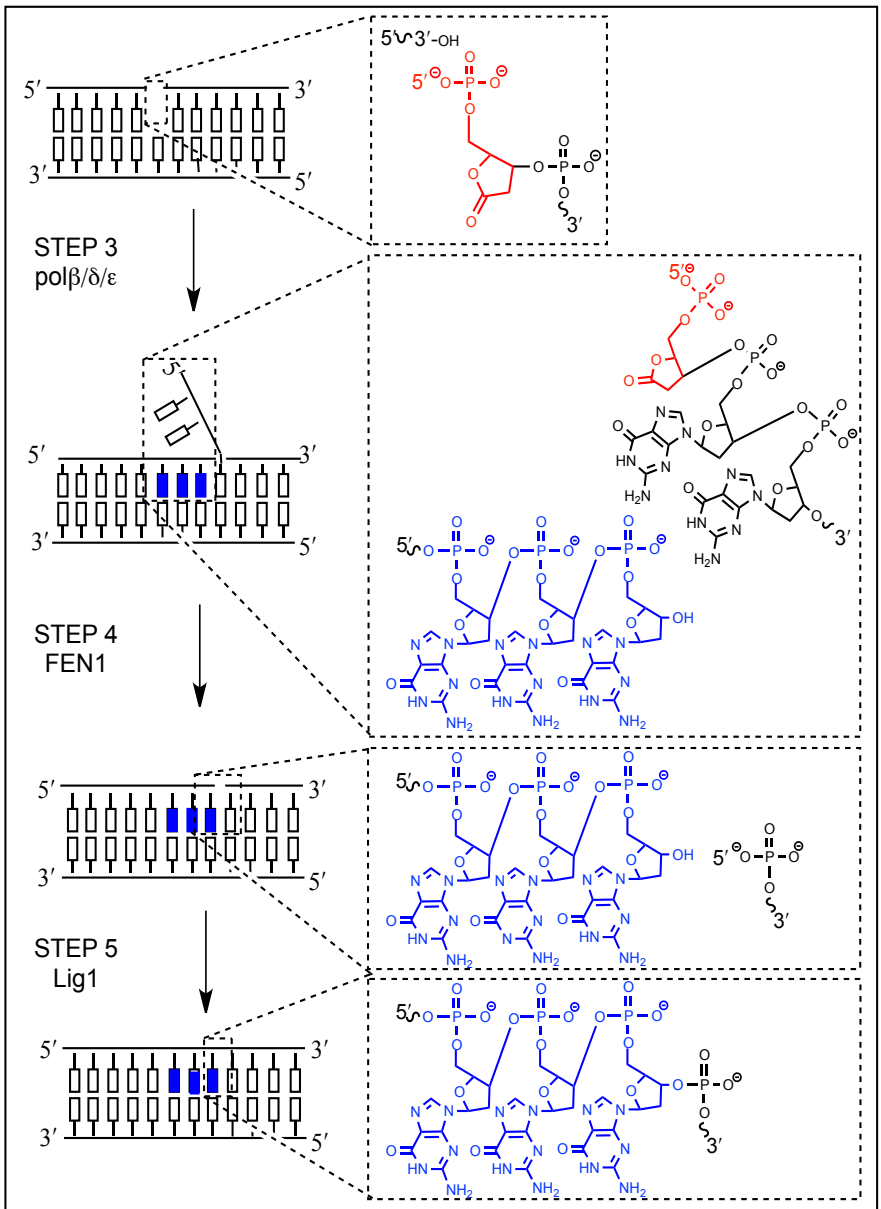

Figure 1.4. Long-patch BER. STEP 1 and 2 are the same as in Figure 1.2. An oxidized abasic site which is known to require LP-BER, 2-deoxyribonolactone, is shown. Pol β, δ, or ε insert multiple nucleotides at the 3'-OH nick site generated by APE1 (STEP 3; we show insertion of three Gs (blue)). FEN1 removes the 5'-flap (STEP 4) and Lig1 seals the nick in the backbone (STEP 5).

or ε (Figure 1.4, Step 3).

The polymerase incorporates, on average, 2-6 nucleotides at the gap site; this number can increase depending on the lesion as well as the sequence context *(33)*. The incorporation of multiple nucleotides at the gap site generates a displaced single-stranded flap of DNA, another key feature of LP-BER. This flap must be removed by flap endonuclease 1 (FEN1) (Figure 1.4, Step 4) so that DNA ligase, Lig1 in LP-BER, can seal the nick (Figure 1.4, Step 5). Importantly, an accessory protein, proliferating cell nuclear antigen (PCNA), has been implicated in binding and coordinating the activity of many LP-BER enzymes *(34)*.

1.7. Kinetics of BER Enzymes

Much of our knowledge about chemistry and substrate specificity of each BER enzyme has been gathered from extensive kinetic studies. The catalytic pathway that an enzyme follows in converting substrate to product is represented by a minimal kinetic scheme, such as that shown in Figure 1.5 for glycosylases (*35*). Arrows represent distinct steps along the pathway and *k* represents the rate associated with that step. (Figure 1.5 is used as an example and represents the minimal kinetic scheme for some, but not all, BER enzymes).

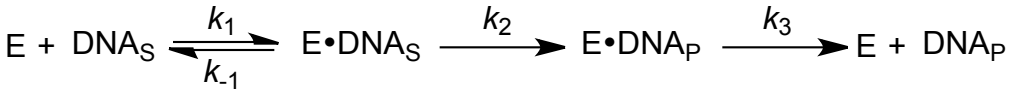

Figure 1.5. Minimal kinetic scheme for DNA glycosylases. Three steps are depicted: binding of glycosylase enzyme (E) to the DNA substrate (DNA_S) (k_1/k_{-1}), glycosidic bond cleavage (and β-elimination, when applicable) (k_2), and DNA product (DNA_P) release (k_3).

The number of reactions an enzyme can catalyze from free substrate to free product per unit of time is represented by k_{cat}. Therefore, k_{cat} is defined by the slow rate-determining step (RDS) of the catalytic pathway. For most BER enzymes, k_{cat} is defined by product release (k_3 in Figure 1.5); as we examine below, this slow rate is an important feature of BER enzymes, and may serve to coordinate individual steps of the pathway. The k_{cat} of BER enzymes range from as slow as 0.05 min^{-1} to as fast as 50 s^{-1}, as determined by steady-state kinetic techniques (Table 1.2). Although k_{cat} is useful for considering an individual BER enzyme, the best way to kinetically compare enzymes is to examine their catalytic efficiency, defined as k_{cat}/K_M (where K_M represents substrate concentration at which the enzyme has reached half maximal velocity). Because catalytic efficiency reflects both the rate at which the enzyme completes the entire catalytic cycle, together with how well the enzyme binds a particular substrate, this term best represents how efficiently an enzyme works. UNG is currently the most catalytically efficient BER enzyme known with k_{cat}/K_M of 500 s^{-1} μM^{-1} (Table 1.2).

Table 1.2. Kinetic parameters of BER enzymes, including DNA Glycosylases used in this work[a,b,c]

Enzyme	k_{cat}	k_{cat}/K_M (s^{-1} μM^{-1})	$k_{chemistry}$	Ref.
UNG	50 s^{-1}	500	115 s^{-1}	8, 66
OGG1	0.05 min^{-1}	0.03	40 min^{-1}	67, 68
APE1	2 s^{-1}	100	~850 s^{-1}[d]	69, 70
polβ (Incorporation)	1.0 s^{-1}	1.5	2-20 s^{-1}[e]	65, 36
(dRP Lyase)	0.075 s^{-1}	0.15	2 s^{-1}[f]	71, 26
Lig1	0.04 s^{-1}	0.4	12 s^{-1}	65, 27

[a] Rates determined at 37 °C
[b] Portion of table adapted from[65]
[c] All kinetics performed on well-matched mixed sequence duplex DNA
[d] Rate of cleavage on tetrahydrofuran abasic site analog
[e] Rate of insertion depends on dNTP
[f] Determined at 15 °C. Value represents the slow phase of a biphasic time course; the fast phase was too fast to measure.

In addition to catalytic efficiency, it is important to call attention to rate of chemistry, $k_{chemistry}$ (k_2 in Figure 1.5) (i.e., cleavage of the DNA backbone by APE1 or incorporation of a nucleotide by pol β). For most, if not all BER enzymes, $k_{chemistry}$ is much faster than k_{cat}. Measuring rates of $k_{chemistry}$, by performing transient-state kinetic experiments, not only provides an understanding of how fast each BER enzyme carries out its required task in BER, but also provides an understanding of substrate specificity. For instance, the rate of nucleotide insertion by pol β varies depending on the nucleotide inserted *(36)*. Furthermore, for many BER enzymes, rates are affected by concentration of a required cofactor. A notable example is Lig1, which requires Mg^{2+} and ATP. At saturating concentrations of Mg^{2+}, enzyme adenylation defines k_{cat}; at limiting concentration of Mg^{2+}, nick-sealing defines k_{cat} (*27*).

1.8. Coordination during SP- and LP-BER

The BER pathway is a highly coordinated process. This coordination is evident in various kinetic studies, as well as by the presence of scaffold accessory proteins. As stated above, the RDS of many BER enzymes is product release. It has been postulated that such a kinetic scheme allows for hand-off of DNA between enzymes of the BER pathway, and prevents exposure of mutagenic and cytotoxic repair intermediates. Such a hand-off, which has also been likened to "passing of a baton" *(37),* suggests a cascade of enzymes acting much like an assembly line. Furthermore, it is known that some BER enzymes stimulate slow product release of the enzyme that precedes it in the cascade. For example, APE1 stimulates product release of many DNA glycosylases *(15,38-40)*.

Likewise, Lig1 plays a role in regulating multinucleotide incorporation of pol δ and ε *(41),* while FEN1 stimulates and coordinates dRP lyase activity of pol β *(42*).

As an alternative to the "passing of the baton" scheme, it has also been proposed that participation of several scaffolding accessory proteins suggests formation of a pre-assembled BER complex *(43*). These scaffolds have no known catalytic function and are not required to reconstitute BER *in vitro*, but are necessary for efficient BER *in vivo*. The scaffold protein XRCC1 can bind APE1, pol β, and Lig3, forming a complex at lesion sites during SP-BER (*28*). Furthermore, PCNA acts as a processivity clamp for pol β, δ, and ε to aid in non-dissociative, accurate DNA replication *(44,45*). PCNA has been shown to complex with many BER enzymes, such as UNG, AAG, MUTYH, NEIL1, APE1, FEN1, and Lig1*(46-49*)*;* accordingly, PCNA has been referred to as a docking station or communication point for such enzymes. Due to extensive interactions amongst BER enzymes, it has been proposed that a pre-assembled PCNA/BER enzyme complex slides along DNA searching for lesions *(50*). PARP1, poly [ADP-ribose] polymerase 1, has also been proposed to contribute to BER. PARP1 poly(ADP)-ribosylates several proteins, including itself, and has a defined role in sensing DNA single-strand breaks, but specific role(s) of PARP1 in BER remain unclear *(51*). It remains to be determined which model is followed *in vivo*, "passing of the baton" or a pre-assembled complex; it is possible that a combination of both is at work during SP- and LP-BER.

1.9. Deficiency in BER

The BER pathway is responsible for repair of many modified DNA nucleobase lesions, and deficiency and/or inactivity of any BER enzyme can have deleterious cellular

outcomes. Deficiency or inactivity of DNA glycosylases can lead to various cancers. For instance, mutation in the OGG1 gene, which inactivates the glycosylase, is linked to esophageal, lung squamous cell carcinomas, orolaryngeal, kidney, and gastric cancers. Similarly, mutations in MUTYH are linked to a form of colorectal cancer known as MUTYH-associated polyposis *(52)*. This mutation leads to MUTYH variants that have decreased affinity and catalytic activity on 8oxoG:A mispairs *(53)*. These are just two examples of several, in which inactivity of a DNA glycosylase leads to cancer. A single-nucleotide polymorphism in APE1 causes increased risk of colorectal cancer *(54)*. Furthermore, APE1 activity is essential for cell viability (*55,56*). This requirement for APE1 is due to the fact that cells rely on APE1 for 95% of all endonuclease activity (*57*). In contrast, for DNA glycosylases, polymerases, and ligases, there is often substrate overlap and therefore, another enzyme can compensate for enzyme deficiency. Mice that produce ~50% of normal levels of pol β have increased amounts of single-stranded breaks and chromosomal aberrations, and are hypersensitive to DNA damaging agents (*58*). Furthermore, mutations in pol β have been detected in ~30% of tumors in humans (*59*). Interestingly, in conjunction with DNA damaging agents, APE1 and pol β are also targets for cancer therapy, with aim of inducing apoptosis in cancer cells by inhibiting APE1 or pol β activity (*60,61*).

1.10. When BER Goes Awry

Although BER is essential for genetic integrity, there are instances when initiation of BER contributes to genetic *instability*; in these instances we consider that BER has gone awry. In particular, repair of 8oxoG in a CAG/CTG trinucleotide repeat (TNR) sequence of the *huntingtin* gene has been linked to expansion of the sequence (*62*). This expansion is the molecular basis for Huntington's disease (HD), one of over 40 TNR disorders. Thus, while BER of 8oxoG typically minimizes the number of point mutations caused by this modified nucleobase, initiated repair in a CAG/CTG sequence context, results in genetic instability.

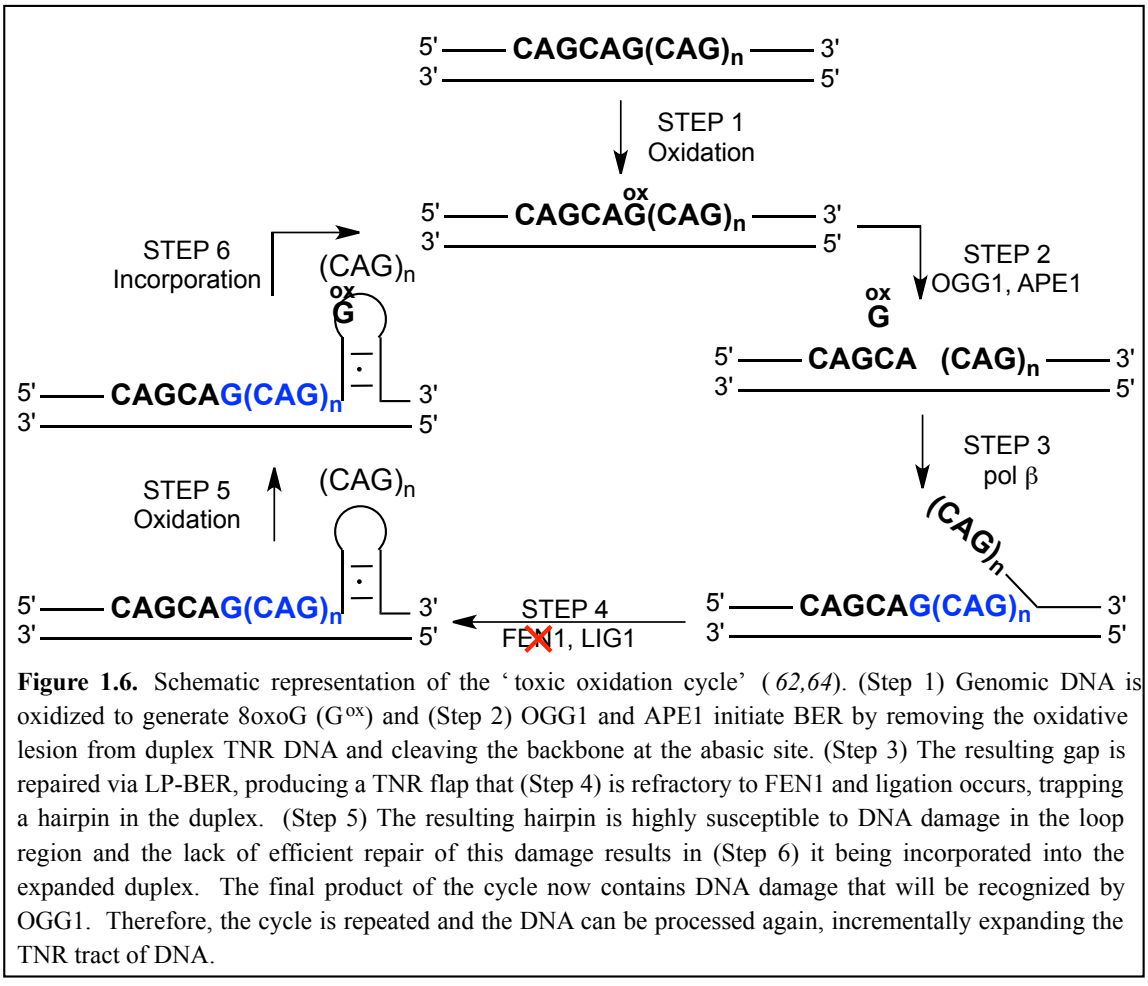

Figure 1.6. Schematic representation of the 'toxic oxidation cycle' (*62,64*). (Step 1) Genomic DNA is oxidized to generate 8oxoG (G^{ox}) and (Step 2) OGG1 and APE1 initiate BER by removing the oxidative lesion from duplex TNR DNA and cleaving the backbone at the abasic site. (Step 3) The resulting gap is repaired via LP-BER, producing a TNR flap that (Step 4) is refractory to FEN1 and ligation occurs, trapping a hairpin in the duplex. (Step 5) The resulting hairpin is highly susceptible to DNA damage in the loop region and the lack of efficient repair of this damage results in (Step 6) it being incorporated into the expanded duplex. The final product of the cycle now contains DNA damage that will be recognized by OGG1. Therefore, the cycle is repeated and the DNA can be processed again, incrementally expanding the TNR tract of DNA.

Both *in vivo* and *in* vitro work suggests repair of 8oxoG in CAG/CTG repeat sequences proceeds down LP-BER as opposed to SP-BER, even in the absence of a modified 5'-dRP group (Figure 1.6)(*63*). It has been proposed that pol β incorporates multiple nucleotides at the gap site, displacing a 5'-flap of CAG repeats (Figure 1.6, Step 3). This 5'-flap could then fold on itself forming a hairpin structure that would be refractory to cleavage by FEN1, but ligated by Lig1, leading to incorporation of excess CAG repeats (Figure 1.6, Step 4). Furthermore, previous work in the Delaney laboratory has shown that Gs in the incorporated CAG hairpin are a hotspot for damage, leading to formation of additional 8oxoG lesions (Figure 1.6, Step 5), and in addition to this accumulation of damage, it was also shown that OGG1 has reduced activity on 8oxoG within these CAG hairpins, leading to persistence of the lesion *(64*). Through DNA replication or nick-induced gap filling synthesis, the damage-containing hairpin can be re-incorporated into duplex DNA, regenerating a substrate for BER (Figure 1.6, Step 6). Thus, a toxic oxidation cycle (TOC) has been proposed in which DNA incrementally expands and is re-oxidized.

1.11. Concluding Remarks and Gap in Knowledge

The BER pathway is fundamental in maintaining the integrity of our genome; without the activity and coordination of the BER enzymes, mutations would persist and cellular toxicity could result, leading to various cancers and aging. Although previous kinetic studies have provided some insight into the molecular mechanism of many of the BER enzymes, much is still unknown about their mechanism, substrate specificity, and coordination with one another. In this body of work, we aim to use transient-state and steady-state kinetic techniques to further understand the substrate specificity of BER

enzymes as well as their molecular mechanism. Importantly, we focus our kinetic studies on the repair of TNR sequence to further examine the TOC so that we may understand the molecular mechanism by which BER leads to CAG repeat expansion.

In order for the proposed TOC to hold true, each enzyme of the BER cascade must perform their required task on CAG repeat DNA. It remains unclear how OGG1 processes an 8oxoG lesion within the context of CAG repeat duplex DNA and consequently if this processing leads to incorrect repair by latter BER enzymes. Furthermore, although it has been shown that APE1 can coordinate and stimulate the product release of OGG1, it is unclear if this holds true for repair in the context of CAG repeat duplex and hairpin constructs. Moreover, it has been proposed that in the presence of APE1, the AP lyase activity of OGG1 is bypassed; instead of the glycosylase cleaving at the abasic site, APE1 cleaves. Understanding which enzyme cleaves the DNA backbone at the abasic site is necessary in understanding the context in which the site is further repaired by latter BER enzymes, and may provide insight into the LP-BER seen for TNR tracts. Understanding such concepts is vital to understanding the initiation of the TOC by OGG1 and APE1.

Although the mechanism and kinetics of APE1 strand incision catalysis has been studied in detail, such studies typically use an abasic site analog, such as the THF site, or a reduced form of the authentic abasic site. Interestingly, much of our knowledge of the molecular mechanism of APE1, including the important amino acids implicated in catalysis, has been revealed from various crystal structures and kinetic studies, most which use APE1 binding or processing THF site containing DNA. In order to gain a better understanding of the mechanism of strand incision by APE1 it would be imperative

to perform structural and kinetic studies of APE1 incising the authentic abasic site. Such mechanistic knowledge would not only be helpful for a better insight into the BER pathway, but also for designing inhibitors of APE1 for chemotherapeutic approaches.

Finally, both *in vivo* and *in vitro* studies of BER of an 8oxoG lesion within CAG TNRs suggest progression down the LP-BER pathway, though, it is not well understood *why* repair progresses down LP-BER versus SP-BER. The polymerase either inserts a single nucleotide or multiple nucleotides at the site of repair; therefore, it is likely that the polymerase, in some part, is responsible for choosing the sub-pathway that completes repair. Kinetic studies examining the ability of pol β to undergo single-nucleotide incorporation as well as multinucleotide incorporation on CAG repeat DNA versus non-repetitive DNA may provide insight into the addition of excess CAG repeats by pol β during the TOC.

Within this text, such questions regarding activity of BER enzymes on CAG repeat and mixed sequence context have been examined by performing enzyme kinetic studies. It is our aim to fully understand each step of the BER cascade to provide useful insight into the mechanism of action of the major BER players alone and in coordination with one another, with the long-term goal to identify possible chemo and neurodegenerative therapeutic targets. Furthermore, exploring the substrate specificity of the BER enzymes will provide further insight into the molecular mechanism by which CAG repeat tracts expand within the context of HD and conceivably other TNR repeat disorders.

1.14. References

(1) Cadet, J., Douki, T., and Ravanat, J. Oxidatively Generated Base Damage to Cellular DNA. *Free Radic. Biol. Med.* **2010**, *49*, 9-21.

(2) Gates, K. S. An Overview of Chemical Processes That Damage Cellular DNA: Spontaneous Hydrolysis, Alkylation, and Reaction with Radicals. *Chem. Res. Tox.* **2009**, *22*, 1747-1760.

(3) Shibutani, S., Takeshita, M., and Grollman, A. P. Insertion of Specific Bases During DNA Synthesis Past the Oxidation-Damaged Base 8-oxodG. *Nature* **1991**, *349*, 431–434.

(4) Friedman, J., and Stivers, J. Detection of Damaged DNA Bases by DNA Glycosylase Enzymes. *Biochemistry*, **2010**, *49*, 4957-4967.

(5) Higley, M., and Llyod, R. Processivity of Uracil DNA Glycosylase. *Mutat. Res.* **1993**, *294*, 109-116.

(6) Francis, A., and David, S. S. *Escherichia coli* MutY and Fpg Utilize a Processive Mechanism for Target Location. *Biochemistry*, **2003**, *42*, 801-810.

(7) Hudglin, M., and O'Brien, P. J. Human Alkyladenine DNA Glycosylase Employs a Processive Search for DNA Damage. *Biochemistry*, **2008**, *47*, 11434-11445.

(8) Kavli, B., Slupphaug, G., Mol, C., Arvai, A., Peterson, S., Tainer, J. A., and Krokan, H. Excision of Cytosine and Thymine from DNA by Mutants of Human Uracil-DNA Glycosylase. *EMBO J.* **1996**, *15*, 3442–3447.

(9) Nash, H. M., Lu, R., Lane, W., and Verdine, G. L. The Critical Active-Site Amine of the Human 8-Oxoguanine DNA Glycosylase, hOgg1: Direct Identification, Ablation and Chemical Reconstitution. *Chem. Biol.* **1997**, *4*, 693–702.

(10) Hazra, T. K., Kow, Y., Hatahet, Z., Imhoff, B., Boldogh, I., Mokkapati, S., Mitra, S., and Izumi, T. Identification and Characterization of a Novel Human DNA Glycosylase for Repair of Cytosine-Derived Lesions. *J. Biol. Chem.* **2002**, *277*, 30417–30420.

(11) Zhao, X., Krishnamurthy, N., Burrows, C. J., and David, S. S. Mutation versus Repair: NEIL1 Removal of Hydantoin Lesions in Single-Stranded, Bulge, Bubble, and Duplex DNA Contexts. *Biochemistry* **2010**, *49*, 1658–1666.

(12) Zhou, J., Liu, M., Fleming, A., Burrows, C. J., and Wallace, S. S. Neil3 and NEIL1 DNA Glycosylases Remove Oxidative Damages from Quadruplex DNA and Exhibit Preferences for Lesions in the Telomeric Sequence Context. *J. Biol. Chem.* **2013**, *288*, 27263–27272.

(13) Michaels, M., Tchou, J., Grollman, A., and Miller, J. A Repair System for 8-Oxo-7,8-Dihydrodeoxyguanine. *Biochemistry* **1992**, *31*, 10964–10968.

(14) Wiebauer, K., and Jiricny, J. Mismatch-Specific Thymine DNA Glycosylase and DNA Polymerase Beta Mediate the Correction of GT Mispairs in Nuclear Extracts from Human Cells. *Proc. Natl. Acad. Sci. U.S.A.* **1990**, *87*, 5842-5845.

(15) Vidal, A. E., Hickson, I., Boiteux, S., and Radicella, J. P. Mechanism of Stimulation of the DNA Glycosylase Activity of hOGG1 by the Major Human AP Endonuclease: Bypass of the AP Lyase Activity Step. *Nucleic Acids Res.* **2001**, *29*, 1285–1292.

(16) Dalhus, B., Forsbring, M., Helle, I., Vik, E., Forstrøm, R., Backe, P., Alseth, I., and Bjoras, M. Separation-of-Function Mutants Unravel the Dual-Reaction Mode of Human 8-Oxoguanine DNA Glycosylase. *Structure* **2011**, *19*, 117–127.

(17) Werner, R. M., and Stivers, J. T. Kinetic Isotope Effect Studies of the Reaction Catalyzed by Uracil DNA Glycosylase: Evidence for an Oxocarbenium Ion-Uracil Anion Intermediate. *Biochemistry* **2000**, *39*, 14054-14064.

(18) McCann, J., and Berti, P. J. Transition-State Analysis of the DNA Repair Enzyme MutY. *J. Am. Chem. Soc.* **2008**, *130*, 5789–5797.

(19) Schärer, O. D., Ortholand, J.-Y., Ganesan, A., Ezaz-Nikpay, K., and Verdine, G. L. Specific Binding of the DNA Repair Enzyme AlkA to a Pyrrolidine-Based Inhibitor. *J. Am. Chem. Soc.* **1995**, *117*, 6623–6624.

(20) Schärer, O. D., Nash, H. M., Jiricny, J., Laval, J., and Verdine, G. L. Specific Binding of a Designed Pyrrolidine Abasic Site Analog to Multiple DNA Glycosylases. *J. Biol. Chem.* **1998**, *273*, 8592–8597.

(21) Chu, A. M., Fettinger, J. C., and David, S. S. Profiling Base Excision Repair Glycosylases with Synthesized Transition State Analogs. *Bioorg. Med. Chem. Lett.* **2011**, *21*, 4969–4972.

(22) Sczepanski, J. T., Wong, R., McKnight, J., Bowman, G., and Greenberg, M. M. Rapid DNA-Protein Cross-Linking and Strand Scission by an Abasic site in a Nucleosome Core Particle. *Proc. Natl. Acad. Sci. U.S.A.* **2010**, *107*, 22475–22480.

(23) Barzilay, G., Mol, C., Robson, C., Walker, L., Cunningham, R. P., Tainer, J. A., and Hickson, I. D. Identification of Critical Active-Site Residues in the Multifunctional Human DNA Repair Enzyme HAP1. *Nat. Struct. Biol.* **1995**, *2*, 561–568.

(24) Erzberger, J. P., and Wilson, D. M. The Role of Mg2+ and Specific Amino Acid

Residues in the Catalytic Reaction of the Major Human Abasic Endonuclease: New Insights from EDTA-Resistant Incision of Acyclic Abasic Site Analogs and Site-Directed Mutagenesis. *J. Mol. Biol.* **1999**, *290*, 447–457.

(25) Beard, W. A., and Wilson, S. H. Structure and Mechanism of DNA Polymerase β. *Chem. Rev.* **2006**, *106*, 361–382.

(26) Prasad, R., Shock, D., Beard, W. A., and Wilson, S. H. Substrate Channeling in Mammalian Base Excision Repair Pathways: Passing the Baton. *J. Biol. Chem.* **2010**, *285*, 40479–40488.

(27) Taylor, M. R., Conrad, J., Wahl, D., and O'Brien, P. J. Kinetic Mechanism of Human DNA Ligase I Reveals Magnesium-Dependent Changes in the Rate-Limiting Step that Compromise Ligation Efficiency. *J. Biol. Chem.* **2011**, *286*, 23054–23062.

(28) Caldecott, K. W. XRCC1 and DNA Strand Break Repair. *DNA Repair (Amst.)* **2003**, *2*, 955–969.

(29) Gao, Y., Katyal, S., Lee, Y., Zhao, J., Rehg, J., and Russell, H. R. DNA ligase III is Critical for mtDNA Integrity but Not Xrcc1-Mediated Nuclear DNA Repair. *Nature* **2011**, *471*, 240-244.

(30) Simsek, D., Furda, A., Gao, Y., Artus, J., Brunet, E., Hadjantonakis, A., Van Houten, B., Shuman, S., McKinnon, P., and Jasin, M. Crucial role for DNA ligase III in Mitochondria but Not in Xrcc1-Dependent Repair. *Nature* **2011**, *471*, 245–248.

(31) Sung, J-S., DeMott, M., and Demple, B. Long-Patch Base Excision DNA Repair of 2-Deoxyribonolactone Prevents the Formation of DNA-Protein Cross-links

with DNA Polymerase Beta. *J. Biol. Chem.* **2005**, *280*, 39095–39103.

(32) Horton, J.K., Prasad, R., Hou, E., and Wilson, S.H. Protection Against Methylation-Induced Cytotoxicity by DNA Polymerase β-Dependent Long Patch Base Excision Repair. *J. Bio. Chem.* **2000**, *275*, 2211-2218

(33) Singhal, R. K., Prasad, R., and Wilson, S. H. DNA Polymerase Beta conducts the Gap-Filling Step in Uracil-Initiated Base Excision Repair in a Bovine Testis Nuclear Extract. *J. Biol. Chem.* **1995**, *270*, 949–957.

(34) Moldovan, G.-L., Pfander, B., and Jentsch, S. PCNA, the Maestro of the Replication Fork. *Cell* **2007**, *129*, 665–679.

(35) Porello, S. L., Leyes, A., and David, S. S. Single-Turnover and Pre-Steady-State Kinetics of the Reaction of the Adenine Glycosylase MutY with Mismatch-Containing DNA Substrates. *Biochemistry*, **1998**, *37*, 14756-14764.

(36) Ahn, J., Kraynov, V., Zhong, X., Werneburg, B.G., Tsai, M-D. DNA Polymerase Beta: Effects of Gapped DNA Substrates on dNTP Specificity, Fidelity, Processivity and Conformational Changes. *Biochemical J.* **1998**, *331*, 79.

(37) Wilson, S. H., and Kunkel, T. A. Passing the Baton in Base Excision Repair. *Nat. Struct. Biol.* **2000**, *7*, 176–178.

(38) Hill, J., Hazra, T., Izumi, T., and Mitra, S. Stimulation of Human 8-Oxoguanine-DNA Glycosylase by AP-Endonuclease: Potential Coordination of the Initial Steps in Base Excision Repair. *Nucleic Acids Res.* **2001**, *29*, 430–438.

(39) Fitzgerald, M., and Drohat, A. C. Coordinating the Initial Steps of Base Excision Repair: Apurinic/apyrimidinic Endonuclease 1 Actively Stimulates Thymine DNA glycosylase by Disrupting the Product Complex. *J. Biol. Chem.* **2008**, *283*,

32680–32690.

(40) Baldwin, M. R., and O'Brien, P. J. Human AP endonuclease 1 Stimulates Multiple-Turnover Base Excision by Alkyladenine DNA Glycosylase. *Biochemistry* **2009**, *48*, 6022–6033.

(41) Pascucci, B., Stucki, M., Jónsson, Z., Dogliotti, E., and Hübscher, U. Long Patch Base Excision Repair with Purified Human Proteins. DNA ligase I as Patch Size Mediator for DNA Polymerases Delta and Epsilon. *J. Biol. Chem.* **1999**, *274*, 33696–33702.

(42) Prasad, R., Dianov, G., Bohr, V., and Wilson, S. H. FEN1 Stimulation of DNA Polymerase Beta Mediates an Excision Step in Mammalian Long Patch Base Excision Repair. *J. Biol. Chem.* **2000**, *275*, 4460–4466.

(43) Dianov, G. L., and Hübscher, U. Mammalian Base Excision Repair: the Forgotten Archangel. *Nucleic Acids Res.* **2013**, *41*, 3483–3490.

(44) Burgers, P. M. Saccharomyces cerevisiae replication factor C. II. Formation and activity of complexes with the proliferating cell nuclear antigen and with DNA polymerases delta and epsilon *J. Biol. Chem.* **1991**, *226*, 22698-22706.

(45) Kedar, P., Kim, S., Robertson, A., Hou, E., Prasad, R., Horton, J. K., and Wilson, S. H. Direct Interaction Between Mammalian DNA Polymerase Beta and Proliferating Cell Nuclear Antigen. *J. Biol. Chem.* **2002**, *277*, 31115–31123.

(46) Maga, G., and Hubscher, U. Proliferating Cell Nuclear Antigen (PCNA): A Dancer with Many Partners. *J. Cell. Sci.* **2003**, *116*, 3051–3060.

(47) Dou, H., Theriot, C., Das, A., Hegde, M., Matsumoto, Y., Boldogh, I.;,Hazra, T., Bhakat, K., and Mitra, S. Interaction of the Human DNA Glycosylase NEIL1

with Proliferating Cell Nuclear Antigen. The Potential for Replication-Associated Repair of Oxidized Bases in Mammalian Genomes. *J. Biol. Chem.* **2008**, *283*, 3130–3140.

(48) Xia, L., Zheng, L., Lee, H.-W., Bates, S., Federico, L., Shen, B., and O'Connor, T. R. Human 3-Methyladenine-DNA Glycosylase: Effect of Sequence Context on Excision, Association with PCNA, and Stimulation by AP Endonuclease. *J. Mol. Biol.* **2005**, *346*, 1259–1274.

(49) Chang, D.-Y., and Lu, A.-L. Functional Interaction of MutY Homolog with Proliferating Cell Nuclear Antigen in Fission Yeast, Schizosaccharomyces pombe. *J. Biol. Chem.* **2002**, *277*, 11853–11858.

(50) Balakrishnan, L., Brandt, P., Lindsey-Boltz, L., Sancar, A. and Bambara, R. A. Long Patch Base Excision Repair Proceeds via Coordinated Stimulation of the Multienzyme DNA Repair Complex. *J. Biol. Chem.* **2009**, *284*, 15158–15172.

(51) Fisher, A., Hochegger, H. Takeda, S., and Caldecott, K. W. Poly(ADP-Ribose) Polymerase 1 Accelerates Single-Strand Break Repair in Concert with Poly(ADP-Ribose) Glycohydrolase. *Mol. Cell. Biol.* **2007**, *27*, 5597–5605.

(52) Al-Tassan, N., Chmiel, N., Maynard, J., Fleming, N., Livingston, A.,Williams, G., Hodges, A., Davies, D., David, S. S., Sampson, J. R., and Cheadle, J. P. Inherited Variants of MYH Associated with Somatic G:C→T:A Mutations in Colorectal Tumors. *Nat. Genet.* **2002**, *30*, 227–232.

(53) Pope, M. A., Chmiel, N. H., and David, S. S. Insight into the Functional Consequences of hMYH Variants Associated with Colorectal Cancer: Distinct Differences in the Adenine Glycosylase Activity and the Response to AP

Endonucleases of Y150C and G365D Murine MYH. *DNA Repair (Amst.)* **2005**, *4*, 315–325.

(54) Karahalil, B., Bohr, V., and Wilson, D. M. Impact of DNA Polymorphisms in Key DNA Base Excision Repair Proteins on Cancer Risk. *Hum. and Exp. Toxicol.* **2012**, *31*, 981–1005.

(55) Xanthoudakis, S., Smeyne, R., Wallace, J., and Curran, T. The Redox/DNA Repair Protein, Ref-1, is Essential for Early Embryonic Development in Mice. *Proc. Natl. Acad. Sci.* **1996**, *93*, 8919-8923.

(56) Fung, H., and Demple, B. A Vital Role for Ape1/Ref1 Protein in Repairing Spontaneous DNA Damage in Human Cells. *Mol. Cell*, **2005**, *17*, 463-470.

(57) Doetsch, P., and Cunningham, R. The Enzymology of Apurinic/Apyrimidinic Endonucleases. *Mutat. Res.* **1990**, *236*, 173-201.

(58) Cabelof, D. C., Guo, Z., Raffoul, J. J., Sobol, R. W., Wilson, S. H., Richardson, A., and Heydari, A. R. Base Excision Repair Deficiency caused by Polymerase Beta Haploinsufficiency: Accelerated DNA Damage and Increased Mutational Response to Carcinogens. *Cancer Res.* **2003**, *63*, 5799–5807.

(59) Starcevic, D., Dalal, S., and Sweasy, J.B. Is There a Link Between DNA Polymerase Beta and Cancer? *Cell Cycle* **2004**, *3*, 996–999.

(60) Fishel, M. L., and Kelley, M. R. The DNA Base Excision Repair Protein Ape1/Ref-1 as a Therapeutic and Chemopreventive Target. *Mol. Aspects. Med.* **2007**, *28*, 375-395.

(61) Yang, J., Parsons, J., Nicolay, N. H., Caporali, S., Harrington, C. F., Singh, R., Finch, D., D'Atri, S., Farmer, P. B., Johnston, P. G., McKenna, W. G., Dianov,

G., and Sharma, R. A. Cells Deficient in the Base Excision Repair Protein DNA Polymerase Beta are Hypersensitive to Oxaliplatin Chemotherapy. *Oncogene* **2010**, *29*, 463–468.

(62) Kovtun, I. V., Liu, Y., Bjoras, M., Klungland, A., Wilson, S. H., and McMurray, C. T. OGG1 Initiates Age-dependent CAG Trinucleotide Expansion in Somatic Cells. *Nature* **2007**, *447*, 447–452.

(63) Liu, Y., Prasad, R., Beard, W. A., Hou, E. W., Horton, J. K., McMurray, C. T.;, and Wilson, S. H. Coordination Between Polymerase Beta and FEN1 can Modulate CAG Repeat Expansion. *J. Biol. Chem.* **2009**, *284*, 28352–28366.

(64) Jarem, D. A., Wilson, N. R., and Delaney, S. Structure-dependent DNA Damage and Repair in a Trinucleotide Repeat Sequence. *Biochemistry* **2009**, *48*, 6655–6663.

(65) Srivastava, D., Berg, B. J., Prasad, R., Molina, J. T., Beard, W. A., Tomkinson, A. E., and Wilson, S. H. Mammalian Abasic Site Base Excision Repair. Identification of the Reaction Sequence and Rate-Determining Steps. *J. Biol. Chem.* **1998**, *273*, 21203–21209.

(66) Drohat, A., Jagashree, J., Ferguson, E., and Stivers, J. T. Role of Electrophilic and General Base Catalysis in the Mechanism of *Escherichia coli* Uracil DNA Glycosylase. *Biochemistry* **1999**, *38*, 11866-11875.

(67) Asagoshi, K., Yamada, T., Terato H., Ohyama, Y., Monden, Y., Arai, T., Nishimura, S., Aburatani, H., Lindahl, T, and Ide, H. Distinct Repair Activities of Human 7,8-Dihydro-8-oxoguanine DNA Glycosylase and Formamidopyrimidine DNA Glycosylase for Formamidopyrimidine and 7,8-

Dihydro-8-oxoguanine. *J. Biol. Chem.* **2000**, *275*, 4956–4964.

(68) Leipold, M., Workman, H., Muller, J., Burrows, C. J., and David, S. S. Recognition and Removal of Oxidized Guanines in Duplex DNA by the Base Excision Repair Enzymes hOGG1, yOGG1, and yOGG2. *Biochemistry* **2003**, *42*, 11373–11381.

(69) Xu, Y.-J., DeMott, M. S., Hwang, J. T., Greenberg, M. M., and Demple, B. Action of Human Apurinic Endonuclease (Ape1) on C1'-oxidized Deoxyribose Damage in DNA, *DNA Repair (Amst.)* **2003**, *2*, 175–185.

(70) Maher, R., and Bloom, L. B. Pre-steady-state kinetic characterization of the AP endonuclease activity of human AP endonuclease 1. *J. Biol. Chem.* **2007**, *282*, 30577–30585.

(71) Prasad, R., Beard, W. A., Strauss, P. R., and Wilson, S. H. Human DNA Polymerase Beta Deoxyribose Phosphate Lyase. Substrate Specificity and Catalytic Mechanism. *J. Biol. Chem.* **1998**, *273*, 15263–15270.

Chapter 2: Initiation and Coordination of DNA Base Excision Repair by Oxoguanine Glycosylase and AP Endonuclease 1 in a Trinucleotide Repeat Tract[†]

[†]**Adapted From:**

Jarem, D.J.[*], Wilson, N.R.[*], Schermerhorn, K.M.[*], and Delaney, S. (2011)

Incidence and Persistence of 8-oxo-7,8-dihydroguanine within a

Hairpin Intermediate Exacerbates a Toxic Oxidation Cycle

Associated with Trinucleotide Repeat Expansion. *DNA Repair 10*, 887-896.

[*]These authors contributed equally to this work

2.1. Abstract

The repair protein oxoguanine glycosylase (OGG1) initiates base excision repair (BER) in mammalian cells by removing the oxidized base 8-oxo-7,8-dihydroguanine (8oxoG) from DNA. Interestingly, OGG1 has been implicated in somatic expansion of the trinucleotide repeat (TNR) sequence CAG/CTG. Furthermore, a 'toxic oxidation cycle' has been proposed for age-dependent expansion in somatic cells. In this cycle, duplex TNR DNA is (1) oxidized by endogenous species; (2) BER is initiated by OGG1 and the DNA is further processed by AP endonuclease 1 (APE1); (3) a stem-loop hairpin forms during strand-displacement synthesis by polymerase β (pol β); (4) the hairpin is ligated and (5) incorporated into duplex DNA to generate an expanded CAG/CTG region. This expanded region is again subject to oxidation and the cycle continues. Our lab previously determined that the hairpin adopted by TNR repeats contains a hot spot for oxidation. This finding prompted us to examine the possibility that the generation of a hairpin during a BER event exacerbates the toxic oxidation cycle due to accumulation of damage. Therefore, in this work we used mixed-sequence and TNR substrates containing a site-specific 8oxoG lesion to define the kinetic parameters of human OGG1 activity on duplex and hairpin substrates. We report that OGG1 activity on TNR duplexes is indistinguishable from a mixed-sequence control. Thus, BER is initiated on TNR sequences as readily as non-repetitive DNA in order to start the toxic oxidation cycle. However, we find that for hairpin substrates OGG1 has reduced affinity and excises 8oxoG at a significantly slower rate as compared to duplexes. Therefore, 8oxoG is expected to accumulate in the hairpin intermediate. This damage-containing hairpin can then be incorporated into duplex, resulting in an expanded TNR tract that now contains

an oxidative lesion. Thus, the cycle restarts and the DNA can incrementally expand. These results contribute to our understanding of the mechanism by which CAG repeats expand during the BER pathway.

2.2. Introduction

The expansion of a CAG/CTG TNR sequence has been identified as the pathogenic signature of several neurodegenerative disorders (*1-3*), with one such disorder being Huntington's disease (HD). In healthy individuals, exon 1 of the HD gene contains 5-35 CAG/CTG repeats; repeat tracts of this length are not prone to expansion (*4*). Sequences containing 36-39 CAG/CTG repeats are described as the pre-mutation allele and are known to be prone to expansion. The disease state is characterized by greater than 40 repeats.

Following expansion of the CAG/CTG sequence, the HD gene is transcribed and translated and results in a protein product with an expanded glutamine tract (*5*). Although the function of the normal HD protein remains an active area of research, it is known that the mutant HD protein, which has a tract of more than 40 glutamine residues, has aberrant properties that cause the death of brain cells (*6*). Indeed, it is the death of these cells that leads to both the mental decline and uncoordinated body movements associated with HD.

Significant insight into the molecular mechanism of the expansion of CAG/CTG sequences was gained from work using an R6/1 mouse model for HD (*7*). In these mice, which harbor a transgene containing exon 1 of the human HD gene, TNR expansion correlated with accumulation of the oxidatively damaged base 8oxoG. Intriguingly, when

the R6/1 mice were crossed with mice lacking the DNA repair protein OGG1, the CAG/CTG repeat expansion was abrogated in somatic cells (*7*). These results indicate that the presence of the OGG1 repair protein is implicated in TNR expansion.

As discussed within the introduction chapter, OGG1 is a glycosylase that initiates the BER process in mammalian cells by excising oxidized bases from DNA, with 8oxoG being the prototypic and most well-studied substrate (*8*). The remaining steps in the BER pathway are believed to occur with APE1 cleaving at the abasic site lesion, pol β inserting a single nucleotide in short-patch (SP) BER, or multiple nucleotides in long-patch (LP) BER, at the nick site, with the latter pathway creating a 5'-flap that is processed by flap endonuclease 1 (FEN1). Finally DNA ligase I (Lig1) ligates the DNA backbone to complete repair. In the context of BER in CAG repeats, pol β is implicated in incorporating multiple nucleotides at the nick site, creating a 5'-flap that can not be processed by FEN1, but is ligatable by Lig1, leading to the incorporation of excess CAG repeats and expansion of the TNR tract (*9*).

The AP lyase activity of OGG1 at an abasic site generates a gap with 3′-phospho α,β-unsaturated aldehyde (3′-dRP) and 5′-phosphate termini (Figure 2.1D) (*9*). APE1 can remove the 3′-dRP to generate the 3′-OH terminus necessary for DNA synthesis by pol β (Figure 2.1E) (*10*). Although OGG1 possesses AP lyase activity it has been shown to be ~500-fold slower than the associated glycosylase step (*11*). Furthermore, it has been shown *in vitro* that APE1 improves the efficiency of repair by stimulating the product release rate of OGG1 and cleaving at the abasic site, which is thought to bypass the AP lyase activity of OGG1, such that OGG1 is acting as a monofunctional glycosylase (Figure 2.1B) (*12, 13*). Thus, it is likely that APE1 and not OGG1, cleaves at

the abasic site *in vivo,* creating a nick in the DNA backbone with 3′-OH and 5′-deoxyribose phosphate (dRP) termini (Figure 2.1C).

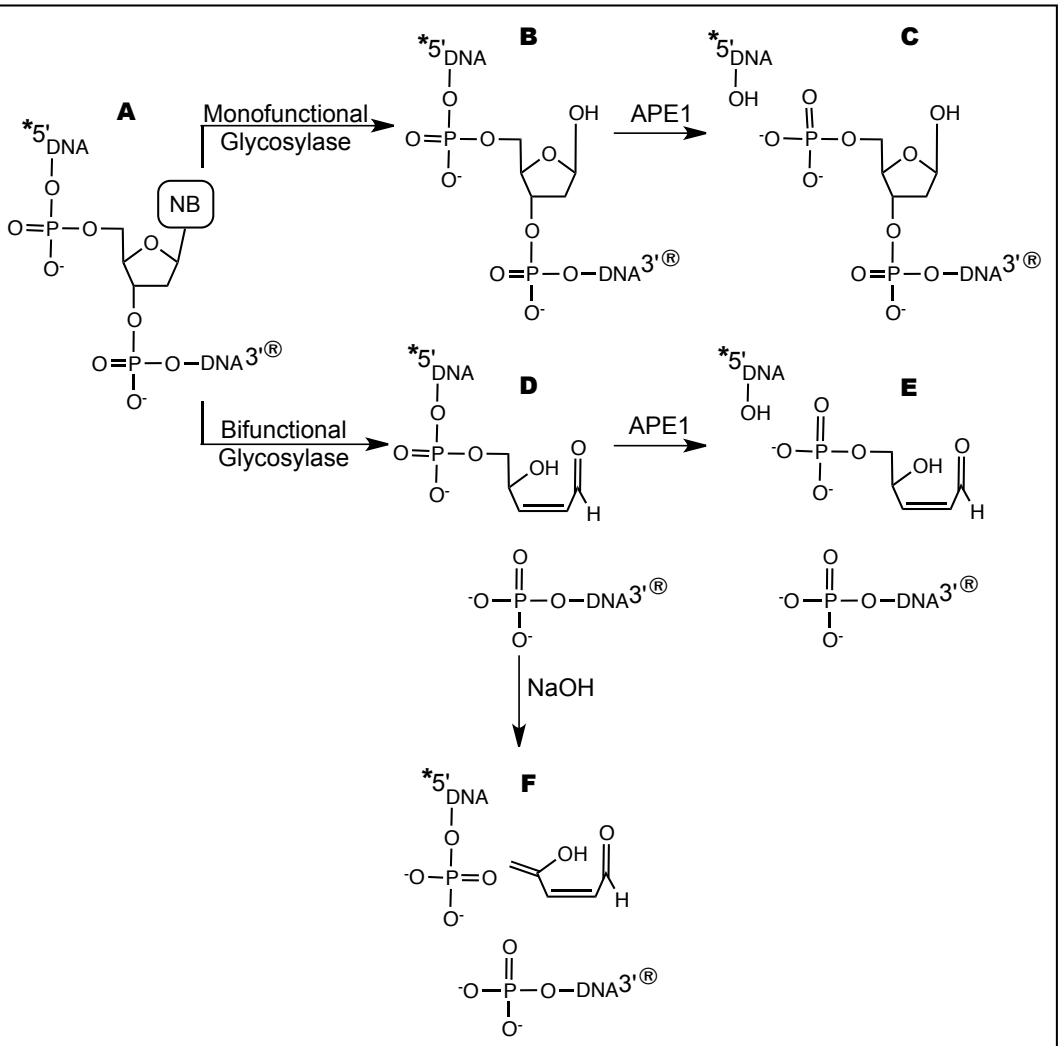

Figure 2.1. DNA structures before and after cleavage by monofunctional and bifunctional glycosylase, and APE1. DNA containing a damaged nucleobase (NB) (A) is processed by either a monofunctional or bifunctional glycosylase. A monofunctional glycosylase removes the NB lesion affording the abasic site product (B), which is recognized and cleaved by APE1 creating a nick in the DNA backbone with 3'-OH and 5'-deoxyribose phosphate (dRP) termini. A bifunctional glycosylase removes the NB lesion and catalyzes β -elimination of DNA backbone using its AP lyase activity, affording a 3'-dRP group and 5'-phosphate termini (D). APE1 can act on the β-elimination product by converting the 3'-dRP group to the 3'-OH (E). Finally in the presence of NaOH, the β-elimination 3'-dRP AP lyase product can be converted to the δ-elimination 3'-phosphate (F). The 5'-* denotes the location of the ^{32}P label while the 3' -® denote the location of the R6G label.

In an effort to elucidate the role of OGG1 in CAG/CTG repeat expansion the OGG1 repair event has been reconstituted *in vitro* (*7*). Two 100 base pair (bp) DNA

duplexes were used as substrates. The first duplex contained 8oxoG flanked on both sides by mixed sequence. In the second duplex the 8oxoG was flanked on the 5′ side by mixed sequence and on the 3′ side by $(CAG)_{19}/(CTG)_{19}$. Using purified human OGG1 which shares 83% sequence homology with murine OGG1 (*14*), 8oxoG was excised from both duplexes (*7*). Furthermore, APE1 also had activity on both duplexes. In contrast, while pol β incorporated a single nucleotide in the mixed-sequence duplex, more than one nucleotide was incorporated in the duplex containing the TNR sequence, suggesting pol β followed the LP-BER pathway (*7*). Following ligation by bacteriophage T4 DNA ligase, a 100 bp product was restored for the mixed-sequence duplex, but expanded products were obtained for the duplex containing the repeat sequence (the length of the expanded products was not reported). In complementary work, when the same 100 bp duplex substrates were incubated with cell extracts from mouse embryonic fibroblasts, instead of purified BER proteins, similar results were obtained (*9*). The mixed-sequence duplex was faithfully repaired, but expansion of the repeat-containing duplex resulted in products containing up to 130 bp. With TNR sequences, LP-BER occurred when the 5′-dRP contained the tetrahydrofuran (THF) analog of the deoxyribose sugar ring that is known to be refractory to the dRPase activity of pol β and, interestingly, also when there was an authentic 5′-dRP group present. In contrast, for the mixed-sequence duplex pol β processed the authentic 5′-dRP group and repair occurred via SP-BER. Therefore, it was suggested that the TNR region, not a modified 5'-dRP group, facilitates LP-BER.

In addition to the duplex conformation, CAG/CTG repeat sequences have been shown to adopt non-B conformations. *In vitro* studies using NMR, optical melting analysis, native gel electrophoresis, differential scanning calorimetry, circular dichroism,

and chemical probes have shown that single-stranded $(CAG)_n$ and $(CTG)_n$ sequences can fold to form intramolecular hairpins and other slipped-structure intermediates (*15-20*). There is also evidence for these TNR sequences to adopt hairpins *in vivo*. Two zinc finger nucleases were designed to cleave the stem of CAG or CTG hairpins but not CAG/CTG duplex (*21*). Expression of either of these nucleases in isogenic HeLa cell lines containing 45 or 102 CAG/CTG repeats resulted in the accumulation of products due to hairpin cleavage.

In previous work we have shown that, relative to $(CAG)_{10}/(CTG)_{10}$ duplex, the hairpin adopted by $(CAG)_{10}$ is hyper-susceptible to modification by peroxynitrite (*22*). Notably, peroxynitrite is known to convert G to several damage products, one of which is 8oxoG (*23-25*). Furthermore, it is the solution-accessible loop of the hairpin that contains a hotspot for DNA damage. Given the demonstrated role of OGG1 in initiating CAG/CTG repeat expansion in both *in vitro* and *in vivo* systems (*7, 9, 26*), in this work we characterized fully the kinetic parameters of OGG1 acting on TNR sequences. We determined the rate of cleavage of the glycosidic bond of 8oxoG, and the rate of product release, in the absence and presence of APE1, for OGG1 acting on DNA substrates with different structural contexts, namely duplex and hairpin, and substrates in which the location of the 8oxoG was varied. Furthermore, comparison of the results obtained for the TNR sequences to those obtained for a mixed-sequence duplex allowed us to define the contribution of sequence context of the damage to enzyme activity. We demonstrate that catalytic activity and rate of product release for TNR duplexes is indistinguishable from a comparable mixed-sequence control, indicating that BER can be initiated by OGG1 just as efficiently in TNR regions as elsewhere in the genome. We also establish

that APE1 can stimulate turnover for both the mixed and TNR duplex substrates, albeit to a lesser extent for repeat sequences. Moreover, we demonstrate that the activity of OGG1 is modulated by the structure of the DNA substrate. With hairpin structures, OGG1 has a reduced affinity for both substrate and product and excises 8oxoG at a slower rate as compared to the corresponding TNR duplex substrates. Finally, we reveal that under the conditions tested here, OGG1 utilizes its AP lyase activity in the presence of over 50 molar excess of APE1. Such evidence suggests that the AP lyase step of OGG1 is functional in the presence of APE1, creating a 5'-phosphate as opposed to the 5'-dRP group at the repair site. Importantly, this work broadens our understanding of the initiation of BER on CAG repeat constructs to further understand the TNR expansion seen in HD.

2.3. Experimental Procedure

2.3.1 Oligonucleotide Synthesis and Purification

Oligonucleotides were synthesized by standard phosphoramidite chemistry using a BioAutomation DNA/RNA synthesizer (*27*). The 8oxoG-CE and deoxyUridine-CE phosphoramidites were purchased from Glen Research and used according to the manufacturer's specifications. For sequences containing 8oxoG, the 5′-dimethoxytrityl (DMT) group was removed by the synthesizer and two rounds of HPLC purification were performed using a Dionex DNAPac PA100 anion-exchange column (4 × 250 mm); 10% acetonitrile (aq) (solvent A) and 0.8 M ammonium chloride in 10% acetonitrile (aq) (solvent B) were used as mobile phases (gradient: solvent B was increased from 30% to 55% over 10 min, 55% to 75% over 5 min, 75% to 90% over 15 min, and 90% to 100%

over 5 min; 1 mL/min). Oligonucleotides were desalted using Sephadex G-25 fine resin after each HPLC purification. Stability of the oligonucleotides containing 8oxoG to the experimental conditions was confirmed by HPLC and mass spectral analysis.

For sequences not containing 8oxoG, the 5′-DMT group was retained to aide in purification. HPLC purification was performed using a Dynamax Microsorb C18 column (10 × 250 mm) with acetonitrile (solvent A) and 30 mM ammonium acetate (solvent B) as mobile phases (gradient: solvent A was increased from 5% to 25% over 25 min; 3.5 mL/min). After the removal of the DMT group by incubation in 80% glacial acetic acid for 12 min at room temperature, a second round of purification was performed (gradient: solvent A was increased from 0% to 15% over 35 min; 3.5 mL/min). Quantification of oligonucleotides was performed at 90 °C using the ε_{260} estimated for single stranded DNA (*28*) and a Beckman Coulter DU800 UV-Vis spectrophotometer equipped with a Peltier thermoelectric device.

2.3.2 OGG1 Transient-State Kinetic Assays (k_2)

Wild-type OGG1 (a gift from Dr. Gregory Verdine, Harvard University) was expressed and purified as described previously (*29*) and total protein concentration was determined using the Bradford assay with bovine γ-globulin as a standard. The concentration of active OGG1 was determined using an active site titration as described previously (*30*) using the 8oxoG-containing duplex Mixed-DUP. The OGG1 preparation was found to be 39% active.

The oligonucleotides containing 8oxoG were 5′-^{32}P end-labeled with T4 polynucleotide kinase (NEB, Ipswich, MA) following the manufacturer's protocol. 5′-

^{32}P-labeled single-stranded DNA (80 nM) with a 1.25-fold excess of the unlabeled complementary oligonucleotide in 20 mM Tris-HCl, 10 mM Na_2EDTA, 140 mM NaCl, pH 7.6 was incubated for 5 min at 90 °C, followed by cooling to room temperature over ~2.5 h. The DNA was diluted to a final concentration of 40 nM in 20 mM Tris-HCl, 10 mM Na_2EDTA, 70 mM NaCl, 100 μg/mL BSA, pH 7.6. This diluted DNA sample and 200 nM OGG1 in 20 mM Tris-HCl, 10 mM Na_2EDTA, 210 μg/mL BSA, pH 7.6 were loaded into separate syringes of a Rapid Quench Flow (RQF) instrument (Kintek) and equilibrated for 5 min at 37 °C. The DNA and OGG1 were then combined in the reaction loop to yield a sample containing 20 nM DNA, 100 nM OGG1 in 20 mM Tris-HCl, 10 mM Na_2EDTA, 35 mM NaCl, 155 μg/mL BSA, pH 7.6. Using the RQF instrument, after 0.5-100 sec the reactions were quenched with NaOH (0.5 M final concentration) and incubated at 90 °C for 2 min. After incubation at 90 °C, 15 μL of denaturing loading buffer (80% formamide, 10 mM EDTA, 0.1% bromophenol blue, 0.1% xylene cyanol) were added, and the samples were stored on dry ice until electrophoresis. Prior to loading onto an 18% denaturing polyacrylamide gel, all samples were incubated at 90 °C for 3 min. The products were visualized by phosphorimagery and the amount of product was plotted versus time. The data were then fitted as described previously (*31*) in order to obtain values for the rate of glycosidic bond cleavage of 8oxoG (k_2).

2.3.4 OGG1 Steady-State Kinetic Assays (k_3)

Oligonucleotides containing 8oxoG were 5′-^{32}P end-labeled with T4 polynucleotide kinase following the manufacturer's protocol. 5′-^{32}P-labeled single-stranded DNA (100 nM) alone (for hairpin samples) or with a 1.25-fold excess of the

unlabeled complementary oligonucleotide (for duplex samples) in 20 mM Tris-HCl, 140 mM NaCl, pH 7.6 was incubated for 5 min at 90 °C, followed by cooling to room temperature over ~2.5 h. Using a dilution buffer (20 mM Tris-HCl, 4 mM $MgCl_2$, 200 μg/mL BSA, pH 7.6) the DNA was then diluted and equilibrated at 37 °C for 5 min. After equilibration at 37 °C, OGG1 (in 20 mM Tris-HCl, 4 mM $MgCl_2$, 200 μg/mL BSA, pH 7.6) and APE1 (NEB; in 20 mM Tris-HCl, 4 mM $MgCl_2$, 200 μg/mL BSA, pH 7.6) were added to yield a final sample of 50 nM DNA, 5 nM OGG1 or 5 nM OGG1/50 nM APE1 in 20 mM Tris-HCl, 70 mM NaCl, 2 mM $MgCl_2$, 100 μg/mL BSA, pH 7.6 (80 μL total sample volume). After addition of OGG1 or OGG1/APE1, the sample was incubated at 37 °C and aliquots of 5 μL were removed as a function of time (0.25-20 min), quenched by the addition of 5 μL of NaOH (0.5 M final concentration), and incubated at 90 °C for 2 min. Following quenching by NaOH/heat treatment, 5 μL of denaturing loading buffer were added and the samples were placed on dry ice until electrophoresis through an 18% polyacrylamide gel. The products were visualized by phosphorimagery and the concentration of product was plotted versus time. Both a burst phase and a linear phase are observed with the slope of the linear phase equal to $k_3 \times$ [active enzyme] (*31*).

2.3.5. Determining AP Lyase Activity of OGG1 in the Presence of APE1

Mixed-DUP and Mixed-U-DUP oligonucleotides containing 8oxoG or uracil were 5′-^{32}P-labeled with T4 polynucleotide kinase following the manufacturer's protocol. Samples were dried *in vacuo*. Following drying, both lesion-containing strands were 3′-Rhodamine 6G-labeled with Rhodamine 6G-ddATP (Perkin Elmer) and Terminal

Transferase (NEB) following the manufacturer's protocol. Care was taken to limit exposure of R6G-containing DNA to light. Samples were dried *in vacuo* then resuspended with a 1.25-fold excess of the unlabeled complementary oligonucleotide in 20 mM Tris-HCl, 140 mM NaCl, 5 mM $MgCl_2$, pH 7.6, to final DNA concentration of 100 nM, and incubated for 5 min at 90 °C, followed by cooling to room temperature over ~2.5 h. Nine 20 μL aliquots of Mixed-DUP (8oxoG) DNA were incubated at 37 °C for 30 min under several different conditions: DNA alone, DNA with 150 nM APE1, DNA with 150 nM OGG1, DNA with 150 nM OGG1 followed by addition of 150 nM APE1 (after 30 min), DNA with 150 nM OGG1 followed by addition of 10 μL 0.75 M NaOH (after 30 min), or DNA with 150 nM OGG1 and 150, 750, 3000 or 7500 nM APE1. All aliquots were quenched with 20 μL of denaturing dye and placed on dry ice. Three 20 μL aliquots of Mixed-U-DUP (uracil) were incubated at 37 °C for 3 or 30 min under several different conditions: DNA with 150 nM APE1 (30 min), DNA with 1 unit uracil DNA glycosylase (UDG) (NEB, Ipswich, MA) (3 min), or DNA with 1 unit UDG and 150 nM APE1 (3 min). All aliquots were quenched with 20 μL of denaturing dye and placed on dry ice. Samples were run on an 18% polyacrylamide gel. The DNA was visualized by phosphorimagery and by fluorescence detection at 550 nm.

2.4. Results and Discussion

2.4.1 DNA Substrates

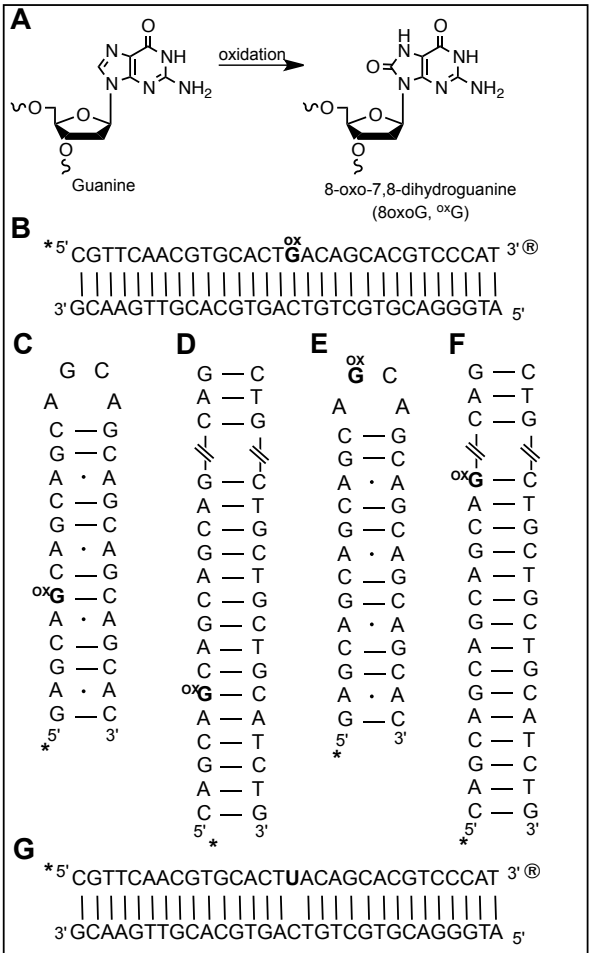

Figure 2.2. Schematic illustrations of lesion-containing DNA substrates used in this work. Shown first is (A) guanine and 8-oxo-7,8-dihydroguanine (8oxoG) followed by (B) mixed-sequence duplex with a centrally located 8-oxoG (Mixed-DUP), (C) $(CAG)_{10}$ hairpin with 8-oxoG in the stem (Stem-HP), (D) duplex obtained by base pairing Stem-HP to $(CTG)_{10}$ (Stem-DUP), (E) $(CAG)_{10}$ hairpin with 8-oxoG in the loop (Loop-HP), (F) duplex obtained by base pairing Loop-HP to $(CTG)_{10}$ (Loop-DUP) and (G) mixed-sequence duplex with centrally located uracil (U) (Mixed-U-DUP). The "*" represents the location of the ^{32}P-radiolabel, while the "®" represents the location of the R6G label

Five 30mer DNA substrates were utilized to obtain the kinetic parameters of OGG1, each of which contains a single, site-specifically incorporated 8oxoG (Fig. 2.2A,B). The substrates differ based on their structure, sequence composition, and/or positioning of the 8oxoG. The first substrate is a 30 bp duplex of mixed sequence with 8oxoG in the 16th bp (Mixed-DUP; Fig. 2.2B). This mixed-sequence duplex has been used previously to establish the rate of glycosidic bond cleavage of 8oxoG in duplex DNA by OGG1 and serves here as a control (*11*). Two substrates are comprised of CAG trinucleotide repeats that adopt an intramolecular fold to form stem-loop hairpins. These hairpins have a loop with 4 bases and a stem comprised of G-C base pairs and A•A mismatches. In one CAG hairpin, the 8oxoG is located in the 2nd repeat, positioning the damage in the stem

of the hairpin (Stem-HP; Fig.2.2C); in the other CAG hairpin, the 8oxoG is in the 5th repeat, positioning the damage in the loop of the hairpin (Loop-HP; Fig. 2.2E). In order to generate CAG/CTG duplexes, the $(CTG)_{10}$ sequence was hybridized with Stem-HP or Loop-HP to yield Stem-DUP (Fig. 2.2D) and Loop-DUP (Fig. 2.2F), respectively; these substrates can be considered the duplex counterparts of Stem-HP and Loop-HP. Notably, in Loop-DUP the 8oxoG is in the center of the 30 bp duplex whereas in Stem-DUP the damage is closer to one end of the duplex. A final sixth DNA substrate containing the same sequence as Mixed-DUP, with uracil instead of 8oxoG at the 16th base pair, was used as a control during OGG1 AP lyase experiments (Mixed-U-DUP; Fig. 2.2G).

2.4.2. Minimal Kinetic Scheme of OGG1

The minimal kinetic scheme used for the analysis of OGG1 activity is provided in Fig. 2.3. The figure shows the three steps of the enzymatic cycle: binding to the DNA substrate $(DNA)_S$, which is described by the rate constants k_1 and k_{-1}, cleavage of the glycosidic bond to excise 8oxoG and subsequent cleavage of the abasic site, which are described by the rate constant k_2, and release of the DNA product $(DNA)_P$, which is described by the rate constant k_3. In this work, using the five 8oxoG containing DNA substrates shown in Fig. 2.1, we characterized the rate of k_2, and k_3.

$$\text{OGG1} + (\text{DNA})_S \underset{k_{-1}}{\overset{k_1}{\rightleftharpoons}} \text{OGG1} \bullet (\text{DNA})_S \xrightarrow{k_2} \text{OGG1} \bullet (\text{DNA})_P \xrightarrow{k_3} \text{OGG1} + (\text{DNA})_P$$

Figure 2.3. Minimal kinetic scheme used for analysis of OGG1 activity. $(DNA)_S$ and $(DNA)_P$ indicate DNA substrate and product, respectively.

2.4.3. Glycosylase Activity of OGG1 is Not Influenced by Sequence Context

With most glycosylases, product release is rate limiting (*32*). Therefore, k_{cat} measured under steady-state conditions is a reflection of the rate of product release rather than the glycosylase step in which the glycosidic bond is cleaved. Indeed, for this reason OGG1 does not follow Michaelis-Menten kinetics (*12*). By carrying out experiments under transient-state single-turnover conditions ([OGG1]>>[DNA]), the enzyme is not required to process more than one substrate and the rate of product release does not contribute to k_{obs}; therefore the rate of excision of 8oxoG is revealed. As described in work from our lab (*28*) and other labs (*14, 37*) single-turnover conditions can be established and k_2 can be determined by incubating the 8oxoG-containing substrates with a 5-fold excess of OGG1. Furthermore, quenching the reactions by addition of NaOH and incubation at 90 °C converts abasic sites to strand breaks, which can be visualized by polyacrylamide gel electrophoresis (PAGE). Thus, quenching with NaOH/heat ensures that the AP lyase activity of OGG1 does not limit the observed rate (*14*). Therefore, k_2 will reflect the rate constant for cleavage of the glycosidic bond (*36*).

In our previous work with TNR substrates we reported a k_2 for OGG1 excising 8oxoG from Stem-HP, Loop-HP, and Stem-DUP (*28*). However, quantitative rate constants describing OGG1 removal of 8oxoG from Loop-DUP and Mixed-DUP could not be obtained using manual methods. After 15 sec at 37 °C, OGG1 had fully converted these two substrates to product; therefore, in our previous work only lower limits for k_2 could be determined. To address this issue, here we used a RQF instrument to determine k_2 for Loop-DUP and Mixed-DUP (Fig. 2.4). OGG1 was found to remove 8oxoG from Loop-DUP and Mixed-DUP at a rate of 56 ± 2.2 min^{-1} and 54 ±

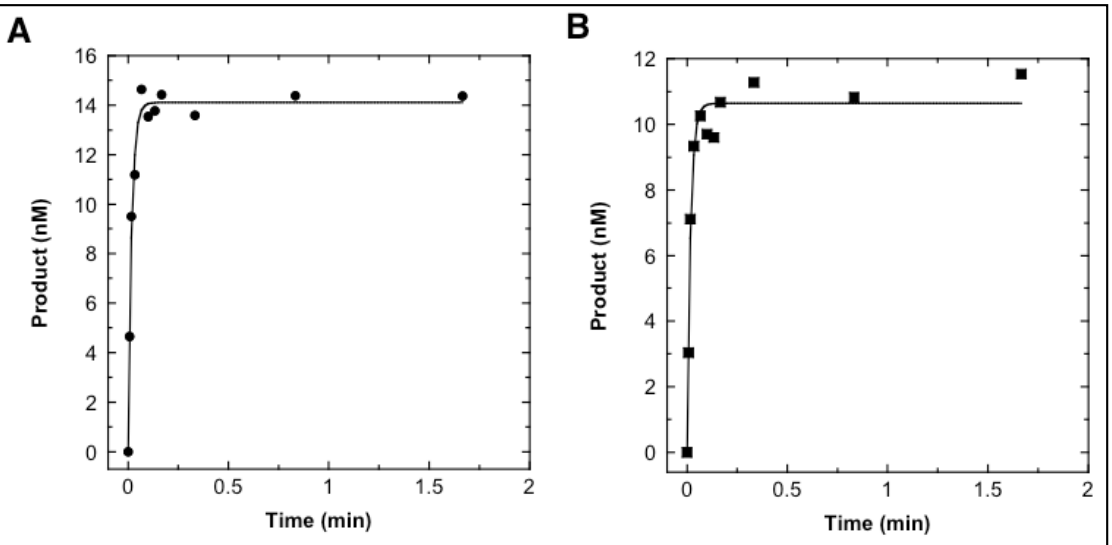

Figure 2.4. Graph of concentration of product as a function of time obtained under single-turnover conditions. Results for (A) Mixed-DUP and (B) Loop-DUP are shown and were obtained using a RQF instrument. Conditions were 20 nM DNA, 100 nM OGG1, 20 mM Tris-HCl, 10 mM Na_2EDTA, 35 mM NaCl, 155 μg/mL BSA, pH 7.6.

11 min^{-1}, respectively (Table 2.1). This rate constant for OGG1 removing 8oxoG from Mixed-DUP is in agreement with the value reported previously for this duplex substrate (*14*). Furthermore, OGG1 removes 8oxoG from Loop-DUP at the same rate as from Mixed-DUP. While the lesion is centrally-located in both duplexes (at the 15^{th} and 16^{th} bp for Loop-DUP and Mixed-DUP, respectively) the sequence context of the lesion is different in these substrates. This result indicates that OGG1 removes 8oxoG at the same rate regardless of sequence context and that non-repetitive and TNR sequences have equal potential to serve as substrates for the initiation of the BER pathway.

Table 2.1: k_2 and k_3 Values Determined for OGG1 with DNA Substrates

Substrate	k_2 (min^{-1})[a]	k_3 (min^{-1})[a]	
		− APE1	+ APE1[c]
Mixed-DUP	54 ± 11	0.040 ± .009	0.348 ± .033
Stem-DUP	2.8 ± 0.17[b]	0.093 ± .016	0.156 ± .027
Stem-HP	1.3 ± 0.11[b]	0.077 ± .008	0.070 ± .012
Loop-DUP	56 ± 2.2	0.046 ± .004	0.163 ± .038
Loop-HP	0.07 ± 0.004[b]	N.D.[d]	N.D.[d]

[a] Error represents standard deviation obtained from a minimum of three experiments.
[b] Values from reference (*28*).
[c] APE1 was present at 10 molar equivalents with respect to OGG1.
[d] No significant turnover observed over 24 h.

Furthermore, comparison of the results obtained here for Loop-DUP with the k_2 results reported previously for Stem-DUP (*22*) reveal that whereas sequence context does not affect k_2, location of the lesion in the duplex does influence the efficiency of OGG1. The k_2 for Stem-DUP is 17-fold slower than Loop-DUP. Although the sequence context of the 8oxoG is identical in these two substrates, positioning the 8oxoG closer to the end of the duplex affects the ability of OGG1 to process the substrate. Indeed, it has been shown previously that position of 8oxoG in a duplex influences the k_2 of OGG1. Literature reports show a 2-fold slower k_2 for an 18 bp duplex with 8oxoG positioned 9 bp from the end than for a 30 bp duplex with 8oxoG 15 bp from the end (*11, 31*).

2.4.4. Rate of Product Release (k_3) by OGG1 is Modulated by DNA Structure

In the minimal kinetic scheme in Fig. 2.3, k_3 is the rate constant associated with the release of product by OGG1. For most glycosylases, including OGG1, the rate of product release is the rate-determining step (*32*). Therefore, by performing experiments under steady-state multiple-turnover conditions ([OGG1]<<[DNA]) the k_{obs} will be k_3. This rate constant provides a measure of the turnover, or k_{cat}, of OGG1 acting on a particular DNA substrate. Representative autoradiograms for the Mixed-DUP substrate are shown in Figure 2.5. Figure 2.6 displays a graph of product concentration as a function of time for experiments performed with Mixed-DUP, Loop-DUP, Stem-DUP, and Stem-HP. In all cases there is an initial burst of product formation, followed by a linear phase, which represents OGG1 operating under steady-state conditions in which the accumulation of product is governed by the rate of product release.

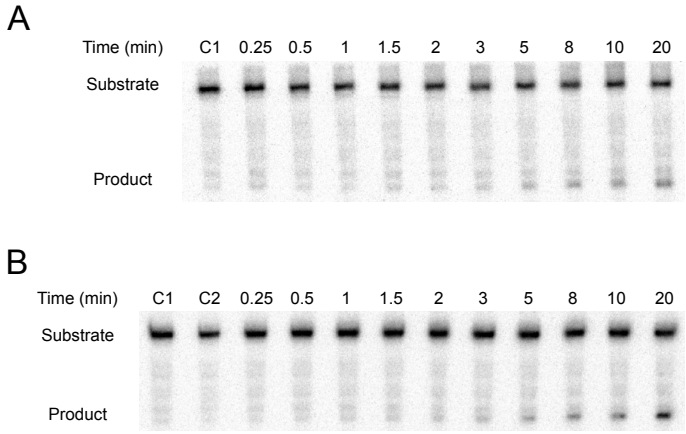

Figure 2.5. Autoradiogram displaying the electrophoretic mobility of the mixed sequence duplex, Mixed-DUP (50 nM) and OGG1 (5 nM) (A) without and (B) with APE1 (50 nM) under multiple-turnover conditions. C1 is a control with no OGG1, C2 is a control with no OGG1, but with APE1. Conditions were 20 mM Tris-HCl, 70 mM NaCl, 2 mM $MgCl_2$, 100 μg/mL BSA, pH 7.6

The duplex substrates Mixed-DUP and Loop-DUP have k_3 values that are the same within error (Table 2.1) and are comparable to a previously reported rate of product release when 8oxoG is in a duplex and is paired to C (*31*). These rates for k_3 are ~1,300-fold slower than those reported for k_2 in this and previous work (*22*). Thus, these data support the notion that the rate-limiting step in the enzymatic cycle for the removal of

8oxoG by OGG1 from both non-repetitive and TNR duplex DNA substrates is product release. It has been proposed that this lingering of glycosylases with their product ensures the proper cascade of events in BER and prevents the exposure of an abasic site (*33, 34*).

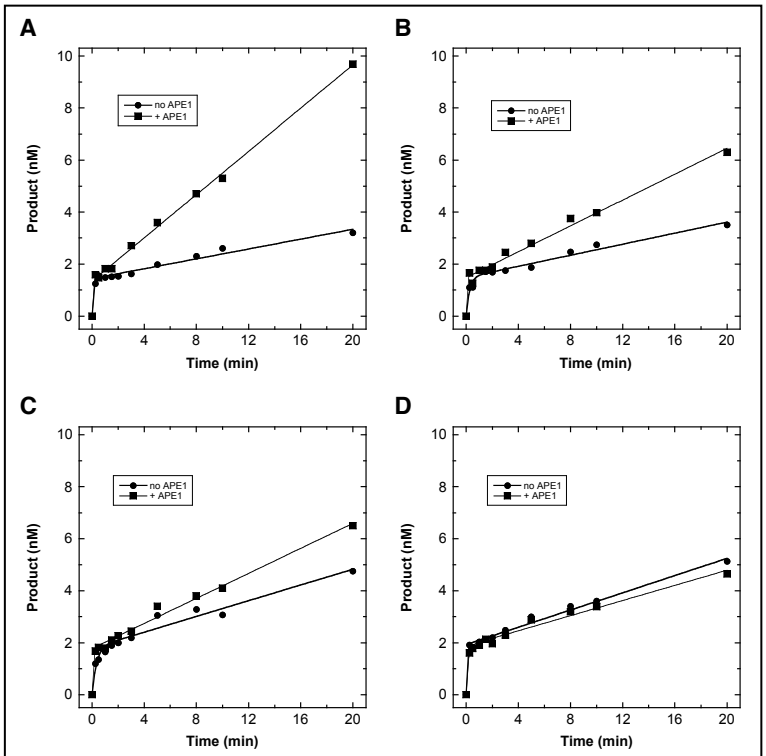

Figure 2.6. Data obtained under multiple-turnover conditions for determination of k_3. Shown is a graph of concentration of product as a function of time for (A) Mixed-DUP, (B) Loop-DUP, (C) Stem-DUP, and (D) Stem-HP. Conditions were 50 nM DNA, 5 nM hOGG1 or 5 nM hOGG1/50 nM APE1 in 20 mM Tris-HCl, 70 mM NaCl, 2 mM $MgCl_2$, 100 μg/mL BSA, pH 7.6.

When compared to Mixed-DUP and Loop-DUP, where the 8oxoG lesion is found in the center of the duplex, the k_3 obtained for both Stem-DUP and Stem-HP is ~2-fold faster. This result indicates that OGG1 releases the Stem-DUP and Stem-HP products more quickly than the Mixed-DUP and Loop-DUP products and reveals that the enzyme has a lower affinity for the product of the reaction obtained with Stem-HP and Stem-DUP. In both of these substrates the 8oxoG is positioned 5 base pairs from one end of the substrate. It has previously been shown for duplex substrates (*11, 31*) that the distance of an 8oxoG from the end of a duplex can influence the catalytic activity of OGG1 and, therefore, it is likely that the affinity of the enzyme for both the substrates and products is also affected.

Using the same concentrations of OGG1 (5 nM) and DNA (100 nM) as for the other substrates, a value for k_3 could not be obtained for Loop-HP even after incubation for 8 h. Only a small amount of product accumulation was observed and no burst or linear phase could be identified (Fig. 2.7). Given the transient nature of the OGG1•Loop-HP interaction, experiments were also performed in which the concentration of Loop-HP was increased to 500 nM. Again, after 24 h only a small amount of product was observed and no discernable burst or linear phase was identified. Notably, although a k_3 could not be determined, a k_2 for the Loop-HP substrate was obtained, albeit 800 times slower than for Loop-DUP. It has been shown that when 8oxoG is paired with G in a duplex, a value for k_2 could be obtained for OGG1, but due to very slow turnover k_3 could not be attained (*31*). Therefore, 8oxoG in a loop of a hairpin or 8oxoG paired to a G in a duplex is a poor substrate for OGG1. When present in excess over OGG1 these substrates reduce the rate of turnover to such an extent that a minimal amount of substrate is converted to product.

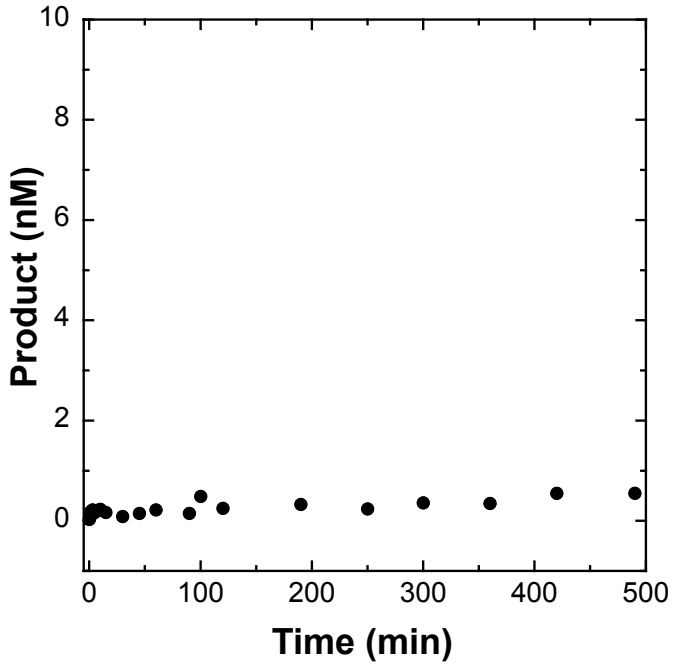

Figure 2.7. Graphical representation of concentration of product as a function of time obtained under multiple-turnover conditions for Loop-HP. Conditions were 50 nM DNA, 5 nM OGG1, 20 mM Tris-HCl, 70 mM NaCl, 2 mM $MgCl_2$, 100 μg/mL BSA, pH 7.6 and incubation at 37 °C.

2.4.5. Rate of Product Release (k_3) by OGG1 in the Presence of APE1

APE1 is the enzyme that follows OGG1 in the BER cascade. APE1 has been shown to improve the efficiency of repair by stimulating the product release rate of OGG1 (*12, 13, 35, 36*). For a mixed-sequence duplex containing 8oxoG, the rate of product release of OGG1 was stimulated 5 to 8-fold in the presence of 10 molar equivalents of APE1 (*12, 36*). Given that APE1 is known to influence the product release rate of OGG1 we also determined the k_3 for OGG1 in the presence of APE1.

We found that the k_3 of OGG1 acting on Mixed-DUP is ~9-fold faster in the presence of 10 molar equivalents of APE1 (Table 2.1, Fig. 2.6 A). The k_3 for the TNR duplex Loop-DUP was stimulated ~3.5-fold in the presence of APE1 (Fig. 2.6 B). This difference in amount of stimulation for the two duplex substrates suggests that while sequence context does not influence k_2 or k_3 of OGG1, the ability of APE1 to stimulate product release of OGG1 may be modulated by sequence. Furthermore, consistent with the observation that proximity of 8oxoG to the end of a duplex influences the catalytic activity of OGG1, we find that APE1 is similarly influenced and for Stem-DUP the k_3 of OGG1 is stimulated ~2-fold in the presence of APE1 (Fig. 2.6 C).

For the hairpin substrate Stem-HP, the addition of APE1 does not stimulate product release of OGG1 (Fig. 2.6 D); the k_3 is the same in the absence and presence of APE1. This lack of stimulation may be a result of the pseudo-duplex nature of Stem-HP. The presence of G-C base pairs and A•A mismatches in Stem-HP result in a stem that is more dynamic than a well-matched duplex. Indeed, we have shown through structural characterizations of CAG repeat hairpins (*22*) that adenines in the A•A mismatches are

more reactive towards the chemical probe diethyl pyrocarbonate than adenines in A-T bp, indicating increased dynamics. This increased dynamics may contribute to the lack of stimulation of OGG1 by APE1 observed for Stem-HP. Lastly, even with the addition of APE1, only a small amount of product accumulated for Loop-HP. No burst or linear phase could be identified and, therefore, a value for k_3 could not be obtained.

2.4.6. AP Lyase Activity of OGG1 is Not Bypassed in the Presence of APE1

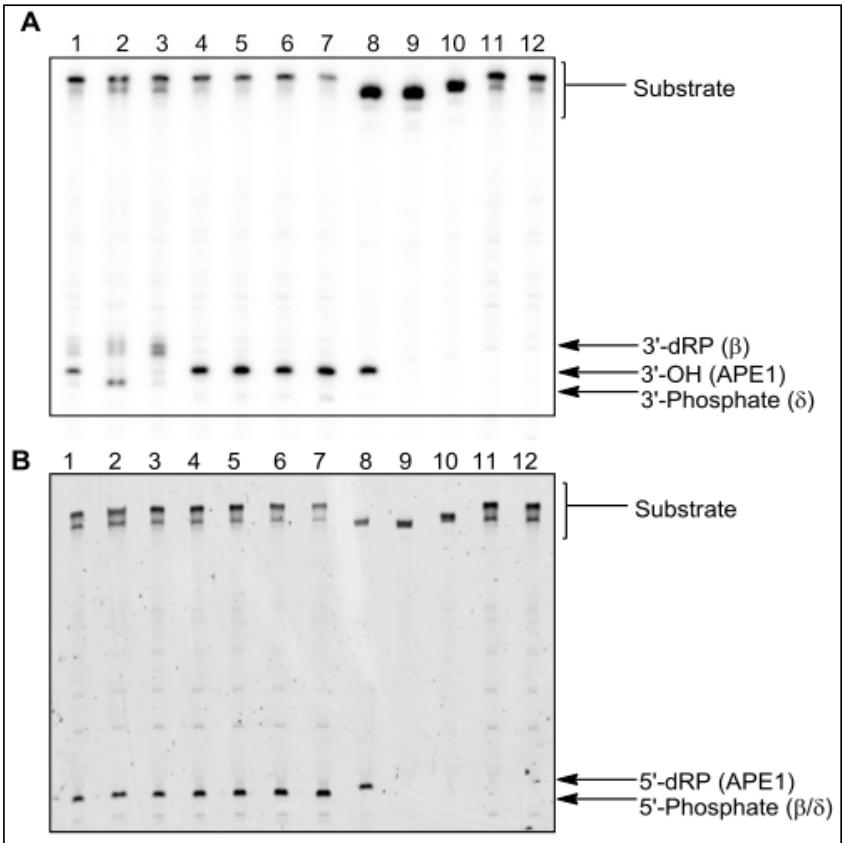

Figure 2.8. Characterization of the AP lyase step of OGG1 in the presence of APE1. Lesion containing strands of Mixed-DUP DNA (8oxoG) and Mixed-U-DUP DNA (uracil) were 5′-^{32}P end-labeled (A) and 3′-R6G end-labeled (B). Reactions were performed with 100 nM duplex DNA in 20 mM Tris-HCl, 140 mM NaCl, 5 mM $MgCl_2$. Mixed–DUP was incubated at 37 °C for 30 min with 150 nM OGG1, followed by the addition of either 150 nM APE1 (Lane 1), 0.75 M NaOH (Lane 2) or nothing (Lane 3). Mixed-DUP was also incubated at 37 °C for 30 min with 150 nM OGG1 and 150-7500 nM APE1 (Lanes 4-7). Mixed-U-DUP DNA was incubated at 37 °C with 1 unit UDG and 150 nM APE1 for 30 min (Lane 8), with 1 unit UDG for 3 min (Lane 9), or alone (Lane 10). Finally Mixed-DUP (8oxoG) was incubated at 37 °C for 30 min alone (Lane 11) or with 150 nM APE1 (Lane 12).

Others have proposed the slow AP lyase activity of bifunctional glycosylases, OGG1 in particular, can be bypassed in the presence of APE1 (*13*). In order to determine if the AP lyase activity of OGG1 is acting in the presence of APE1, 8oxoG-containing DNA was incubated with

OGG1 and equal molar to a 50-fold molar excess of APE1. We first perform several controls to examine the electrophoretic mobility of DNA processed by a monofunctional glycosylase alone and in the presence of APE1, and by a bifunctional glycoslylase alone. APE1 incubated with the monofunctional DNA glycosylase UDG and uracil containing DNA, creates a nick in the DNA backbone with 3′-OH and 5′-dRP termini (Figure 2.1C, Figure 2.8A,B Lane 8). Bifunctional OGG1 incubated with 8oxoG containing DNA creates a nick in the DNA backbone with 3′-dRP and 5′-phosphate termini, utilizing the AP lyase activity of OGG1 (Figure 2.1D, Figure 2.8A,B Lane 3). Furthermore, addition of NaOH to 8oxoG DNA incubating with OGG1 converts the 3′-dRP β-elimination product (Figure 2.1D, Figure 2.8A Lane 3) to the 3′-phosphate δ-elimination product (Figure 2.1F, Figure 2.8A, Lane 2). Moreover, addition of APE1 to 8oxoG DNA that has undergone β-elimination, converts the 3′-dRP group (Figure 2.1D, Figure 2.8A Lane 3) to the 3′-OH (Figure 2.1E, Figure 2.8A Lane 1). Importantly, we wanted to examine the electrophoretic mobility of DNA processed by a bifunctional glycosylase in the presence of APE1. Interestingly, when 8oxoG DNA was incubated with OGG1 in the presence of equal molar to 50 times more APE1 (Figure 2.8A,B Lanes 4-7), a nick in the DNA backbone was observed with species running at the same electrophoretic mobility as the 3′-OH and 5′-phosphate termini (Figure 2.1 E). Such termini are produced only if OGG1 performs AP lyase activity followed by APE1 processing to convert the 3'-dRP group to the 3'-OH. These results indicate that the AP lyase activity of OGG1 occurs even in the presence of a large excess of APE1. These results contradict those obtained in a similar experiment by Vidal, et al. (*13*); during the incubation of 3'-^{32}P labeled 34mer 8oxoG DNA with OGG1 and APE1 in equal molar to 50-fold excess, product with the same

electrophoretic mobility as APE1 incubated with UDG and uracil-containing DNA was observed. The results obtained by Vidal, et al. suggest as more APE1 was added, the AP lyase step of OGG1 was not utilized. Although a slightly different DNA construct in a lower salt buffer was used in the Vidal study, such differences do not warrant such opposing results. The results obtained here suggest that initiation of BER by OGG1 removing an 8oxoG lesion does not create a 5'-dRP group, but instead creates a 5'-phosphate, and therefore the dRP lyase activity of polβ is not utilized during downstream nick site processing.

2.4.7. Implications for TNR Expansion and a Toxic Oxidation Cycle

DNA glycosylases initiate the BER pathway by recognition and excision of a damaged base, and are followed in action by downstream proteins and particular polymerases that incorporate unmodified bases in place of the damaged DNA (*8*, *10*, *12*). Such repair events typically help to maintain genetic stability by minimizing mutations that occur due to errors in DNA replication. However, the presence of OGG1 has been implicated in the disease-initiating CAG/CTG repeat expansion (*7*). Indeed, it has been demonstrated that if BER is initiated by OGG1 on TNR duplex DNA, pol β ultimately catalyzes the addition of excess TNR repeats (*7*, *9)*. Therefore, OGG1 contributes to TNR expansion by initiating BER on damage-containing duplex DNA.

Here, by determining the rate of glycosidic bond cleavage, and the rate of product release of OGG1 for TNR duplex DNA, we provide a comprehensive description of the kinetic parameters for the initiating event in TNR expansion. With respect to duplex substrates, we found that the kinetic parameters describing OGG1 activity on CAG/CTG

sequences and mixed-sequences are indistinguishable when the 8oxoG is located the same distance from the end of the substrate. These results indicate that OGG1 is not more or less likely to initiate BER on TNR duplexes than on non-repetitive sequences, but rather processes these substrates with the same efficiency. While the ability of OGG1 to excise 8oxoG was found to be influenced by the proximity of the damage to the end of the duplex, the processing of genomic DNA is likely not affected by this property of OGG1 since most damage will not be located near a double-stranded end. It is of note, that although product release by OGG1 is stimulated by APE1 on both TNR and mixed-sequence duplexes the effect is larger for mixed-sequence duplexes.

Due to our previous studies that identified hairpin TNR structures as containing hot spots for oxidative damage, we were also motivated to examine the ability of OGG1 to initiate BER on such DNA substrates. We describe here that these non-B conformations are poor substrates for OGG1. It is noteworthy that although OGG1 can process these hairpin substrates to a small extent, the enzyme-DNA interaction is transient. This transient interaction provides insight into the differential catalytic activity of OGG1 observed for hairpin substrates relative to duplex substrates and suggests that hairpins are not biologically relevant substrates for OGG1. Additionally, this data suggests it is unlikely that OGG1 contributes to stabilization of a hairpin during a repair or replication-dependent expansion mechanism.

Taken together, the data presented in this work provide further insight into the mechanistic pathway by which OGG1 and BER contribute to a toxic oxidation cycle (Fig. 7). We have shown here that the first step of this pathway, initiation of BER by OGG1 on duplex DNA, occurs with high efficiency regardless of sequence context. More

simply, the TNR repeats do not decrease the likelihood for this process to occur. We determined previously that hairpins contain hot spots for oxidative damage, particularly in the loop region that is solvent exposed. Importantly, it is these same hairpin conformations that are proposed to form during LP-BER mediated TNR expansion. *Therefore the likelihood of DNA oxidation within a TNR region is greatly increased during the process that is intended to remove oxidative damage.* Here, we provide a kinetic analysis of OGG1 activity on hairpin substrates containing 8oxoG and demonstrate that the probability that oxidative damage is removed from hairpins is dramatically reduced relative to duplex. In fact, we were unable to measure k_3 for OGG1 in the presence of a hairpin containing an 8oxoG lesion in the loop due to the transient interaction of OGG1 with the substrate and product of the glycosylase reaction, respectively. Due to the solvent accessibility of the loop-region of the CAG hairpin, an 8oxoG lesion forms and accumulates in the hairpin intermediate. This hairpin DNA is ligated and incorporated into duplex resulting in an expanded duplex, which now contains oxidative damage, poising the system to begin the toxic oxidation cycle again. Furthermore, although others have suggested the presence of APE1 leads to bypass of the AP lyase activity of OGG1, under conditions tested here, such bypass was not observed. These results suggest a 5'-dRP group would not form during BER initiated by OGG1 and therefore the dRP lyase activity of pol β would not be utilized. Importantly, inhibition of pol β dRP lyase activity, which prevents the conversion of the 5'-dRP group to the 5'-phosphate, is implicated in forcing LP-BER in a mixed sequence context. Therefore, in the case of OGG1 initiating BER in a CAG repeat tract, it is unlikely that inhibition of pol β dRP lyase activity is a contributing factor to LP-BER seen for CAG repeat tracts. It

is currently unclear what factors lead to multiple nucleotide incorporation by pol β at a nick site found within CAG repeats. We postulate that pol β initiates LP-BER over SP-BER due to the intrinsic ability of repetitive DNA to form secondary structures. A future characterization of multinucleotide incorporation by pol β within a CAG repeat tract, as explored in Chapter 4 of this work, will shed light on this topic.

2.5. Concluding Remarks

These data not only contribute to our understanding of substrate specificity of OGG1 and APE1, but they also contribute to our understanding of the proposed toxic oxidation cycle (*7*) in which somatic TNR expansion contributes to the onset and progression of HD. In this model of TNR expansion the repetitive duplex DNA is oxidized, BER is initiated by OGG1, formation and ligation of a TNR hairpin into the DNA occurs during a LP-BER event, and the hairpin is incorporated into duplex to generate an expanded CAG/CTG sequence. Several models have been proposed for hairpin incorporation into duplex and involve a subsequent round of replication or nick-induced gap-filling synthesis (*3*). The expanded CAG/CTG duplex is then oxidatively damaged to restart the cycle. Here we show that OGG1 would effectively initiate this cycle by removing 8oxoG from duplex TNR DNA. However, the hairpin intermediate is hyper-susceptible to oxidative damage and 8oxoG is not efficiently processed at the hotspot location. Incorporation of the 8oxoG-containing hairpin results in expanded duplex, which now contains oxidative damage. Therefore, we describe a system in which the final step of the cycle regenerates a substrate for the toxic process and works to incrementally expand the TNR DNA.

2.6. References

(1) Kozlowski, P., De Mezer, M., and Krzyzosiak, W., Trinucleotide repeats in human genome and exome, *Nucleic Acids Res.*, **2010**, *38*, 4027-4039.

(2) López Castel, A., Cleary, J.D., and Pearson, C.E., Repeat instability as the basis for human diseases and as a potential target for therapy. *Nat. Rev. Mol. Cell Biol.*, **2010**, *11*, 165- 170.

(3) McMurray, C., Mechanisms of trinucleotide repeat instability during human development. *Nat. Rev. Genet.*, **2010**, *11*, 786-799.

(4) The Huntington's Disease Collaborative Research Group, A novel gene containing a trinucleotide repeat that is expanded and unstable on Huntington's disease chromosomes. *Cell*, **1993**, *72*, 971-983.

(5) McMurray, C., Huntington's disease: New hope for therapeutics, *Trends Neurosci*., **2001**, *24*, 32-38.

(6) Cummings, C.J., and Zoghbi, H.Y., Trinucleotide repeats: Mechanisms and pathophysiology. *Annu. Rev. Genomics Hum. Genet.*, **2000**, *1*, 281-328.

(7) Kovtun, I.V., Liu, Y., Bjoras, M., Klungland, A., Wilson, S.H., and McMurray C.T., OGG1 initiates age-dependent CAG trinucleotide expansion in somatic cells, *Nature*, **2007**, *447,* 447-452.

(8) David, S., O'Shea, V., and Kundu, S., Base-excision repair of oxidative DNA damage. *Nature*, **2007**, *447*, 941-950.

(9) Liu, Y., Prasad, R., Beard, W., Hou, E., Horton, J., McMurray, C., and Wilson, S., Coordination between Polymerase β and FEN1 can modulate CAG repeat expansion. *J. Biol. Chem*., **2009**, *284*, 28352-28366.

(10) Beard, W., and Wilson S.H., Structure and mechanism of DNA polymerase β. *Chem. Rev.*, **2006**, *106*, 361-382.

(11) Krishnamurthy, N., Haraguchi, K., Greenberg, M., and David, S., Efficient removal of formamidopyrimidines by 8oxoGuanine glycosylases. *Biochemistry*, **2007**, *47*, 1043-1050.

(12) Hill, J., Hazra, T., Izumi, T., and Mitra, S., Stimulation of human 8oxoGuanine-DNA glycosylase by AP-endonuclease: Potential coordination of the initial steps in base excision repair. *Nucleic Acids Res*., **2001**, *29*, 430-438.

(13) Vidal, A., Hickson, I., Boiteux, S., and Radicella, J., Mechanism of stimulation of the DNA glycosylase activity of OGG1 by the major human AP endonuclease: Bypass of the AP lyase activity step. *Nucleic Acids Res*., **2001**, *29*,1285-1292.

(14) Aburatani, H., Hippo, Y., Ishida, T., Takashima, R., Matsuba, C., Kodama, T., Takao, M., Yasui, A., Yamamoto, K., Asano, M., Fukasawa, K., Yoshinari, T., Inoue, H., Ohtsuka, M., and Nishimura, S., Cloning and characterization of mammalian 8- hydroxyguanine-specific DNA glycosylase/apurinic, apyrimidinic lyase, a functional mutM homologue. *Cancer Res*., **1997**, *57*, 2151-2156.

(15) Degtyareva, N., Barber, C., Sengupta, B., and Petty, J., Context dependence of trinucleotide repeat structures. *Biochemistry*, **2010**, *49*, 3024-3030.

(16) Paiva, A., and Sheardy, R., Influence of sequence context and length on the structure and stability of triplet repeat DNA oligomers. *Biochemistry*, **2004**, *43*, 14218- 14227.

(17) Pearson, C., Tam, M., Wang, Y., Dar, A., Cleary, J., and Nichol, K., Slipped-strand DNAs formed by long (CAG)·(CTG) repeats: Slipped-out repeats and slip-out junctions, *Nucleic Acids Res*., **2002**, *30*, 4534-4537.

(18) Degtyareva, N., Reddish, M., Sengupta, B., and Petty, J. Structural studies of a trinucleotide repeat sequence using 2-aminopurine. *Biochemistry*, **2009**, *48*, 2340-2346.

(19) Mitas, M., Trinucleotide repeats associated with human disease. *Nucleic Acids Res.*, **1997**, *25*, 2245-2253.

(20) Gacy, A., Goellner, G., Juranić, N., Macura, S., and McMurray, C., Trinucleotide repeats that expand in human disease form hairpin structures in vitro. *Cell*, **1995**, *81*, 533-540.

(21) Liu, G., Chen, X., Bissler, J., Sinden, R., and Leffak, M., Replication-dependent instability at (CTG)•(CAG) repeat hairpins in human cells. *Nat. Chem. Biol.*, **2010**, *6*, 652-659.

(22) Jarem, D., Wilson, N., and Delaney, S., Structure-dependent DNA damage and repair in a trinucleotide repeat sequence. *Biochemistry*, **2009**, *48*, 6655-6663.

(23) Denicola, A., Freeman, B., Trujillo, M., and Radi, R., Peroxynitrite reaction with carbon dioxide/bicarbonate: Kinetics and influence on peroxynitrite-mediated oxidations. *Arch. Biochem. Biophys.*, **1996**, *333*, 49-58.

(24) Niles, J., Wishnok, J., and Tannenbaum, S., Peroxynitrite-induced oxidation and nitration products of guanine and 8oxoGuanine: Structures and mechanisms of product formation. *Nitric Oxide,* **2006**, *14*, 109-121.

(25) Gu, F., Stillwell, W., Wishnok, J., Shallop, A., Jones, A., and Tannenbaum, S. Peroxynitrite- induced reactions of synthetic oligo 2‘-deoxynucleotides and DNA containing guanine: Formation and stability of a 5-Guanidino-4-nitroimidazole lesion. *Biochemistry*, **2002**, *41*, 7508-7518.

(26) Goula, A., Berquist, B., Wilson D.M. III, Wheeler, V., Trottier, Y., and Merienne, K., Stoichiometry of base excision repair proteins correlates with increased somatic CAG instability in striatum over cerebellum in Huntington's disease transgenic mice. *PLoS Genet.*, **2009**, *5*, e1000749.

(27) Beaucage, S.L., and Caruthers, M.H., Synthetic strategies and parameters involved in the synthesis of oligodeoxyribonucleotides according to the phosphoramidite method. *Curr. Protoc. Nucleic Acid Chem*., **2000**, 3.3.1-3.3.20.

(28) Warshaw, M.M, Tinoco, I. Jr, Optical properties of sixteen dinucleoside phosphates. *J. Mol. Biol.*, **1966**, *20*, 29-38.

(29) Nash, H., Lu, R., Lane, W., and Verdine, G., The critical active-site amine of the human 8-oxoguanine DNA glycosylase, OGG1: Direct identification, ablation and chemical reconstitution. *Chem. Biol.*, **1997**, *4*, 693-702.

(30) Porello, S., Leyes, A., and David, S., Single-turnover and pre-steady-state kinetics of the reaction of the adenine glycosylase MutY with mismatch-containing DNA substrates. *Biochemistry*, **1998**, *37*, 14756-14764.

(31) Leipold, M.D., Workman, H., Muller, J.G., Burrows C.J., and David S.S., Recognition and removal of oxidized guanines in duplex DNA by the base excision repair enzymes OGG1, yOGG1, and yOGG2. *Biochemistry*, **2003**, *42*, 11373-11381.

(32) David, S., and Williams, S., Chemistry of glycosylases and endonucleases involved in base-excision repair. *Chem. Rev.*, **1998**, *98*, 1221-1262.

(33) Wilson, S.H., and Kunkel, T., Passing the baton in base excision repair. *Nat. Struct. Mol. Biol.*, **2000**, *7*, 176-178.

(34) Prasad, R., Shock, D., Beard, W., and Wilson, S.H., Substrate channeling in mammalian base excision repair pathways: Passing the baton. *J. Biol. Chem.*, **2010**, *285*, 40479-40488.

(35) Sidorenko, V.S., Nevinsky, G.A., and Zharkov, D.O., Specificity of stimulation of human 8-oxoguanine-DNA glycosylase by AP endonuclease. *Biochem. Bioph. Res. Co.*, **2008***, 368*, 175-179.

(36) Sidorenko, V.S., Nevinsky G.A., and Zharkov D.O., Mechanism of interaction between human 8oxoGuanine-DNA glycosylase and AP endonuclease. *DNA Repair*, **2007***, 6*, 317-328.

Chapter 3: Transient-state kinetics of apurinic/apyrimidinic (AP) endonuclease 1 acting on an authentic AP site and commonly-used substrate analogs: The effect of diverse metal ions and base mismatches[†]

[†]**Adapted From:**

Schermerhorn, K.M. and Delaney, S. (2013) Transient-state kinetics of apurinic/apyrimidinic (AP) endonuclease 1 acting on an authentic AP site and commonly-used substrate analogs: The effect of diverse metal ions and base mismatches, *Biochemistry 52*, 7669-7677

3.1 Abstract

APE1 is a Mg^{2+}-dependent enzyme responsible for incising the DNA backbone 5' to an apurinic/apyrimidinic (AP) site. Here, we use rapid quench flow (RQF) techniques to provide a comprehensive kinetic analysis of the strand incision activity ($k_{chemistry}$) of APE1 acting on an authentic AP site along with two widely-used analogs, a reduced AP site and a tetrahydrofuran (THF) site. In the presence of biologically-relevant Mg^{2+}, APE1 incises all three substrates at a rate faster than the resolution of the RQF, $\geq$700 s^{-1}. To obtain quantitative values of $k_{chemistry}$ and facilitate comparison of the authentic substrate versus the substrate analogs, we replaced Mg^{2+} with Mn^{2+} or Ni^{2+}, or introduced a mismatch 5′ to the lesion site. Both strategies were sufficient to slow $k_{chemistry}$ and resulted in rates within the resolution of the RQF. In all cases where quantitative rates were obtained, $k_{chemistry}$ for the reduced AP site is indistinguishable from the authentic AP site. Notably, there is a small decrease, ~1.5-fold, in $k_{chemistry}$ for the THF site relative to the authentic AP site. These results highlight a role in strand incision for the C1' oxygen of the AP site, and warrant consideration when designing experiments using substrate analogs.

3.2 Introduction

Apurinic/apyrimidinic (AP) sites are generated by the repair activity of DNA glycosylases, damaging chemical agents, and by spontaneous hydrolysis of the purine glycosidic bond (*1*, *2*). If left unrepaired, AP sites are both cytotoxic and mutagenic to a cell, and therefore repair of these sites is essential to maintaining genomic integrity (*3*, *4*).

Apurinic/apyrimidinic endonuclease 1 (APE1), a Mg^{2+}-dependent base excision repair (BER) enzyme, is the major human AP endonuclease responsible for incising the

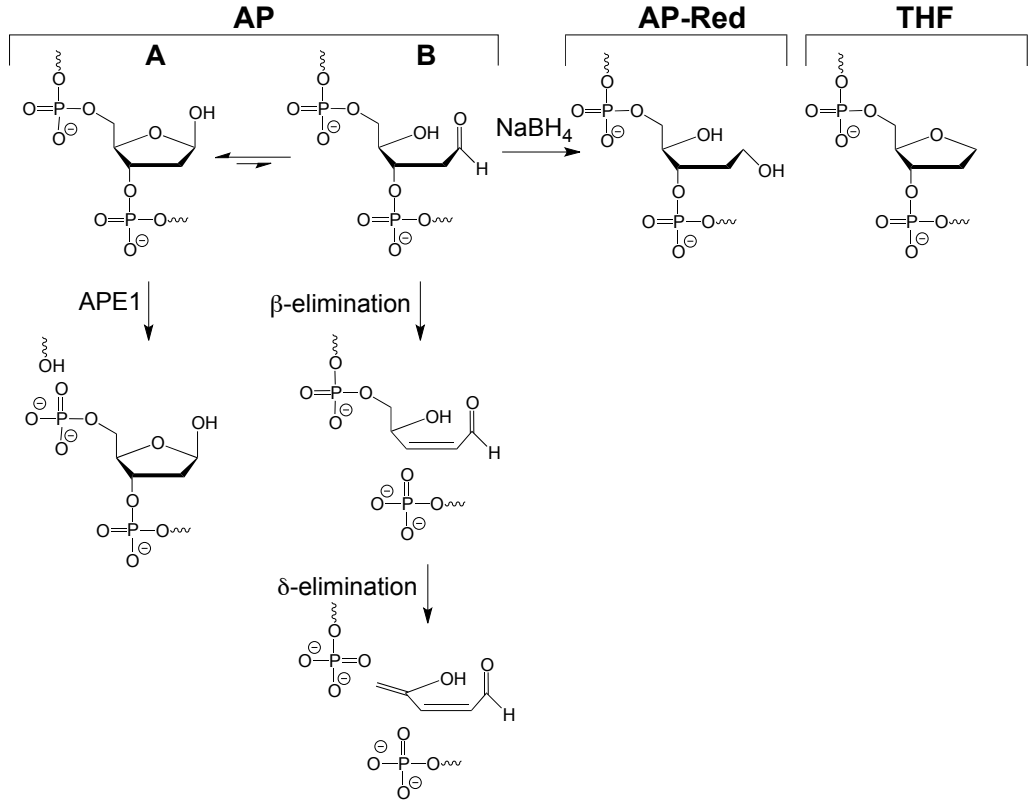

Figure 3.1. Structures of AP, AP-Red, and THF. The authentic AP site exists as an equilibrium between the ring-closed hemiacetal (A) and ring-opened aldehyde (B). The ring-opened aldehyde is subject to β-elimination, and can further be converted to the β,δ-elimination product under basic conditions. The ring-opened aldehyde can be reduced by $NaBH_4$ to generate the AP-Red substrate. APE1 incises the AP site, to create a nick with a 3′-OH and 5′-dRP group.

DNA phosphodiester backbone 5' to AP sites, generating a nick with 3'-OH and 5'-deoxyribose phosphate (dRP) termini (Figure 3.1) (*5*). Repair of the resulting nick is completed by DNA polymerase and DNA ligase. In addition to its endonuclease activity, APE1 is known to have 3'-phosphodiesterase and 3'-phosphatase activity, 3' to 5' exonuclease activity, as well as a role in regulating the redox state of several transcription factors (*6*-*8*). APE1 also stimulates the rate of product release for many DNA

glycosylases, where the action of a glycosylase precedes APE1 in the BER cascade (*9-13*). Finally, APE1 has been shown to stimulate the dRPase activity as well as the strand displacement synthesis activity of DNA polymerase β (*14*, *15*).

An important consideration for DNA containing an AP site is that the lesion exists as an equilibrium between the ring-closed hemiacetal (Figure 3.1A) and ring-opened aldehyde (Figure 1B) forms. Furthermore, the ring-opened aldehyde is known to undergo β-elimination, resulting in a strand break with 3'-α,β-unsaturated aldehyde and 5'-phosphate termini (*16*). Because of the instability of the authentic AP site, analogs that do not undergo β-elimination are often used. Two commonly-used analogs are the reduced AP site, which is generated by reduction of an authentic AP site with $NaBH_4$, and the tetrahydrofuran (THF) site. To date, all x-ray crystal structures of APE1 bound to DNA utilize the THF AP site analog (*17*, *18*).

Several previous studies examined the kinetics of APE1 endonuclease activity. Steady-state rates for APE1 acting on an authentic AP site (*19-21*), a THF site (*20-24*), and a reduced AP site (*16*, *25*) are the same within error, ~2-10 s^{-1}. More recently, the first transient-state characterization of APE1 strand incision was reported (*24*); using rapid quench flow (RQF) techniques and a THF-containing substrate, it was reported that the steady-state rate of APE1 is limited by a slow step that follows strand incision chemistry, likely product release, and that the rate of strand incision ($k_{chemistry}$) is at least 850 s^{-1}. With respect to the authentic AP site, to date all transient-state kinetics have been performed using stop-flow fluorescence (SFF) techniques, which monitor conformational changes within APE1 (*20*, *21*). One notable SFF study compared APE1 processing the authentic AP and THF sites; interestingly, for the THF substrate an

additional conformational change in the APE1/DNA complex was observed prior to the chemistry step (*21*).

In this work we use RQF techniques and report the first experiments to monitor directly the strand incision activity of APE1 on the biologically-relevant authentic AP site. The rate of APE1 strand incision for authentic, reduced and THF AP sites was determined in the presence of Mg^{2+}, Mn^{2+}, or Ni^{2+}. Furthermore, we also investigated APE1 strand incision chemistry on substrates with mismatches 5' to the lesion. These varied experimental conditions allow for a comprehensive comparison of the strand incision activity of APE1 acting on an authentic AP site and the substrate analogs. The results highlight the destabilizing effects of different metal ions, and mismatches located 5' to the AP site. Furthermore, these results merit consideration when designing experiments using substrate analogs.

3.3 Experimental Procedure

3.3.1 Oligonucleotide Synthesis and Purification

DNA oligonucleotides used in this work are listed in Table 3.1, and were synthesized using standard phosphoramidite chemistry on a BioAutomation DNA/RNA synthesizer. The modified phosphoramidites deoxyuridine (5'-dimethoxytrityl-5-*O*-acetyl-2'-deoxyuridine,3'-[(2-cyanoethyl)-(*N*,*N*-diisopropyl)]-phosphoramidite) and tetrahydrofuran (5′-*O*-dimethoxytrityl-1′, 2′-dideoxyribose-3′-[(2-cyanothyl)-(*N*,*N*-diisopropyl)]-phosphoramidite) were used in synthesis of lesion-containing strands (denoted as LS in Table 3.1) and were obtained from Glen Research. During synthesis the 5′-DMT was retained to aid in HPLC purification. Two rounds of HPLC purification

were performed on each oligonucleotide as previously described (*26*). The 5′-DMT group was removed and quantification of each oligonucleotide was performed using the ε_{260} values estimated for single-stranded DNA (*27*) and a Beckman Coulter DU800 UV-VIS Spectrophotometer.

Table 3.1. DNA Oligonucleotides Used in this Study

Name	Sequence
LS[a]	5′-CGTTCAACGTGCACTXACAGCACGTCCCAT-3′
WM	3′-GCAAGTTGCACGTGACTGTCGTGCAGGGTA-5′
MM1[b]	3′-GCAAGTTGCACGTGTCTGTCGTGCAGGGTA-5′
MM2[b]	3′-GCAAGTTGCACGTCACTGTCGTGCAGGGTA-5′
MM3[b]	3′-GCAAGTTGCACGAGACTGTCGTGCAGGGTA-5′
MM4[b]	3′-GCAAGTTGCACCTGACTGTCGTGCAGGGTA-5′

[a] LS indicates the lesion-containing strand where X denotes location of AP, AP-Red, THF, or Uracil site.
[b] Mismatched nucleotide is underlined.

3.3.2 DNA Duplex Assembly and Characterization

Oligonucleotides containing THF or Uracil were 5′-^{32}P end-labeled using T4 Polynucleotide Kinase (New England Biolabs) following the manufacturer's protocol. Assembly of the 30mer duplex substrate was achieved by annealing 30 pmol (for transient-state experiments) or 300 pmol (for steady-state experiments) of the 5′-radiolabeled lesion-containing strand in the presence of a 1.5-fold excess of the desired complement [either well matched (WM) or containing a mismatch (MM1, MM2, MM3, or MM4)] in 300 μL of 50 mM HEPES-KOH, 100 mM KCl, pH 7.5.

To generate a duplex containing the reduced AP site, the uracil-containing duplex was incubated with 1.5 units of uracil DNA glycosylase (UDG; New England Biolabs) and freshly prepared $NaBH_4$ (final concentration of $NaBH_4$ was 0.1 M) overnight at 37 ˚C. The DNA was desalted using a 0.5 mL, 3,000 MW Amicon centrifugal filter. To generate a duplex containing the authentic AP site, the uracil-containing duplex was

incubated with 1.5 units of UDG for 30 min at 37 ˚C. Due to the lability of the authentic AP substrate, UDG was not removed from the authentic AP site samples, therefore THF DNA was also incubated with 1.5 units of UDG for 30 min at 37 ˚C.

The stability of the duplex substrates formed using the WM complement was assessed immediately following the incubation with UDG. For each substrate, three 15 μL aliquots of the lesion-containing duplexes were prepared and 15 μL of Buffer A (50 mM HEPES-KOH, 100 mM KCl, 10 mM $MgCl_2$ and 0.24 mg/mL BSA, pH 7.5) was added. The first aliquot was then quenched with 50 μL 100 mM EDTA, followed by 40 μL of denaturing dye (80% formamide, 10 mM EDTA, 1 mg/mL xylene cyanol). The second aliquot was quenched with 50 μL of 0.1 M NaOH followed by 40 μL of denaturing dye. The first and second aliquots were placed on dry ice until gel electrophoresis. A third aliquot was quenched with 50 μL of 100 mM EDTA and immediately dried *in vacuo,* resuspended in 105 μL denaturing dye, and heated to 90 ˚C for 3 min prior to gel loading. A separate 15 μL aliquot of each duplex was incubated with 15 μL of APE1 (final concentration of 500 nM APE1), diluted in Buffer A, for 5 min at 37 ˚C, and quenched with 50 μL of 100 mM EDTA followed by 40 μL denaturing dye and placed on dry ice. All reactions were also carried out on uracil-containing duplex not treated with UDG, as a control. All samples were loaded onto an 18% denaturing PAGE gel (33 × 42 cm, 0.4 mm thick) and were electrophoresed for ~3 h at 80 W and the results were visualized using phosphorimagery.

3.3.3 Expression and Purification of human APE1

Escherichia coli BL21(DE3) pLysS cells were transformed via heat shock with

the pXC53 plasmid carrying the APE1 gene (a gift from Dr. Samuel Wilson, NIEHS) (*16*). The transformed cells were grown at 37 ˚C in 2 L of LB media containing 100 μg/mL ampicillin to an OD_{600} of 0.6-0.7, at which time cells were induced with isopropyl β-D-1-thiogalactopyranoside to a final concentration of 1 mM. After 2 h of growth at 37 ˚C, the cells were pelleted by centrifugation (3,000 × *g*, 30 min, 4 ˚C). The supernatant was discarded, and the cells were frozen with liquid nitrogen and stored at −80 ˚C until purification of APE1. Upon thawing, cells were resuspended in lysozyme buffer (10 mM Tris-HCl, pH 8.0, 1 mM EDTA, 1 mM PMSF, 1 μg/mL pepstatin, 1 μg/mL leupeptin) at room temperature for 30 min. The incubation continued for another 20 min after the addition of NaCl to a final concentration of 1 M. Cells were then lysed using a French press. Lysates were clarified by centrifugation (24,336 × *g*, 20 min, 4 ˚C). Purification of the protein was completed using both HiTrap SP HP and Heparin HP columns (GE Healthcare) as previously described (*21*). The purity of APE1 was >90% as assessed by SDS-PAGE. The total concentration of APE1 was determined by the Bradford method using bovine γ-globulin as a standard. The APE1 preparation was >80% active as determined by steady-state kinetic experiments and all APE1 concentrations given below or in figure captions are active enzyme concentrations.

It is noteworthy that the purified APE1 contained trace amounts of Mg^{2+}. For transient-state kinetics experiments using different metal ions, it was important to ensure that this trace Mg^{2+} is removed. Therefore, we performed an EDTA chelation experiment (Figure 3.2). The authentic AP site-WM duplex was prepared as described above. Two 40 μL APE1 aliquots (1000 nM) were prepared in either Buffer A or Buffer B (50 mM HEPES-KOH, 100 mM KCl and 0.24 mg/mL BSA, pH 7.5). A 5 μL aliquot of AP-WM

DNA was mixed with 5 µL Buffer A. A second 5 µL DNA aliquot was mixed with 5 µL of APE1 in Buffer A. Seven 5 µL aliquots of APE1 in Buffer B were initially mixed with EDTA to a concentration of 0-40 mM, followed by addition of 5 µL of AP-WM DNA, which created samples with a final concentration of 0-20 mM EDTA. All samples were incubated at 37 ˚C for 3 min, followed by addition of 10 µL denaturing dye and placed on dry ice. All samples were loaded onto an 18% denaturing PAGE gel (33 × 42 cm, 0.4 mm thick) and were electrophoresed for ~3 h at 80 W and the results were visualized using phosphorimagery. We found that a final reaction concentration of 0.25 mM EDTA was sufficient to chelate the trace amount of Mg^{2+} present following expression and purification of APE1 (Figure 3.2).

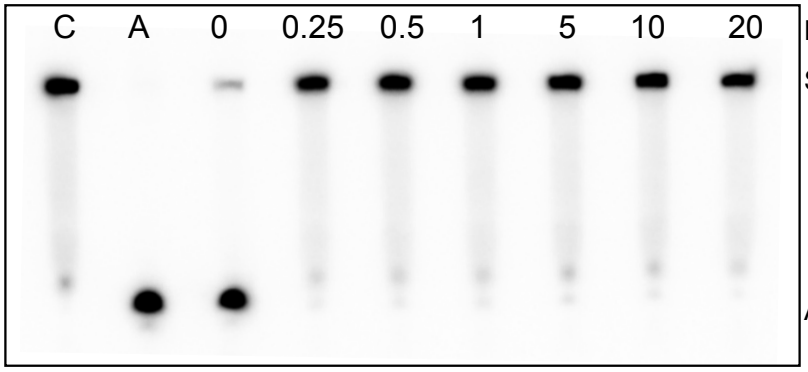

Figure 3.2. Autoradiogram revealing concentration of EDTA needed to chelate Mg^{2+} present in our APE1 aliquots after purification. Samples contained 30 pmol uracil DNA (annealed to WM complement) in 300 µ L of 50 mM HEPES-KOH, 100 mM KCl, pH 7.5 and were incubated with 1.5 units of UDG for 30 min at 37 ˚C. Following UDG incubation, samples were mixed with an equal volume of Buffer B and incubated with APE1 to a final concentration of 500 nM and 0-20 mM EDTA (EDTA added to APE1 prior to DNA) for 3 min at 37 ˚C and quenched with denaturing dye. Two controls were performed: one in which just DNA + Buffer B was incubated without enzyme for 3 min at 37 ˚C (C) and one in which DNA+ Buffer A, APE1 (500 nM final concentration) (A) were incubated for 3 min at 37 ˚C; both controls were quenched with denaturing dye.

3.3.4 APE1 Transient-State Kinetic Assays

APE1 transient-state kinetic assays were performed using a Rapid Quench Flow instrument (RQF-3, KinTek Corp.). DNA duplex and enzyme aliquots were prepared freshly for each time course. To limit β-elimination in the authentic AP site DNA, a separate UDG reaction, used to create the authentic AP site, was performed prior to each time course.

For metal ion dependence kinetics, the lesion-containing strand was annealed to the WM complement. For each time course, a 300 μL aliquot of 1000 nM APE1 in Buffer B containing EDTA to chelate Mg^{2+} (50 mM HEPES-KOH, 100 mM KCl, 500 nM EDTA, and 0.24 mg/mL BSA, pH 7.5), was prepared. For each time course, two controls were performed. In the first control, used to demonstrate inactivity of the APE1 aliquot in the absence of additional metal ions, a 15 μL aliquot of DNA was manually mixed with 15 μL of the prepared APE1 aliquot and incubated for 3 min at 37 ˚C, followed by addition of 50 μL of 100 mM EDTA, to quench the reaction, and 40 μL of denaturing dye, then placed on dry ice. The second control, performed at the end of the RQF time course, was used to demonstrate the stability of the DNA throughout the time course; DNA and Buffer B, in the absence of enzyme, were mixed in the RQF instrument, followed by quenching with 100 mM EDTA by the RQF and manual addition of 40 μL denaturing dye and placed on dry ice until electrophoresis. Following initial chelation reaction and immediately prior to RQF reactions, $MgCl_2$, $MnCl_2$ or $NiCl_2$, to a concentration of 10 mM, was added to the APE1 aliquot. It is important to note that by mixing an equal volume of enzyme and DNA by the RQF, the final concentration of DNA and enzyme was 50 nM and 500 nM, respectively, and final concentration of

EDTA and divalent metal ions was 250 nM and 5 mM, respectively. RQF reactions were allowed to proceed for 2-15,000 msec at 37 ˚C prior to quenching by the addition of 50 µL of 100 mM EDTA by the RQF. Once the sample was expelled from the RQF, 40 µL of denaturing dye was added and samples were placed on dry ice until separation on a

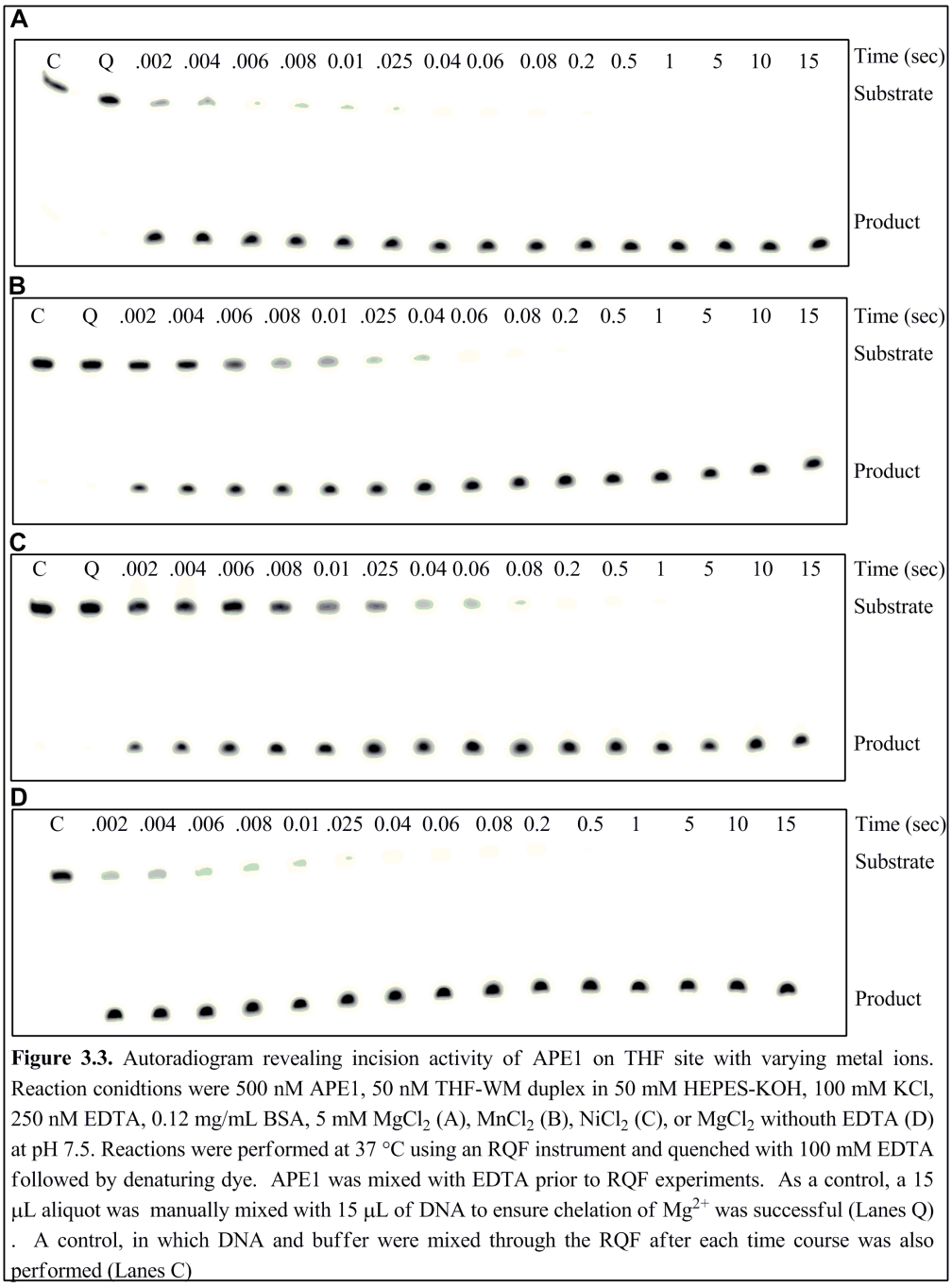

Figure 3.3. Autoradiogram revealing incision activity of APE1 on THF site with varying metal ions. Reaction conidtions were 500 nM APE1, 50 nM THF-WM duplex in 50 mM HEPES-KOH, 100 mM KCl, 250 nM EDTA, 0.12 mg/mL BSA, 5 mM $MgCl_2$ (A), $MnCl_2$ (B), $NiCl_2$ (C), or $MgCl_2$ withouth EDTA (D) at pH 7.5. Reactions were performed at 37 °C using an RQF instrument and quenched with 100 mM EDTA followed by denaturing dye. APE1 was mixed with EDTA prior to RQF experiments. As a control, a 15 µL aliquot was manually mixed with 15 µL of DNA to ensure chelation of Mg^{2+} was successful (Lanes Q) . A control, in which DNA and buffer were mixed through the RQF after each time course was also performed (Lanes C)

18% denaturing PAGE gel (33 × 42 cm, 0.4 mm thick). The samples were run for ~2 hrs at 80 W. The products were visualized by phosphorimagery (Figure 3.3). Additionally, a transient-state kinetic time course was run, as described above, for each lesion in the presence of $MgCl_2$ but lacking EDTA, to ensure addition of EDTA did not affect strand incision chemistry rates. Kinetic experiments were also performed using authentic AP DNA annealed to the WM complement as described above, in the presence of 0.5, 1, 2.5, and 5 mM $MgCl_2$; such experiments allowed us to determine the Mg^{2+} concentration that provided maximal strand incision, 5 mM, which was used in subsequent experiments (Figure 3.4).

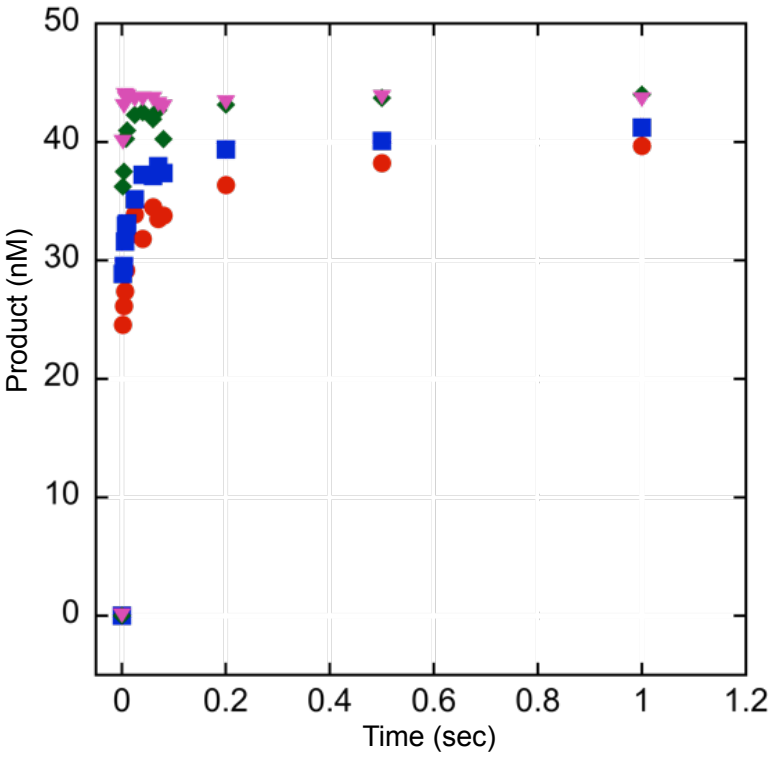

Figure 3.4. Transient-state kinetic time courses of strand incision activity of APE1 acting on AP DNA in the presence of varying concentration of $MgCl_2$. Experimental conditions were 50 nM DNA, 500 nM APE1, 50 mM HEPES-KOH, 100 mM KCl, 0.12 mg/mL BSA, 0.25 mM EDTA, and 0.5 (red), 1 (blue), 2.5 (green) or 5 (pink) mM $MgCl_2$, pH 7.5. Reactions were performed at 37 ˚C using a RQF instrument and quenched with 100 mM EDTA.

For 5' mismatch kinetics, the lesion-containing strand was annealed to either MM1, MM2, MM3, or MM4. For each time course, a 300 µL aliquot of 1000 nM APE1 in Buffer A was prepared. RQF reactions and gel electrophoresis proceeded as described above.

For all kinetic time courses, 100 mM

EDTA was used to quench each time point. A control was performed to ensure a concentration of 100 mM EDTA was sufficient to quench the reaction (data not shown). A 15 μL aliquot of prepared APE1, after addition of either Mg^{2+}, Mn^{2+}, or Ni^{2+}, was mixed with 50 μL of 100 mM EDTA, followed by 15 μL of DNA and incubated for 60 s in the RQF at 37 ˚C followed by the addition of 40 μL of denaturing dye and placed on dry ice until gel electrophoresis. The results were visualized by phosphorimagery.

For all transient-state kinetic experiments, Kaleidagraph was used to fit data from the full time course as previously described to obtain the rate of strand incision chemistry ($k_{chemistry}$) (*28*). Importantly, the fastest reaction time that can be performed on the RQF instrument is 2 msec, which provides an upper limit to the rate that can be determined of 700 s^{-1}. This rate is calculated by assuming two half-lives have passed, or at least 75% of substrate has been converted to product at the 2 msec time point. This 75% substrate turnover was chosen as the cut-off point as rates obtained from burst kinetic plots are determined by the slope of the burst; 75% product formation is a point reliably on the burst portion and not the plateau. It is of note that this methodology provides a conservative estimate of the capability of the RQF instrument. Two-tailed, student's T-test was performed to obtain the p-values for transient-state rates for THF-containing DNA compared to authentic AP DNA.

3.3.5 APE1 Steady-State Kinetic Assays

DNA substrates, annealed to WM complement, were created as described above. For each time course, a 300 μL aliquot of 100 nM APE1 in Buffer A was prepared. RQF instrumentation was used to rapidly mix and quench DNA and APE1 to a final

concentration of 500 nM DNA and 50 nM APE1. RQF reactions were allowed to proceed for 2-100 msec and quenched and gel electrophoresed as described above. The products were visualized by phosphorimagery. Both a burst phase and a linear phase are observed with the slope of the linear phase equal to $k_{ss} \times$ [active enzyme] (*28*). It is important to note that we have defined the steady-state rate as k_{ss} while this reference defines the steady-state rate as k_3. The active enzyme concentration of >80% was determined by extrapolating the linear phase line through the y-axis. The reported steady-state rates are from a single data set and reported error is the error associated with the fit. Two additional steady-state kinetic assays were performed with varying substrate concentrations (250 nM and 1000 nM) and rates comparable to those reported here were obtained.

3.4 Results

3.4.1 Characterization of DNA Substrates

DNA duplexes containing an authentic AP site (AP DNA), reduced AP site (AP-Red DNA), or THF site (THF DNA) were used to obtain the kinetic parameters of human APE1. Prior to performing kinetic experiments, we confirmed the lability of the authentic AP site, and observed formation of the β-elimination product *during* gel electrophoresis as seen in Figure 3.5. as a smear in the gel (AP Lane 1). This smear, which was also observed in our kinetic time course experiments with AP DNA, was included as substrate during quantitation, and is likely due to the increased temperature incurred during electrophoresis. The β-elimination product is formed *prior* to electrophoresis when the AP DNA is dried *in vacuo* and heated to 90 ˚C prior to loading (AP Lane 2).

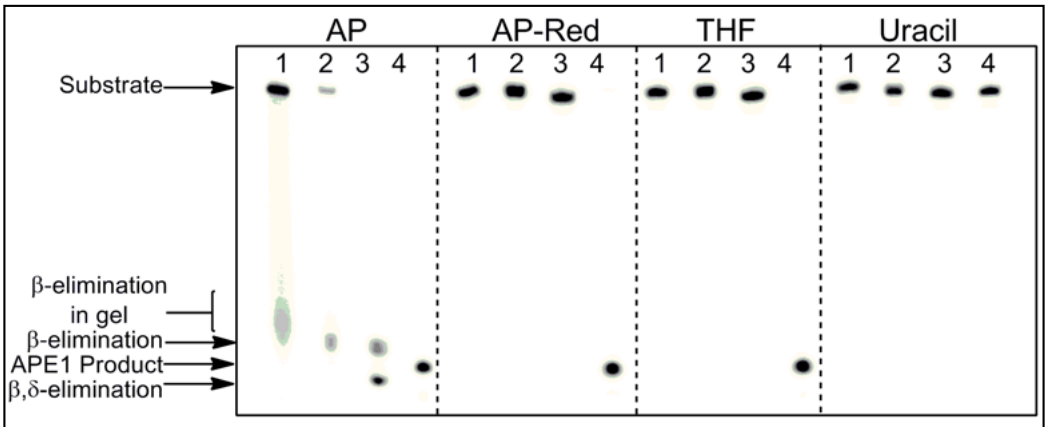

Figure 3.5. Susceptibility of DNA substrates to β and β,δ-elimination. Autoradiogram revealing β-elimination of authentic AP site before and during gel electrophoresis. Samples contained 30 pmol uracil or THF-containing duplex (annealed to WM complement) in 300 ¬µL of 50 mM HEPES-KOH, 100 mM KCl, pH 7.5 and were incubated with 1.5 units of UDG for 30 min at 37 ˚C. For AP-Red, uracil-containing DNA and $NaBH_4$ (final concentration of 0.1M) was incubated overnight with 1.5 units of UDG at 37 ˚C. Following incubation, samples were mixed with an equal volume of Buffer A and subjected to the following: quenching by addition of EDTA and denaturing dye (lanes 1); addition of EDTA followed by *in vacuo* drying, resuspension in denaturing dye, and heating to 90 ˚C for 3 min (lanes 2); quenching with 0.1 M NaOH and denaturing dye (lanes 3). All substrates were also allowed to react with APE1, to a final concentration of 500 nM, for 3 min at 37 ˚C (lane 4). Uracil-containing duplex in the absence of UDG was also used as a control.

Furthermore, we can convert the AP site to the β,δ-elimination product in the presence of 0.1 M NaOH (AP Lane 3). Finally, reaction of AP DNA with APE1 leads to complete conversion to the APE1 product (AP Lane 4). Important for the experiments conducted here, β-elimination of the AP site can be avoided by not heating the samples above 37 °C, and not drying the samples.

As anticipated, the AP-Red and THF DNA are not susceptible to β-elimination and no strand cleavage is observed when the DNA is dried, heated, treated with NaOH, or electrophoresed (Figure 3.5; AP-Red and THF Lanes 1-3). Treatment of both the AP-Red and THF DNA with APE1 leads to conversion to the APE1 product (Figure 3.5; AP-Red and THF Lanes 4).

3.4.2 Transient-State Kinetics of APE1: Dependence on Metal Ion

In order to determine $k_{chemistry}$ for APE1 incising the AP, AP-Red, and THF DNA, transient-state kinetic time courses were performed in which the concentration of APE1 was 10-fold greater than the concentration of DNA. Mixing of the enzyme with each DNA substrate and rapid quenching of the reaction was achieved using an RQF instrument. Experiments were performed in the presence of 5 mM Mg^{2+}, Mn^{2+}, or Ni^{2+}. This concentration of Mg^{2+} is biologically relevant, and we also observed maximal strand incision at this concentration (Figure 3.4). For all three DNA substrates, in the presence of Mg^{2+}, Mn^{2+}, or Ni^{2+}, we observe a rapid burst in product formation followed by a

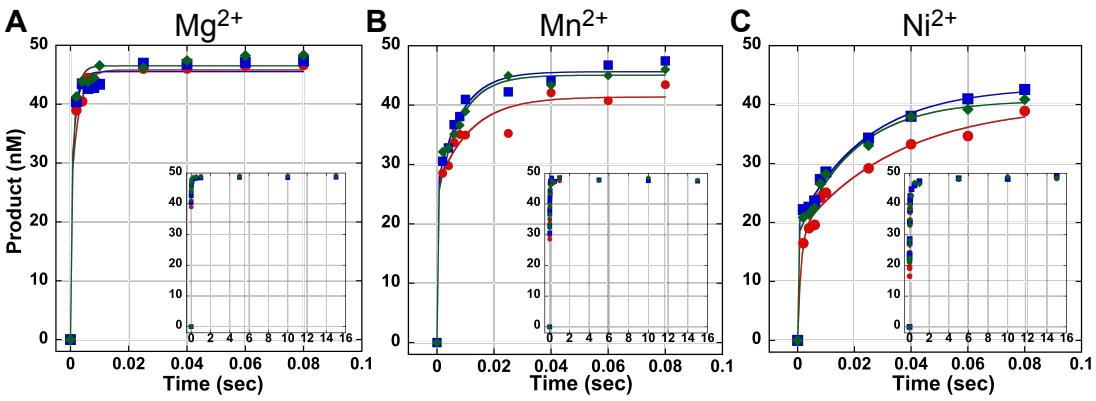

Figure 3.6. Transient-state kinetic time courses of strand incision activity of APE1 acting on AP (blue), AP-Red (green) or THF (red) DNA in the presence of 5 mM (A) Mg^{2+}, (B) Mn^{2+}, (C) or Ni^{2+}. Inset depicts the full time course. Experimental conditions were 50 nM DNA, 500 nM APE1, 50 mM HEPES-KOH, 100 mM KCl, 0.12 mg/mL BSA, 0.25 mM EDTA, and 5 mM $MgCl_2$, $MnCl_2$, or $NiCl_2$, pH 7.5. Reactions were performed at 37 ˚C using a RQF instrument and quenched with 100 mM EDTA.

product plateau (Figure 3.6A-C). In the presence of the biologically-relevant ion Mg^{2+}, APE1 incises all three DNA substrates very rapidly, and is faster than the resolution of the RQF with $k_{chemistry} \geq 700\ s^{-1}$ (Table 3.2). Initial attempts to slow strand incision by performing experiments at 4 ˚C, instead of 37 ˚C, were unsuccessful as $k_{chemistry}$ was still faster than the resolution of the RQF (data not shown). However, in the presence of Mn^{2+} or Ni^{2+}, $k_{chemistry}$ is slowed for all three substrates and is within the resolution of the

instrument; this decrease in $k_{chemistry}$ can be observed qualitatively in Figure 3.6 (inset) as more points in the burst region of the graph for Mn^{2+} or Ni^{2+}, relative to Mg^{2+}. Furthermore, in the presence of Mn^{2+} or Ni^{2+}, $k_{chemistry}$ for the THF DNA is ~1.5 times slower than AP DNA and AP-Red DNA.

Table 3.2. Dependence on Metal Ions: Strand Incision Rates of APE1 Acting on AP, AP-Red, or THF DNA[a,b]

	$k_{chemistry}$ (s^{-1})		
Substrate	Mg^{2+}	Mn^{2+}	Ni^{2+}
AP	≥700	329 ± 16	155 ± 17
AP-Red	≥700	325 ± 30	167 ± 1
THF	≥700	234 ± 46[c]	111 ± 18[d]

[a] Measured at 37 ˚C under transient-state conditions using RQF instrumentation.
[b] Error represents the standard deviation from at least four experiments.
[c] p=0.008 when compared to AP DNA using student's T test.
[d] p=0.01 when compared to AP DNA using student's T test.

3.4.3 Transient-State Kinetics of APE1: Dependence on 5' Mismatch

We also determined the influence on $k_{chemistry}$ of mismatches placed 1, 2, 3, or 4 base pairs (bp) from the 5' side of the AP, AP-Red, or THF site (Table 3.1). These experiments were performed in the presence of 5 mM Mg^{2+}. In all cases we observe a

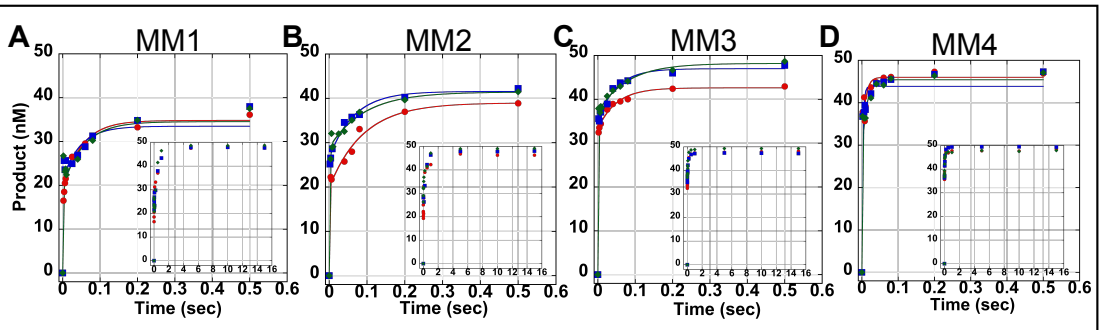

Figure 3.7. Transient-state kinetic time courses of strand incision activity of APE1 acting on AP (blue), AP-Red (green), or THF (red) DNA containing a mismatch (A) 1, (B) 2, (C) 3, or (D) 4 bp on the 5' side of the lesion. Inset depicts the full time course. Experimental conditions were 50 nM DNA, 500 nM APE1, 50 mM HEPES-KOH, 100 mM KCl, 0.12 mg/mL BSA, 0.25 mM EDTA, and 5 mM $MgCl_2$, pH 7.5. Reactions were performed at 37 ˚C using a RQF instrument and quenched with 100 mM EDTA.

rapid burst in product formation followed by a product plateau (Figure 3.7A-D). We observed the slowest value of $k_{chemistry}$ when the mismatch is adjacent to the lesion, and observe a recovery in $k_{chemistry}$ as the mismatch is moved away from the lesion site (Table 3.3). Indeed, for AP DNA and AP-Red DNA, when the mismatch is 3 bp away, $k_{chemistry}$ is $\geq$ 700 s^{-1} and is again faster than the resolutions of the RQF. For THF DNA, the mismatch must be 4 bp away before the resolution of the RQF is exceeded. Furthermore, in the prescence of a 5' mismatch, 1 or 2 bp away from the lesion, $k_{chemistry}$ for the THF DNA is ~1.5 times slower than AP DNA and AP-Red DNA. Experiments were also performed in which an A•A mismatch was placed

Table 3.3. Dependence on 5' Mismatches: Strand Incision Rates of APE1 Acting on AP, AP-Red, or THF DNA[a,b]

	$k_{chemistry}$ (s^{-1})[a,b]			
Substrate	MM-1	MM-2	MM-3	MM-4
AP	156 ± 29	312 ± 29	≥700	≥700
AP-Red	163 ± 21	307 ± 24	≥700	≥700
THF	116 ± 29[c]	194 ± 32[d]	575 ± 65	≥700

[a] Measured at 37 °C under transient-state conditions using RQF instrumentation.
[b] Error represents the standard deviation from at least four experiments.
[c] p=0.04 when compared to AP DNA using student's T test.
[d] p=0.008 when compared to AP DNA using student's T test.

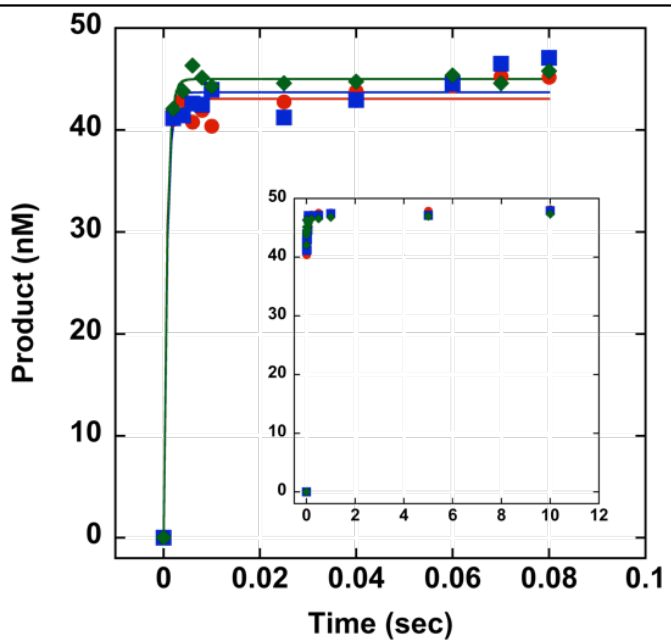

Figure 3.8 . Transient-state kinetic time courses of strand incision activity of APE1 acting on AP (blue), AP-Red (green), or THF (red) DNA containing a 3′ mismatch adjacent to the lesion. Inset depicts the full time course. Experimental conditions were 50 nM DNA, 500 nM APE1, 50 mM HEPES-KOH, 100 mM KCl, 0.12 mg/mL BSA, 0.25 mM EDTA, and 5 mM $MgCl_2$, pH 7.5. Reactions were performed at 37 °C using a RQF instrument and quenched with 100 mM EDTA.

immediately to the 3' side of each lesion; $k_{chemistry}$ was faster than the resolution of the RQF for all three lesions (Figure 3.8).

3.4.4 Steady-State Kinetics of APE1

In order to compare the steady-state rate (k_{ss}) of APE1 acting on authentic AP, AP-Red, and THF DNA, we performed steady-state kinetic time courses in which the concentration of DNA was 10 times greater than the concentration of APE1. As with the transient-state experiments, we used the RQF instrument to rapidly mix and quench each reaction. As seen in Figure 3.9, for each time course we observe an initial burst of product formation followed by a linear accumulation of product. The initial burst represents the fast chemistry step that leads to the initial turnover of product. The linear phase signifies a slow step that occurs after chemistry, likely product release, and defines the steady-state rate. The steady-state rates for each lesion, 2.2 ± 0.3 s^{-1}, 2.4 ± 0.3 s^{-1}, and 2.4 ± 0.2 s^{-1}, for AP, AP-Red and THF, respectively, are the same within error.

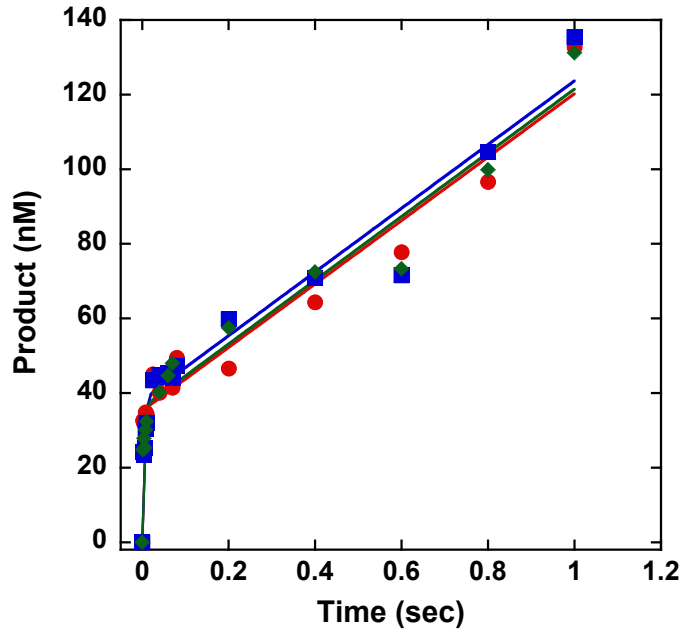

Figure 3.9. Steady-state kinetic time courses of APE1 acting on an AP (blue), AP-Red (green) or THF (red) site in the presence of 5 mM $MgCl_2$. Experimental conditions were 500 nM DNA and 50 nM APE1 in 50 mM HEPES-KOH, 100 mM KCl, 0.24 mg/mL BSA, 0.25 mM EDTA 5 mM $MgCl_2$, pH 7.5. Reactions were performed at 37 °C using a RQF instrument and quenched with 100 mM EDTA.

3.5 Discussion

3.5.1 Steady-State and Transient-State Kinetics of APE1 in the Presence of Mg^{2+}

We report the first RQF-derived value of $k_{chemistry}$ for APE1 incising an authentic AP site, $\geq 700\ s^{-1}$, making APE1 one of the fastest BER enzymes known to date. Indeed, in the presence of Mg^{2+}, strand incision by APE1 is very rapid and $k_{chemistry}$ is faster than the resolution of the RQF for AP, AP-Red, and THF DNA. Our results are consistent with the only other APE1 transient-state experiments performed using RQF instrumentation in which $k_{chemistry}$ for THF DNA is limited by the resolution of the instrument (*24*). Also consistent with literature reports, our steady-state rates for APE1 acting on AP-Red and THF analogs are indistinguishable from the authentic AP DNA (*16*, *19-25*). It has previously been suggested that the high copy number of APE1 (350,000-7,000,000 per cell) may serve to counteract the slow steady-state rate (*7*).

In other experiments performed using SFF, $k_{chemistry}$ of $68\ s^{-1}$ and $97\ s^{-1}$ have been reported for APE1 processing a THF and authentic AP site, respectively (*20*). Notably at $\geq 700\ s^{-1}$, the rates we obtain are significantly faster; however, SFF experiments do not directly measure strand incision, but rather monitor conformational changes of the enzyme during processing of the DNA substrate, and may underestimate the rate.

3.5.2 Transient-State Kinetics of APE1 in the Presence of Mn^{2+} or Ni^{2+}

A divalent metal ion is required for APE1 strand incision (*29-32*). Examination of x-ray crystal structures of APE1 bound to the incised product of THF-containing DNA, and the results of several site-directed mutagenesis studies have led to the proposal that the divalent metal ion coordinates to an oxygen of the electrophilic phosphate, as well as

residues in the APE1 active site pocket, such as E96 (*29-32*). Via these interactions the metal ion is thought to stabilize and correctly orient the DNA backbone for strand incision, as well as polarize the P-O bond to facilitate nucleophilic attack of an activated water molecule. A previous study reported a qualitative comparison of APE1 activity in the presence of several metal ions, including Mg^{2+}, Mn^{2+}, and Ni^{2+}(*29*); activity was greatest with Mg^{2+}, and reduced with Mn^{2+} or Ni^{2+}. Indeed, we report, depending on the lesion, the $k_{chemistry}$ was reduced at least 2-3 fold in the presence of Mn^{2+}, and at least 4-6.5 fold in the presence of Ni^{2+}. This reduction of strand incision chemistry is likely due to slightly altered positioning of the larger Mn^{2+} or Ni^{2+} ions in the active site, and an altered orientation of the DNA backbone. However, we cannot rule out the possibility that different metal ions may change the mechanism of strand incision altogether. Nevertheless, by slowing strand incision and obtaining quantitative values, we reveal that in the presence of Mn^{2+} or Ni^{2+}, $k_{chemistry}$ for AP DNA and AP-Red DNA are indistinguishable. Furthermore, albeit a small difference, the rate of strand incision is statistically different for THF DNA where $k_{chemistry}$ is ~1.5 times slower than the authentic AP DNA.

3.5.3 Transient-State Kinetics of APE1 in the Presence of 5' Mismatches

While varying the metal ion allowed us to obtain quantitative values for $k_{chemistry}$, and to compare directly APE1 strand incision on the authentic AP site versus the substrate analogs, we considered the possibility that changing the metal ion also changed the mechanism of APE1; if this were the case, the observed difference between THF and the authentic AP site may not be biologically relevant. Thus, we sought an alternate

method to slow strand incision. Previous work has qualitatively shown that activity of APE1 on THF-containing DNA is reduced when a mismatch is directly 5' or 3' to the lesion site, with the 5' mismatch having a more dramatic effect (*22,38*). Similar results were also observed for the removal of an 8-oxo-7,8-dihydroguanine lesion by OGG1, another BER enzyme; the presence of a 5′ mismatch was more detrimental to activity than a 3′ mismatch (*33*). Not surprisingly, when we positioned a mismatch 1, 2, 3, or 4 bp from the lesion, we saw the greatest reduction in $k_{chemistry}$, at least ~5-fold, when the mismatch was immediately adjacent to the lesion. As the mismatch moved away from the lesion, $k_{chemistry}$ recovered to values comparable to those obtained for the well-matched substrates. The decreased rate of strand incision in the presence of the 5' mismatches is likely due to distortion of the DNA backbone within the APE1 active site, in particular, distortion of the electrophilic phosphate 5' to the lesion site; as the mismatch is moved further from the lesion, the effect is diminished. Interestingly, similar results have been established for the repair of bistranded authentic AP sites by APE1; duplex substrates contained two AP sites on opposite strands, positioned 1, 3, or 5 bp apart, and strand incision was monitored at one of the AP sites. A reduction in incision by APE1 was observed when the second AP site was 1 or 3 bp away; conversely, when the second AP site was 5 bp away, no reduction in incision was observed (*34*). In this work, although the identity of the mismatch varies in different locations (i.e., MM-1 contains a T•T mismatch whereas MM-2 has a C•C mismatch), the purpose of these experiments is not to compare the effect of mismatches at different locations, but rather to compare $k_{chemistry}$ obtained for AP, AP-Red, and THF when the mismatch is the same distance from the lesion. Indeed, consistent with the results obtained in the presence of Mn^{2+} or Ni^{2+}, a

~1.5-fold reduction in $k_{chemistry}$ is observed for THF DNA relative to AP and AP-Red DNA when the mismatch is 1 or 2 bp away.

3.5.4 Highlighting Structural Differences Between the Authentic AP site and Analogs

The transient-state kinetic experiments performed within this body of work revealed a small yet significant decrease in $k_{chemistry}$ for APE1 incising THF DNA compared to substrates containing an authentic AP or reduced AP site. This decrease was apparent when experiments were conducted in the presence of Mn^{2+} or Ni^{2+}, or when a 5' mismatch was 1 or 2 bp from the lesion. It is important to note, for experiments performed in the presence of Mg^{2+}, differences in the way that APE1 may process the THF lesion are likely masked by the limitation of the RQF instrument. A feature distinguishing the THF site from the authentic and reduced AP site is the lack of a C1' oxygen. Since strand incision is observed for THF DNA, this oxygen is not required for catalytic activity; however, its presence (or the presence of a C1'-OH) may play a role in stabilizing and optimally orienting the authentic AP and AP-Red substrates in the APE1 active site pocket. An extensive hydrogen bonding network is present in active site, and contributes to formation of the activated water molecule which serves as the nucleophile for the strand incision chemistry (*35*, *36*). Interestingly, examination of several x-ray crystal structures of APE1 bound to THF DNA reveal that the primary amine of N212 would be within hydrogen-bonding distance of a C1' oxygen (*17*). However, we cannot be certain that the APE1 binding pocket would be the same when an authentic AP substrate is bound. While the role of N212 remains unclear, site-directed mutagenesis studies of APE1 incising authentic AP DNA suggest this residue is important for

substrate recognition; the role of N212 on THF containing DNA has not been explored (*37*). A THF lesion would lack the ability to form a hydrogen bond at the C1' position, and may be oriented slightly differently within the active site, explaining the small reduction in $k_{chemistry}$. Additionally, both the authentic AP and AP-Red lesions possess a ring-opened form; notably, the THF site is locked in the ring-closed form. The additional flexibility of the ring-opened form may allow for optimal orientation within the active site of APE1 and also may explain the differences we observe in $k_{chemistry}$ for authentic AP and AP-Red compared to the THF containing DNA. It is noteworthy that previous APE1 kinetic studies also observed differences in the processing of THF DNA compared to authentic AP DNA; such studies used SFF techniques which detected conformational changes in APE1 (*21*). When observing directly strand incision we obtain similar results indicating that the C1′ oxygen or flexibility of the lesion directly influences strand incision.

3.6 Concluding Remarks

Due to the wide spectrum of APE1 activity, as well as its cellular importance, it is not surprising that APE1 is a widely-studied BER enzyme. Here within, by examining the kinetics of APE1 on an authentic AP site and commonly-used analogs, we highlight the destabilizing effects of different metal ions and 5' mismatches on APE1 stand incision chemistry further expanding our understanding of the strand incision chemistry carried out by APE1. Transient-state kinetics performed in the presence of the biologically relevant Mg^{2+} reveal strand incision by APE1 on all lesions, is $\geq 700\ s^{-1}$, making APE1 the fastest BER enzyme to date. Furthermore, kinetics-based experiments using diverse

metal ions and 5' mismatches suggest a role for the C1' oxygen and ring-opened flexibility of the AP site for optimal strand incision, and reveal that with respect to strand incision, the AP-Red analog cannot be distinguished from the authentic substrates, whereas the THF analog is processed slightly differently. Further structural and mechanistic work investigating novel AP site analogs as well as structural studies of APE1 bound to authentic AP or AP-Red DNA may shed light into the kinetic differences observe within this work, and may pinpoint the source of the differences. Importantly, due to multitude of studies which use substrate analogs to studying BER enzymes and their mechanism of action, this work calls to attention the significance of choosing substrate analogs, and understanding the implications such analogs can have on experimental results.

3.7 References

(1) Lindahl, T., and Nyberg, B. Rate of depurination of native deoxyribonucleic acid, *Biochemistry* **1972**, *11*, 3610–3618.

(2) Wilson, D. M., III, and Barsky, D. The major human abasic endonuclease: formation, consequences and repair of abasic lesions in DNA, *Mut. Res./DNA Repair* **2001**, *485*, 283–307.

(3) Loeb, L. A., and Preston, B. D. Mutagenesis by apurinic/apyrimidinic sites, *Ann. Rev. Genet.* **1986**, *20,* 201-230

(4) Schaaper, R. M., Kunkel, T. A., and Loeb, L. A. Infidelity of DNA synthesis associated with bypass of apurinic sites, *Proc. Natl. Acad. Sci. U.S.A.* **1983**, *80*, 487–491.

(5) Demple, B., and Harrison, L. Repair of Oxidative Damage to DNA: Enzymology and Biology, *Annu. Rev. Biochem.* 1994, *63*, 915–948.

(6) Seki, S., Hatsushika, M., Watanabe, S., Akiyama, K., Nagao, K., and Tsutsui, K. cDNA cloning, sequencing, expression and possible domain structure of human APEX nuclease homologous to Escherichia coli exonuclease III, *Biochim. Biophys. Acta* **1992**, *1131*, 287–299.

(7) Chen, D. S., Herman, T., and Demple, B. Two distinct human DNA diesterases that hydrolyze 3′-blocking deoxyribose fragments from oxidized DNA, *Nucleic Acids Res.* **1991**, *19*, 5907–5914.

(8) Xanthoudakis, S., Miao, G., Wang, F., Pan, Y. C., and Curran, T. Redox activation of Fos-Jun DNA binding activity is mediated by a DNA repair enzyme, *EMBO J.* 1992, *11*, 3323–3335.

(9) Hill, J. W., Hazra, T. K., Izumi, T., and Mitra, S. Stimulation of human 8-oxoguanine-DNA glycosylase by AP-endonuclease: potential coordination of the initial steps in base excision repair. *Nucleic Acids Res.* **2001**, *29*, 430–438.

(10) Vidal, A. E., Hickson, I. D., Boiteux, S., and Radicella, J. P. Mechanism of stimulation of the DNA glycosylase activity of hOGG1 by the major human AP endonuclease: bypass of the AP lyase activity step, *Nucleic Acids Res.* **2001**, *29*, 1285–1292.

(11) Fitzgerald, M. E., and Drohat, A. C. Coordinating the Initial Steps of Base Excision Repair: Apurinic/apyrimidinic endonuclease 1 actively stimulates thymine DNA glycosylase by disrupting the product complex, *J. Biol. Chem.* **2008**, *283*, 32680–32690.

(12) Baldwin, M. R., and O'Brien, P. J. Human AP endonuclease 1 stimulates multiple-turnover base excision by alkyladenine DNA glycosylase, *Biochemistry* **2009**, ***48***, 6022–6033.

(13) Baldwin, M. R., and O'Brien, P. J. Nonspecific DNA binding and coordination of the first two steps of base excision repair., *Biochemistry* **2010**, *49*, 7879–7891.

(14) Bennett, R. A., Wilson, D. M., Wong, D., and Demple, B. Interaction of human apurinic endonuclease and DNA polymerase beta in the base excision repair pathway, *Proc. Natl. Acad. Sci. U.S.A.* **1997**, *94*, 7166–7169.

(15) Sukhanova, M. V., Khodyreva, S. N., Lebedeva, N. A., Prasad, R., Wilson, S. H., and Lavrik, O. I. Human base excision repair enzymes apurinic/apyrimidinic endonuclease1 (APE1), DNA polymerase beta and poly(ADP-ribose) polymerase 1: interplay between strand-displacement DNA synthesis and proofreading

exonuclease activity, *Nucleic Acids Res.* **2005**, *33*, 1222–1229.

(16) Strauss, P. R., Beard, W. A., Patterson, T. A., and Wilson, S. H. (1997) Substrate Binding by Human Apurinic/Apyrimidinic Endonuclease Indicates a Briggs-Haldane Mechanism, *J. Biol. Chem.* **1997**, *272*, 1302–1307.

(17) Mol, C. D., Izumi, T., Mitra, S., and Tainer, J. A. DNA-bound structures and mutants reveal abasic DNA binding by APE1 and DNA repair coordination, *Nature* **2000**, *403*, 451–456.

(18) Tsutakawa, S. E., Shin, D. S., Mol, C. D., and Izumi, T. Conserved Structural Chemistry for Incision Activity in Structurally Non-homologous Apurinic/Apyrimidinic Endonuclease APE1 and Endonuclease IV DNA repair, *J. Biol. Chem.* **2013***, 288*, 8445-8455

(19) Xu, Y.-J., DeMott, M. S., Hwang, J. T., Greenberg, M. M., and Demple, B. (2003) Action of human apurinic endonuclease (Ape1) on C1'-oxidized deoxyribose damage in DNA, *DNA Repair (Amst.)* **2003**, *2*, 175–185.

(20) Timofeyeva, N. A., Koval, V. V., Knorre, D. G., Zharkov, D. O., Saparbaev, M. K., Ishchenko, A. A., and Fedorova, O. S. Conformational dynamics of human AP endonuclease in base excision and nucleotide incision repair pathways, *J. Biomol. Struct. Dyn.* **2009**, *26*, 637–652.

(21) Kanazhevskaya, L. Y., Koval, V. V., Zharkov, D. O., Strauss, P. R., and Fedorova, O. S. Conformational transitions in human AP endonuclease 1 and its active site mutant during abasic site repair, *Biochemistry* **2010**, *49*, 6451–6461.

(22) Wilson, D. M., Takeshita, M., Grollman, A. P., and Demple, B. Incision activity of human apurinic endonuclease (Ape) at abasic site analogs in DNA, *J. Biol. Chem.*

1995, *270*, 16002–16007.

(23) Mundle, S. T., Delaney, J. C., Essigmann, J. M., and Strauss, P. R. Enzymatic mechanism of human apurinic/apyrimidinic endonuclease against a THF AP site model substrate, *Biochemistry* **2009**, *48*, 19–26.

(24) Maher, R. L., and Bloom, L. B. Pre-steady-state kinetic characterization of the AP endonuclease activity of human AP endonuclease 1, *J. Biol. Chem.* **2007**, *282*, 30577–30585.

(25) Lucas, J. A., Masuda, Y., Bennett, R. A. O., Strauss, N. S., and Strauss, P. R. Single-Turnover Analysis of Mutant Human Apurinic/Apyrimidinic Endonuclease, *Biochemistry* **1999**, *38*, 4958–4964.

(26) Jarem, D. A., Wilson, N. R., and Delaney, S. Structure-dependent DNA damage and repair in a trinucleotide repeat sequence, *Biochemistry* **2009**, *48*, 6655–6663.

(27) Warshaw, M. M., and Tinoco, I. Optical properties of sixteen dinucleoside phosphates, *J. Mol. Biol.* **1966**, *20*, 29–38.

(28) Leipold, M. D., Workman, H., Muller, J. G., Burrows, C. J., and David, S. S. Recognition and removal of oxidized guanines in duplex DNA by the base excision repair enzymes hOGG1, yOGG1, and yOGG2, *Biochemistry* **2003**, *42*, 11373–11381.

(29) Barzilay, G., Mol, C. D., Robson, C. N., Walker, L. J., Cunningham, R. P., Tainer, J. A., and Hickson, I. D. Identification of critical active-site residues in the multifunctional human DNA repair enzyme HAP1, *Nat. Struct. Biol.* **1995**, *2*, 561–568.

(30) Kane, C. M., and Linn, S. Purification and characterization of an

apurinic/apyrimidinic endonuclease from HeLa cells, *J. Biol. Chem.* **1981**, *256*, 3405–3414.

(31) Masuda, Y., Bennett, R. A., and Demple, B. (1998) Rapid dissociation of human apurinic endonuclease (Ape1) from incised DNA induced by magnesium, *J. Biol. Chem.* **1998**, *273*, 30360–30365.

(32) Erzberger, J. P., and Wilson, D. M. The role of Mg2+ and specific amino acid residues in the catalytic reaction of the major human abasic endonuclease: new insights from EDTA-resistant incision of acyclic abasic site analogs and site-directed mutagenesis, *J. Mol. Biol.* **1999,** *290*, 447–457.

(33) Sassa, A., Beard, W. A., Prasad, R., and Wilson, S. H. DNA sequence context effects on the glycosylase activity of human 8-oxoguanine DNA glycosylase, *J. Biol. Chem.* **2012**, *287*, 36702–36710.

(34) Chaudhry, M. A., and Weinfeld, M. Reactivity of human apurinic/apyrimidinic endonuclease and Escherichia coli exonuclease III with bistranded abasic sites in DNA, *J. Biol. Chem.* **1997**, *272*, 15650–15655.

(35) Gorman, M. A. (1997) The crystal structure of the human DNA repair endonuclease HAP1 suggests the recognition of extra-helical deoxyribose at DNA abasic sites, *EMBO J. 16*, 6548–6558.

(36) Rothwell, D. G., Hickson, I. D. Asparagine 212 is Essential for Abasic Site Recognitions by the Human DNA Repair Endonuclease HAP1, *Nucleic Acids Res.* **1996**, *24*, 4217-4221.

(37) Rothwell, D. G., and Hickson, I. D. Asparagine 212 is essential for abasic site recognition by the human DNA repair endonuclease HAP1, *Nucleic Acids Res.*

1996, *24*, 4217–4221.

(38) Kanazhevskaya, L. Y., Koval, V. V., Vorobjev, Y. N., and Fedorova, O. S. Conformational Dynamics of Abasic DNA upon Interactions with AP Endonuclease 1 Revealed by Stopped-Flow Fluorescence Analysis. *Biochemistry* **2012**, *51*, 1306−1321.

Chapter 4: Single-Nucleotide and Multinucleotide Incorporation by DNA Polymerase β on CAG Repeat and Mixed-Sequence DNA Constructs

4.1 Abstract

The DNA base excision repair (BER) pathway, a cascade of enzymes responsible for repairing single-nucleobase lesions, has been implicated in the expansion of a CAG trinucleotide repeat (TNR) tract. During BER, a DNA glycosylase in coordination with AP endonuclease, removes the single-nucleobase lesion and cleaves the DNA backbone. Here, DNA polymerase β (pol β) must insert the correct nucleotide, so that DNA ligase I (Lig1) can seal the DNA backbone and complete the repair. Interestingly, BER can proceed down one of two sub-pathways, short-patch (SP) or long-patch (LP) BER. In SP-BER, pol β incorporates a single nucleotide at the gap and Lig1 completes the repair. In LP-BER, a DNA polymerase incorporates multiple nucleotides, displacing a 5'-flap of DNA that is further processed to complete the repair. The BER of an oxidized form of guanine within the CAG repeat track of exon 1 of the huntingtin gene proceeds down the LP-BER pathway, leading to the incorporation of multiple CAG repeats at the nick site by pol β, and creation of a 5′ flap of CAG repeats. The 5'-flap of CAG repeats is incorporated back into duplex DNA leading to the expansion of the repeat tract; this expansion is the molecular basis for the neurological disorder Huntington's disease. It is currently unclear why pol β proceeds down LP-BER versus SP-BER within the CAG repeat tract. In this work, we examine single-nucleotide and multinucleotide incorporation by pol β on mixed and CAG repeat substrates to understand the context of SP and LP-BER on differing DNA sequences. Using single-nucleotide kinetic incorporation assays, we reveal that pol β inserts a single guanine nucleotide across a cytosine on both mixed and repeat constructs at similar rates, ~ 5 s^{-1}. Furthermore, pol β dissociates from mixed and repeat constructs at similar rates, ~ 2 s^{-1}. Multinucleotide

incorporation assays reveal that pol β incorporates more nucleotides on CAG repeat constructs compared to mixed sequence after 30 s incubation, ~23 compared to ~16, respectively. Furthermore, strand displacement activity assays reveal pol β can displace a 5'-flap of CAG repeats more readily than a 5'-flap of mixed sequence DNA. These results suggest that while pol β initially processes both mixed and repeat constructs similarly, the increased strand displacement activity and multinucleotide incorporation activity seen for pol β on CAG repeat DNA compared to mixed-sequence DNA may explain progression down LP-BER by pol β in a CAG repeat tract.

4.2. Introduction

Trinucleotide repeat (TNR) tracts are naturally occurring microsatellites found throughout our genome and are genetically unstable; through various cellular processes, the repeat number can expand or contract (*1*). DNA replication and DNA repair along with the ability for TNR tracts to form non-B DNA conformations, such as stem-loop hairpins, are implicated in playing a role in the instability of these repeat tracts (*2*-5). Expansion of these TNR tracts is linked to over 40 human neurological disorders (*6*). Huntington's disease (HD) is a notable example characterized by the expansion of (CAG)/(CTG) repeats. Interestingly, the expansion of the (CAG)/(CTG) repeat tract seen in HD is most pronounced in post-mitotic skeletal and brain tissue, ruling out DNA replication as a route by which these tracts expand in non-dividing cells (*3*).

As introduced earlier in this body of work, the initiation of base excision repair (BER) by the DNA glycosylase oxoguanine glycosylase (OGG1) in removal of an 8-oxo-

7,8-dihydroguanine (8oxoG) lesion has been implicated in leading to the expansion of the CAG repeat tract seen in HD (*3*). Canonical BER of an 8oxoG lesion begins by action of OGG1 and apurinic/apyrimidinic endonuclease 1 (APE1) in removing the 8oxoG lesion and cleaving the DNA backbone, leading to a nick with 3'-OH and 5'-deoxyribose phosphate (dRP) or a one nucleotide gap with 3'-OH and 5'-phosphate termini (*7*). Here, BER can proceed down one of two sub-pathways, short-patch (SP) or long-patch (LP). In SP-BER, polymerase β (pol β) incorporates a single-nucleotide at the nick site along with converting the 5'-dRP group, if present, to the 5'-phosphate, so that a ligase can complete the repair event (*7*). Experimental evidence suggests that when pol β cannot covert the 5'-dRP group to the 5'-phosphate, the polymerase will proceed down LP-BER (*8*,*9*). During LP-BER, a polymerase adds multiple nucleotides at the lesion site, displacing a 5'-flap of nucleotides that is further cleaved by flap endonuclease 1 (FEN1) so that DNA ligase I (Lig1) can complete repair. BER performed within the context of the CAG repeat tract of the huntingtin gene is thought to progress down LP-BER regardless of the ability for pol β to remove the 5'-dRP group; multiple nucleotides are inserted by pol β, displacing a 5'-flap of CAG repeats that can fold to form a CAG stem-loop hairpin that is refractory to cleavage by FEN1, but ligated into the DNA by Lig1, leading to the incorporation of excess CAG repeats, thus creating a mechanism for expansion of the repeats (*3*,*10*). Notably, work in the Delaney laboratory has implicated the formation of a second 8oxoG lesion within the newly formed hairpin to contribute to the expansion mechanism, resulting in a toxic oxidation cycle (TOC) (*11*,*12*). Importantly, the incorporation of multiple nucleotides by pol β at the gap site is a critical turning point in BER within the context of CAG repeats. It is here that BER is awry; pol β should incorporate a single

guanine in an SP-BER event, but instead incorporates multiple repeats in an LP-BER fashion, ultimately causing the TOC. Understanding why pol β undergoes LP-BER versus SP-BER in the context of CAG repeat DNA is integral to understanding the mechanism of repair-based trinucleotide repeat expansion.

Pol β, a 39 kDa member of the X-family of polymerases, is the smallest human polymerase and has two catalytic domains: an 8 kDa amino-terminal dRP lyase domain which binds to the 5' dRP or 5' phosphate of the gap site, and a 31 kDa carboxy-terminal domain which binds to the 3'-OH of the gap site (*13*, *14*). The presence of both catalytic domains is required for optimal gap site binding and processing (*15*). The dRP lyase domain contains a nucleophilic lysine residue, Lys 72, which is responsible for converting the 5'-dRP group to the 5'-phosphate required for nick-sealing by Lig1 (*14*). The dRP lyase domain also has activity on intact AP sites, causing β-elimination of the AP site, much like bifunctional DNA glycosylases, again affording the 5'-phosphate (*14*). Interestingly, inhibition of pol β dRP lyase activity, typically thought to occur due to oxidation of the dRP group, is known to force LP-BER in the context of mixed-sequence DNA (*8*, *9*); *in vitro* experiments studying LP-BER typically use a tetrahydrofuran (THF) containing dRP group to inhibit pol β dRP lyase activity and force LP-BER (*10*, *16*). In contrast, LP-BER seen in the context of CAG repeat DNA is known to occur even in the presence of an unmodified dRP group (*10*). Moreover, as presented earlier in this work, we observe the action of the AP lyase step of OGG1 in coordination with APE1 to create a gap with 3'-OH and 5'-phosphate termini; therefore, in the case of BER initiated by OGG1, a 5'-dRP is likely never formed along the BER cascade. Taken together, such

evidence suggests the inability of polβ to remove a modified 5′-dRP group is not contributing to the initiation of LP-BER in CAG repeat tracts.

The 31 kDa polymerase domain of pol β is responsible for catalyzing nucleotidyl transfer from an incoming dNTP to the 3'-OH of the DNA backbone at the gap site, causing the release of pyrophosphate (PPi); such reaction requires two Mg^{2+} metal ions. One metal ion, referred to as the catalytic metal ion, coordinates to the 3'-OH of the growing primer, while the other metal ion, referred to as the nucleotidyl binding metal, coordinates to the α-phosphate of the bound dNTP, and assists in dNTP binding and PPi release (*17*).

The kinetic scheme for polβ nucleotide incorporation shows an ordered binding of polymerase to the DNA, followed by binding of the dNTP (Figure 4.1 Step 1, 2) (*17*).

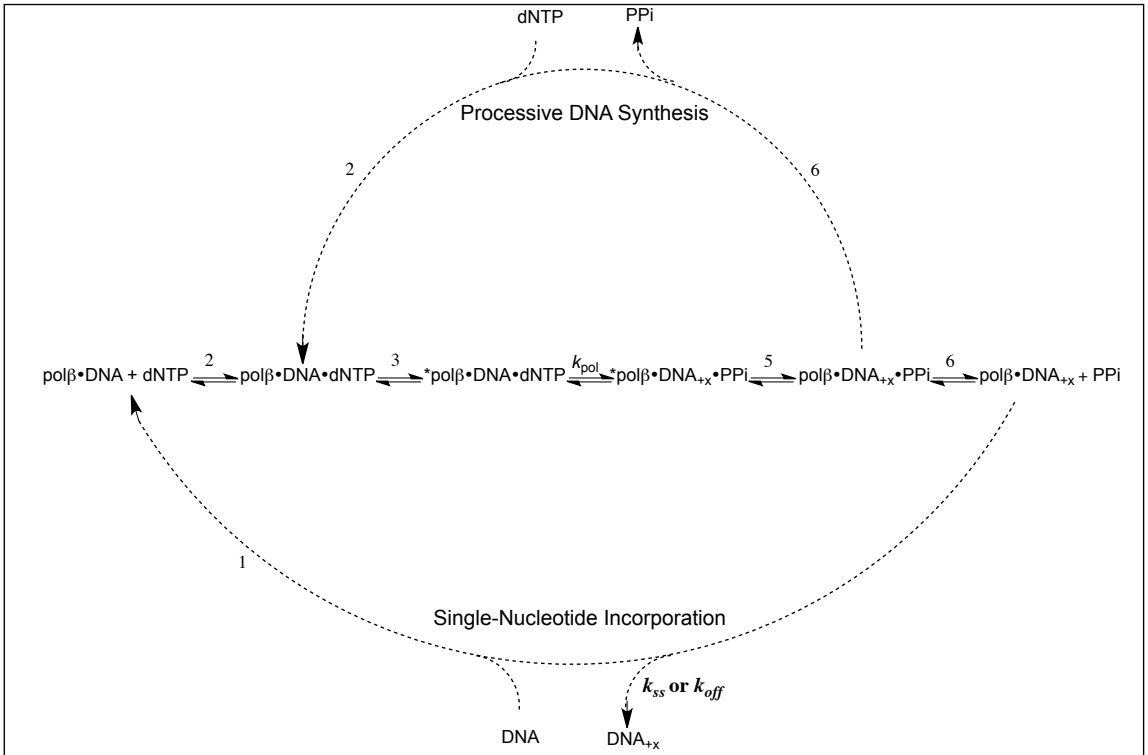

Figure 4.1. Single-nucleotide and processive DNA synthesis kinetic scheme for pol β. The six-step elongation cycle consists of DNA binding (1), nucleotide binding (2), a conformation change that aids in nucleotide discrimination (3), nucleotidyl transfer (4, k_{pol}), a conformation change (5) that permits PPi release (6). For single-nucleotide incorporation the DNA then dissociates from pol β (k_{off}) (bottom pathway). For Processive DNA synthesis (top pathway), a new dNTP binds after PPi release and the cycle continues. Figure adopted from reference 17.

Upon binding of the correct dNTP, the polymerase undergoes a conformation change from an "open" form to a "closed" form (Figure 4.1 Step 3) which aids in correct nucleotide discrimination and brings the 3'-OH present at the nick site in close proximity to the bound dNTP to allow for nucleotidyl transfer and formation of a new oxygen-phosphate bond; the rate of nucleotidyl transfer is represented by k_{pol} (Figure 4.1 k_{pol}). Previous pol β kinetic experiments reveal k_{pol} for *correct* nucleotide insertion ranges from 2 – 20 s^{-1}, and differs based on the nucleotide inserted; the fastest k_{pol} is observed for A inserted opposite of T, while the slowest k_{pol} is seen for G inserted opposite of C (*18*,*19*). A second conformational change (Figure 4.1 Step 5) allows for release of PPi (Figure 4.1 Step 6) followed by dissociation of the DNA from the polymerase (Figure 4.1 k_{off}). This pathway describes the events that occur during a single-nucleotide incorporation event, i.e. SP-BER (Figure 4.1, bottom pathway). Both conformational changes are thought to be faster than nucleotidyl transfer chemistry, and therefore are not rate limiting (*20*); moreover, similar to other BER enzymes, dissociation of the polymerase enzyme from the DNA is rate-determining and defines k_{cat}, typically called k_{off} in the context of polymerase kinetics (*13*). The k_{off} rate for pol β ranges from 0.5 – 2.5 s^{-1}, and varies based on the functional groups present at the nick site; faster dissociation rates are seen without the presence of the 5'-phosphate, while slower dissociation rates are observed in the presence of the 5'-phosphate (*15,18*,*19*).

In scenarios in which the polymerase adds multiple nucleotides in a single binding event, the polymerase is said to be processive (Figure 4.1, top pathway). The processivity of a polymerase is a reflection of how many nucleotides the polymerase can add before dissociating from the DNA, and is determined by the ratio of averages of

k_{pol}/k_{cat}. Replicative DNA polymerases, or those involved in DNA replication, such as δ and ε, are able to replicate thousands of base pairs in a single binding event, and are therefore highly processive polymerases (*21*). Pol β is weakly processive due to the similar magnitude of k_{pol}, ~ 10 s^{-1}, and k_{off}, ~ 2.5 s^{-1} (*18,19*).

Within the context of processive DNA replication, the polymerase may also be required to displace a downstream strand of DNA nucleotides as it is undergoing nucleotidyl transfer chemistry. For example, this action, typically referred to as the strand displacement activity of the polymerase, is required by pol δ during replication through Okazaki fragments (*22*). Again, different polymerases have differing strand displacement abilities, and having high processivity does not equate to high strand displacement activity. While pol δ has high processivity, it has weak strand displacement activity (*22*). This weak activity is greatly enhanced by the presence of the processivity clamp, proliferating cell nuclear antigen (PCNA). Importantly, PCNA, a donut-shaped protein that completely encircles the DNA duplex, binds many human polymerases, including δ, ε, and β, and aids in non-dissociative processive replication (*23*). Qualitative strand displacement assays suggest pol β alone has weak strand-displacement activity (*24*). Furthermore, within the context of BER, the presence and APE1 has been shown to increase pol β strand displacement activity (*16*).

Due to the poor processivity and strand displacement activity of pol β, it has been proposed that in the context of LP-BER on mixed sequence DNA, pol β incorporates a single nucleotide at the gap site and then dissociates. Next, a highly processive polymerase, such at δ or ε, takes over, adding multiple nucleotides to the nick site with the help of PCNA, creating a patch size of 2-6 nucleotides (*25*). Remarkably, in the

context of reconstituted BER from mouse embryonic fibroblasts on CAG repeat DNA, mouse cell lines null in pol β had a *reduction* in expanded CAG repeat products compared to the wild-type pol β efficient counterparts (*10*). Such evidence directly implicates pol β as the key polymerase in adding multiple nucleotides during the proposed BER-based expansion model. Moreover, reconstituted BER on a 100mer DNA construct containing an 8oxoG lesion flanked 5' by mixed-sequence and 3' by $(CAG)_{19}/(CTG)_{19}$, revealed correct processing by OGG1 and APE1, followed by multinucleotide incorporation by pol β. Interestingly, a unique pattern was observed in the autoradiogram for multinucleotide incorporation by pol β in the repeat tracts (*10*). Distinct, intense banding at each adenine within the repeat was attributed to pol β pausing. Pausing is thought to occur when a polymerase encounters structures and/or duplex regions that are difficult to processes, such as well-matched stem-loop hairpins or high GC content (*26*-*28*). This pausing is thought to lead to the dissociation of the polymerase from the DNA (*29*). The authors speculate that the pausing observed at each A within the repeat tract was likely due the presence of downstream CAG hairpins within the DNA construct; DNA structural studies were not performed to confirm the presence of these structures (*10*).

In this work, we investigate single-nucleotide and multinucleotide incorporation by pol β on both mixed and CAG repeat DNA constructs to gain further insight into the mechanism by which CAG repeat DNA expands within the context of the HD gene. We perform transient-state and steady-state single-nucleotide incorporation kinetics of pol β on mixed and CAG repeat constructs to determine and compare the kinetic parameters associated with SP-BER. Furthermore, we compare the processivity of pol β on both

mixed and CAG repeat constructs to understand how sequence context may influence processive multinucleotide incorporation. Finally, we aim to determine if pol β has similar strand displacement activity on both CAG repeat and mixed-sequence constructs. The results obtained here contribute to our understanding of the molecular mechanism by which pol β incorporates multiple nucleotides during the repair of a DNA lesion contained with a CAG repeat tract and ultimately provides further evidence for the toxic oxidization cycle we propose for expansion of the TNR tracts.

4.3 Experimental Procedure

4.3.1 Oligonucleotide Synthesis and Purification

DNA oligonucleotides used in this work were synthesized using standard phosphoramidite chemistry on a BioAutomation DNA/RNA synthesizer (Table 4.1) (*30*). A chemical phosphorylation reagent (CPR) ([3-(4,4'-Dimethoxytrityloxy)-2,2-dicarboxyethyl]propyl-(2-cyanoethyl)-(N,N-diisopropyl)-phosphoramidite) was used in synthesis of 5'-phosphate containing strands, and was obtained from Glen Research. During synthesis the 5′-DMT was retained to aid in HPLC purification. Two rounds of HPLC purification were performed using a polystyrene-divinyl benzene reverse phase column (PLRP-S; Polymer Labs) (4.6 × 250 mm) at 90 °C using 100 mM TEAA in acetonitrile:water (99%:1%) (solvent A) and 100 mM TEAA in acetonitrile:water (1%:99%) (solvent B) as the mobile phases (gradient: solvent A was increased from 5 to 25% over 25 min; 1.0 mL/min for first round, gradient: solvent A was increased from 0 to 15% over 35 min; 1.0 mL/min for second round). For all strands, the 5′-DMT group was removed following the first round of HPLC; after 5'-DMT removal, strands synthesized

with CPR were incubated in NH_4OH overnight at 55 ºC to afford the 5'-phosphate. Quantification of each oligonucleotide was performed using the ε_{260} values estimated for single-stranded DNA (*31*) and a Beckman Coulter DU800 UV-VIS Spectrophotometer.

Table 4.1. Sequence of DNA Oligonucleotides Used in this Study[a]

Name	Sequence
22mer	5′- CGAGTCATCTAGCATCCGTACA-3′
77mer-M[b]	5′- PACTCGTTACGTGATCGTGTACTGCATGTGTATGTCGTATGATGTCTATGTCTC GAACTACGTAGACTTACTCATTGC-3′
77mer-R[b,c]	5′- PCAGCAGCAGCAGCAGCAGCAGCAGCAGCAGCAGCAGCAGCAGCAGCA GCAGCAGTACGTAGACTTACTCATTGC-3′
100mer-M[d]	3′- GCTCAGTAGATCGTAGGCATGT**C**TGAGCAATGCACTAGCACATGACGTACACA TACAGCATACTACAGATACAGAGCTTGATGCATCTGAATGAGTAACG-′5
100mer-R[c,d]	3′- GCTCAGTAGATCGTAGGCATGT**C**GTCGTCGTCGTCGTCGTCGTCGTCGTC GTCGTCGTCGTCGTCGTCGTCGTCATGCATCTGAATGAGTAACG -5′

[a] Sequences were adopted from reference 10.
[b] P denotes location of phosphate group.
[c] Repeat regions are underlined.
[d] Cystosines at gap site in duplex constructs are in bold.

4.3.2 Expression and Purification of pol β

TAP56 *Escherichia coli* cells pre-transformed with pWL11 plasmid containing the pol β gene were grown at 37 ºC in 2 L of LB media containing 50 μg/mL ampicillin to an OD_{560} ~ 0.2 at which time the temperature was increased to 42 ºC for 3 h to induce protein expression. After 3 h growth at 42 ºC, cells were pelleted by centrifugation (3,000 × *g*, 30 min, 4 ˚C) (*32*). The supernatant was discarded and the cells were frozen with liquid nitrogen and stored at −80 ˚C until purification of pol β. The purification of pol β was adapted from two previously performed protocols (*19*, *32*). Upon thawing on ice, cells were resuspended in buffer A (50 mM Tris-HCl, 1 mM EDTA, 1 mM PMSF, 10 mM $Na_2S_2O_5$ and 1 μg/mL pepstatin A) containing 0.5 M NaCl. Cells were then lysed using a French press; lysates were clarified by centrifugation (24,336 × *g*, 20 min, 4 ˚C). The supernatant was diluted with buffer A to a final concentration of 0.2 M NaCl. The

diluted supernatant was loaded onto a 5 mL DEAE-cellulose column (Bio-Rad) in tandem with a 5 mL phosphocellulose column (Sigma Aldrich), both pre-equilibrated with buffer A supplemented with 0.1 M NaCl, using a peristaltic pump. Both columns were washed with 5 column volumes of buffer A supplemented with 0.2 M NaCl. The DEAE-cellulose column was disconnected, and the phosphocellulose column was washed with another 5 column volumes of buffer A supplemented with 0.2 M NaCl. Pol β was eluted with 5 column volumes of buffer A supplemented with 1 M NaCl. The eluted protein was dialyzed overnight (6,000 – 8,000 MW dialysis tubing) in 2 L of buffer A supplemented with 0.1M NaCl. Following dialysis, pol β was loaded onto a pre-equilibrated (buffer A supplemented with 0.1 M NaCl) 5 mL HiTrap Heparin column (GE Healthcare); then washed with 5 column volumes of buffer A supplemented with 0.1 M NaCl. Using a salt gradient in buffer A from 0.1 M NaCl to 1 M NaCl, pol β was eluted off the column. Fractions containing pol β, as confirmed by SDS-PAGE analysis, were pooled and dialyzed overnight (6,000 – 8,000 MW dialysis tubing) in buffer A supplemented with 0.1 M NaCl. Following dialysis, pol β was loaded onto a pre-equilibrated 1 mL HiTrap Q anion-exchange column (GE Healthcare) and the *flow-through* containing pol β was collected and concentrated using an Amicon 5,000 MW cut-off concentration. The purity of pol β was >95% as assessed by SDS-PAGE. Pol β was resuspended in storage buffer (25 mM Tris-HCl, 1 mM DTT, 100 mM NaCl, 0.1 mM EDTA and 50% glycerol) and flash frozen. The concentration of pure pol β was determined by the Bradford method using bovine γ-globulin as a standard.

4.3.3 Determination of Active Enzyme Concentration and Dissociation Rates of pol β

The 22mer oligonucleotide was 5′-^{32}P end-labeled with T4 polynucleotide kinase (NEB, Ipswich, MA) following the manufacturer's protocol. The 5′-^{32}P-labeled 22mer (400 nM) was incubated with a 1.5-fold excess of unlabeled 77mer-M or 77mer-R and a 1.25-fold excess (with respect to 22mer) of the unlabeled 100mer complementary oligonucleotide, in 50 mM Tris-HCl, 0.1 mM Na_2EDTA, 50 mM NaCl, pH 7.6 (Buffer B) for 5 min at 90 °C, followed by cooling to room temperature over ~2.5 h. The DNA was diluted to a final concentration of 200 nM and preincubated with 40 nM polβ in 50 mM Tris-HCl, 0.1 mM Na_2EDTA, 50 mM NaCl, 5 mM $MgCl_2$ 100 μg/mL BSA, 10 % glycerol, 5 mM DTT, pH 7.8 (Buffer C) in a total volume of 300 μL. This diluted DNA/pol β sample and 200 μM dGTP (NEB) in 300 μL of Buffer C were loaded into separate sample syringes of a Rapid Quench Flow (RQF) instrument (Kintek) and equilibrated for 5 min at 37 °C. The DNA/pol β and dGTP were then combined in the reaction loop to yield a sample containing 100 nM DNA, 20 nM pol β, and 100 μM dGTP in Buffer C. Using the RQF instrument, after 0.02-5 s the reactions were quenched with EDTA (~65 mM final concentration) followed by the addition of 40 μL denaturing dye (80% formamide, 10 mM EDTA, 1 mg/mL xylene cyanol and 1 mg/mL bromophenol blue). At the end of each time course, a control was performed in which DNA/pol β was incubated with Buffer C lacking dGTP in the RQF for 5 s and quenched as described above. The samples were stored on dry ice until electrophoresis. Prior to loading onto a 20% denaturing polyacrylamide gel, all samples were incubated at 90 °C for 3 min. The products were visualized by phosphorimagery and the amount of product was plotted versus time. Both a burst phase and a linear phase are observed with the slope of the linear phase equal to k_{off} × [active enzyme], where an active enzyme concentration

of ~ 50% was determined by extrapolating the linear phase line through the y-axis (*18*, *19*).

4.3.4 Determination of Single-nucleotide dGTP insertion rates of pol β

Both 100mer DNA constructs were assembled as described above, with the 22mer 5'-^{32}P labeled. Following annealing, the DNA was diluted to 60 nM and preincubated with 300 nM active pol β in Buffer C. This diluted DNA/pol β sample and 800 μM dGTP in 300 μL of Buffer C were loaded into separate sample syringes of an RQF instrument and equilibrated for 5 min at 37 °C. The DNA/pol β and dGTP were then combined in the reaction loop to yield a sample containing 30 nM DNA, 150 nM active pol β, and 400 μM dGTP in Buffer C. Using the RQF instrument, after 0.02-15 s the reactions were quenched with EDTA (~65 mM final concentration) followed by the addition of 40 μL denaturing dye. At the end of each time course, a control was performed in which DNA/pol β was incubated with Buffer C lacking dGTP in the RQF for 5 s and quenched as described above. The samples were stored on dry ice until electrophoresis. Prior to loading onto a 20% denaturing polyacrylamide gel, all samples were incubated at 90 °C for 3 min. The products were visualized by phosphorimagery and the amount of product was plotted versus time. The data were then fitted to a burst equation as described previously to obtain rates of k_{pol} (*18*, *19*).

4.3.5 Pol β Multinucleotide Incorporation Assays

Both mixed and repeat 100mer constructs were assembled as described above. A similar second set of mixed and repeat 100mer constructs were assembled as described

above, but lacked the presence of the 77mer strand. Each DNA construct was diluted to 100 nM and preincubated with 100 nM active pol β in Buffer C. This diluted DNA/pol β sample and 200 μM each dNTP (NEB) in 300 μL of Buffer C OR 200 μM each dNTP and 5 mg/mL calf-thymus (CT) DNA (Invitrogen) in 300 μL of Buffer C were loaded into separate sample syringes of an RQF instrument and equilibrated for 5 min at 37 °C (*33*). DNA/pol β and dNTPs with or without CT DNA, were then combined in the reaction loop to yield a sample containing 50 nM DNA, 50 nM active pol β, and 100 μM each dNTP with or without 2.5 mg/mL CT-DNA in Buffer C. Using the RQF instrument, after 0.02-60 s the reactions were quenched with EDTA (~65 mM final concentration) followed by the addition of 40 μL denaturing dye. At the end of each time course, two controls were performed. In the first, DNA/pol β was incubated with Buffer C lacking dNTPs in the RQF for 60 s and quenched as described above. In the second, 50 nM pol β, 2.5 mg/mL CT-DNA and 100 μM each dNTPs in Buffer C were preincubated for 30 s manually, followed by the addition of 50 nM DNA construct for 60 s. The control was quenched manually with 100 mM EDTA (~65 mM final concentration) and denaturing dye. The samples were stored on dry ice until electrophoresis. Prior to loading onto a 20% denaturing polyacrylamide gel, all samples were incubated at 90 °C for 3 min. The products were visualized by phosphorimagery.

4.4 Results

4.4.1 DNA substrates

Two 100mer DNA constructs were used to obtain the kinetic parameters of pol β. Each 3-part DNA construct contains a 22mer and 77mer annealed to their 100mer

complement, creating a site-specific gap in the DNA backbone with 3'-OH and 5'-phosphate termini (Table 4.1, Figure 4.2). Notably, standard phosphoramidite chemistry yields DNA with both 3' and 5'-OH groups; 77mer constructs which bear a 5'-phosphate were exposed to a chemical phosphorylation reagent during DNA synthesis to convert the 5'-OH to the desired 5'-phosphate. The presence of a 5'-phosphate at the gap site is required for optimal binding, and therefore optimal processing by the polymerase. These constructs were adopted from reference 10, and mimic the gap site that would be generated by initiation of BER by OGG1 and APE1 on an 8oxoG lesion. The two DNA substrates differ based on their sequence context downstream from the gap site; the first construct is completely mixed sequence (Figure 4.2A), while the second contains $(CAG)_{19}/(CTG)_{19}$ repeats adjacent to the gap site, followed by 20 base pairs (bp) of mixed sequence (Figure 4.2C). Both mixed and repeat constructs contain a cytosine on the 100mer complementary strand at the gap site. To assess the processivity of pol β, the above mixed and repeat constructs were also created in the absence of the 77mer (Figure 4.2 B,D).

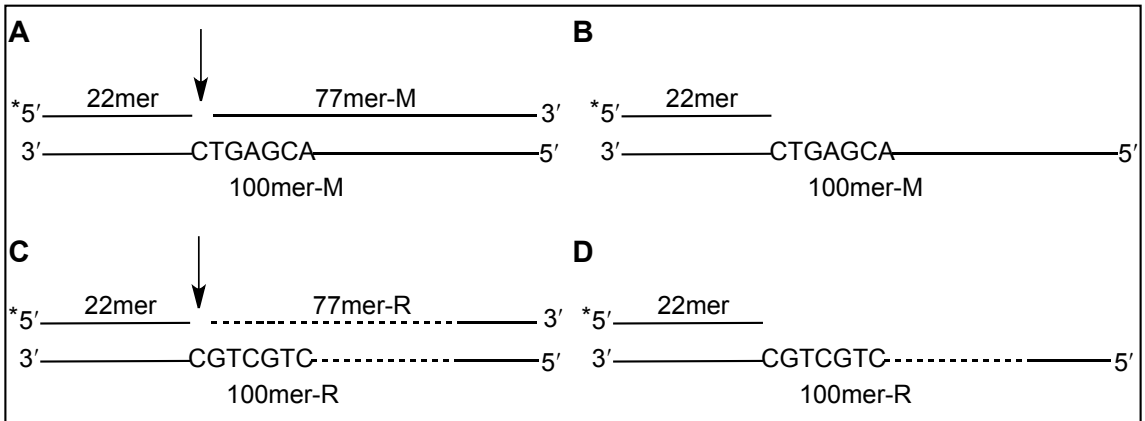

Figure 4.2. Schematic representation of mixed (A,B) and repeat (C,D) DNA constructs used in this study, with (A,C) or without (B,D) a downstream 77mer. Solid lines represent mixed sequence context, while dashed lines represent repeat sequence context. Arrows denote the location of a gap site (A,C), the 5′ * denotes the location of a ^{32}P label, "M" denotes mixed DNA constructs, while "R" denotes repeat DNA constructs.

4.4.2 Dissociation Rates (k_{off}) of Pol β

In order to obtain the rates of pol β dissociating from the 100mer mixed and repeat constructs, steady-state kinetic time courses were performed in which a 5-fold excess of DNA was preincubated with pol β (to allow for pol β /DNA binding) followed

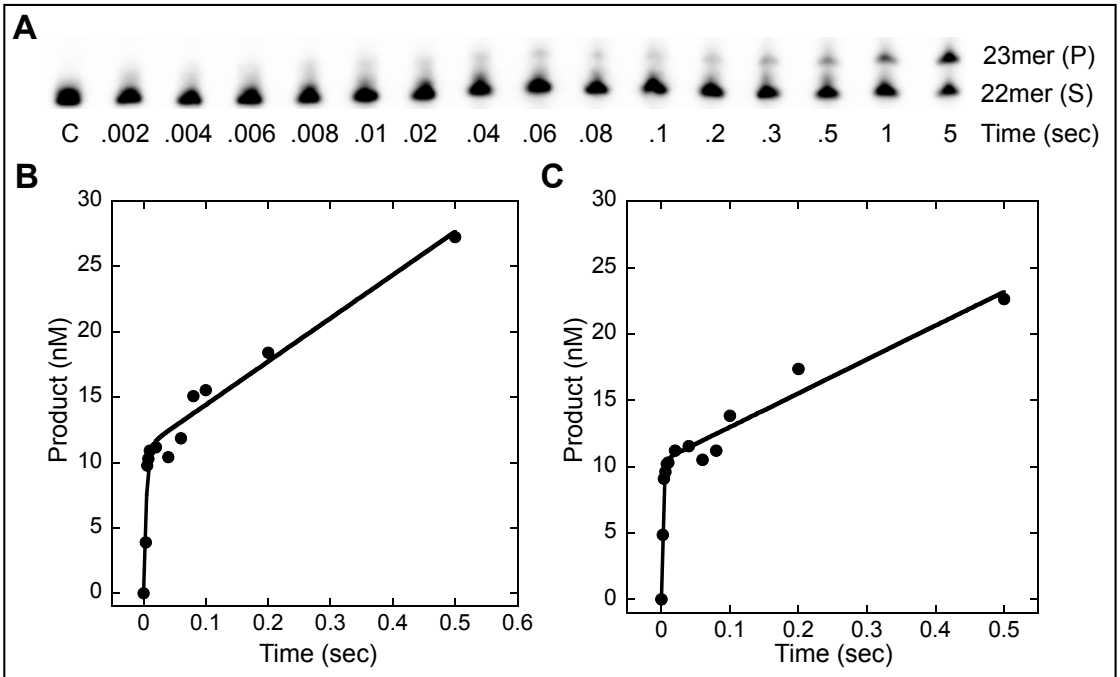

Figure 4.3. Autoradiogram (A) of single-nucleotide dGTP incorporation on mixed 100mer DNA construct and steady-state single-nucleotide dGTP incorporation time courses by pol β on (B) mixed or (C) repeat 100mer DNA constructs. Experimental conditions were 20 nM pol β, 100 nM DNA construct, 100 μM dGTP in 50 mM Tris-HCl, 50 mM NaCl, 0.1 mM Na_2EDTA, 5 mM $MgCl_2$, 100 μg/mL BSA, 10% glycerol, and 5 mM DTT, pH 7.8. Reactions were performed at 37 °C using an RQF instrument and quenched with 100 mM EDTA.

by rapid mixing with dGTP and quenching by an RQF instrument. As seen in Figure 4.3A, we see a disappearance of the 22mer substrate and appearance of the 23mer product over time, indicating the incorporation of a single guanine nucleotide to the 22mer radiolabeled substrate. The formation of product versus time was graphed for both mixed and repeat constructs (Figure 4.3B,C). Figure 4.3B and C reveal an initial burst of production accumulation followed by a linear accumulation of product over time. The initial burst represents the fast nucleotide insertion of pol β leading to the first turnover of

22mer substrate to the 23mer product. The linear phase represents a slow step occurring after the fast nucleotide insertion that has been attributed to release of the DNA from the polymerase, and limits the steady-state rate. The steady-state k_{off} rates of pol β dissociating from the mixed sequence and repeat sequence constructs, as obtained from the linear phase, are 2.5 ± 0.3 s^{-1} and 1.8 ± 0.4 s^{-1}, respectively (Table 4.2).

Table 4.2. Steady-State and Transient-State Kinetic Parameters of dGTP Incorporation by Pol β

Substrate	k_{pol} (s^{-1})[a,b]	k_{off} (s^{-1})[b,c]
100mer-M[d]	4.9 ± 0.3	2.5 ± 0.3
100mer-R[d]	5.5 ± 0.4	1.8 ± 0.4

[a] Measured at 37 ˚C under transient-state conditions using RQF instrumentation.
[b] Error represents the standard deviation from two experiments.
[c] Measured at 37 ˚C under steady-state conditions using RQF instrumentation.
[d] DNA constructs contain 77mer.

4.4.3 Single-Nucleotide Incorporation Rates (k_{pol}) of dGTP by Pol β

In order to obtain the rates of dGTP nucleotidyl transfer, k_{pol}, by pol β, transient-state kinetic time courses were performed on both mixed and repeat 100mer constructs. Each DNA construct was

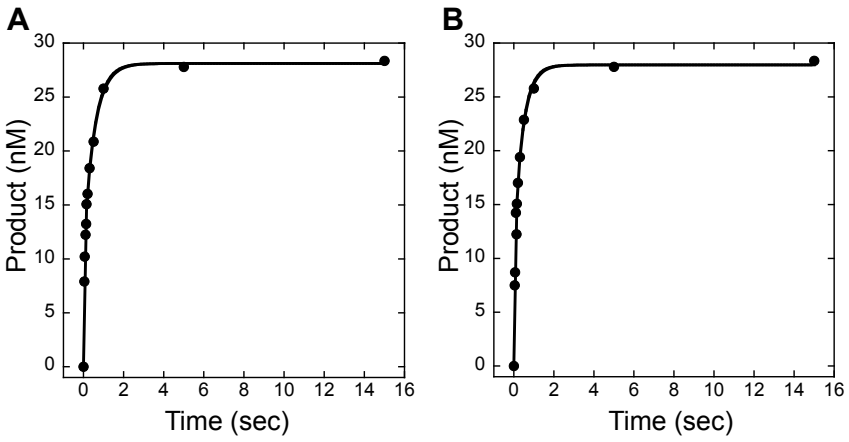

Figure 4.4. Transient-state single-nucleotide incorporation of dGTP by pol β on (A) mixed and (B) repeat 100mer DNA constructs. Experimental conditions were 50 nM DNA construct, 150 nM active pol β, 400 μM dGTP in 50 mM Tris-HCl, 50 mM NaCl, 0.1 mM Na_2EDTA, 5 mM $MgCl_2$, 100 μg/mL BSA, 10% glycerol and 5 mM DTT at pH 7.8. Reactions were performed at 37 °C using an RQF instrument and quenched with 100 mM EDTA.

preincubated with a 5-fold excess of active pol β followed by the addition of saturating dGTP, 400 μM, by the RQF instrument. The reactions were quenched with 100 mM EDTA (~65 mM final concentration) delivered by the RQF instrument. For both DNA substrates, we observe a rapid burst of product accumulation followed by a plateau (Figure 4.4A,B). The rates of pol β dGTP incorporation, k_{pol}, obtained from the slope of the burst phase, for the mixed and repeat constructs are 4.9 ± 0.3 s^{-1} and 5.5 ± 0.4 s^{-1}, respectively (Table 4.2).

4.4.4 Multinucleotide Incorporation by Pol β

To compare the ability of pol β to undergo multinucleotide incorporation on the mixed and repeat DNA constructs, both constructs were preincubated with an equal molar concentration of active pol β followed by the addition of 100 μM of all four dNTPs by the RQF. The reactions were quenched using 100 mM EDTA (~65 mM final concentration) delivered by the RQF instrument. For both mixed and repeat constructs,

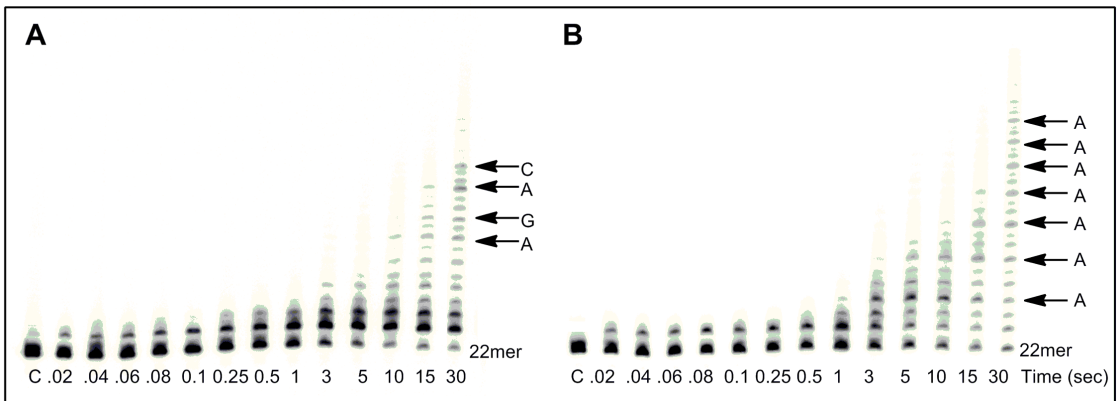

Figure 4.5. Autoradiogram revealing multinucleotide incorporation by pol β on (A) mixed and (B) repeat constructs with a downstream 77mer present. Arrows and accompanying letters highlight the nucleotide of major pause sites by pol β. Experimental conditions were 50 nM DNA construct, 50 nM active pol β, 100 μM each dNTP in 50 mM Tris-HCl, 50 mM NaCl, 0.1 mM Na_2EDTA, 5 mM $MgCl_2$, 100 μg/mL BSA, 10% glycerol, and 5 mM DTT at pH 7.6. Reactions were performed at 37 °C using an RQF instrument and quenched with 100 mM EDTA. Control lane (C) represents DNA with pol β in buffer, lacking dNTPs.

we observe the disappearance of the 22mer substrate and the appearance of 23mer product followed by appearance of higher- order DNA products over time, suggesting multinucleotide incorporation by pol β on both constructs (Figure 4.5, A,B). The longest DNA products were observed at the longest incubation time; for the mixed-sequence construct, we can reliably count the incorporation of 16 nucleotides after 30 s incubation with pol β, for the repeat-sequence construct, we can reliably count the incorporation of 23 nucleotides after 30 s incubation with pol β. Moreover, pol β seems to initiate multinucleotide incorporation to a larger extent on the repeat construct compared to the mixed construct; this is most evident by examining the abundance of the 22mer substrates and 23mer single-nucleotide incorporation product left in the 3-10 s time points. Furthermore, for both DNA constructs, we observe the appearance of intense bands, marked with arrows, in the lanes in which we see multinucleotide incorporation. For the mixed-sequence construct, these bands appear after the incorporation of 8, 10, 13 and 16 nucleotides, corresponding to incorporation of an A, G, A and C respectively. For the repeat-sequence construct, these bands appear at each adenine within the CAG repeat tract, yielding a periodic incorporation pattern.

4.4.5 Processivity of Pol β

To assess the ability of pol β to undergo multinucleotide incorporation in a *single* DNA binding event for both the mixed and repeat 100mer constructs, we performed the above multinucleotide incorporation assays in the presence of a large excess of DNA trap. Both the mixed and repeat DNA constructs were preincubated with equal molar active pol β, again to ensure prebinding of pol β to our construct, and rapidly mixed with

all four dNTPs in the presence of a large excess of the calf thymus DNA trap. If the polymerase were to dissociate from our radiolabeled DNA construct within the reaction time frame, it would reassociate with the excess of calf thymus DNA rather than our radiolabeled construct, allowing us to observe the extent of nucleotide incorporation during a single polβ-binding event. A control, in which pol β, all four dNTPs and calf thymus DNA trap were pre-incubated for 30 s, followed by the addition of the radiolabeled DNA construct for 60 s, confirmed the calf thymus DNA trap as a viable strategy (Figure 4.6 Lanes C*)(*33*). Again, much like the multinucleotide incorporation assays performed in the absence of the trap, we observe the disappearance of the 22mer substrate and the appearance of 23mer product followed by appearance of higher-order DNA products over time, suggesting multinucleotide incorporation by pol β on both constructs (Figure 4.6A,B). The extent to which we observe multinucleotide

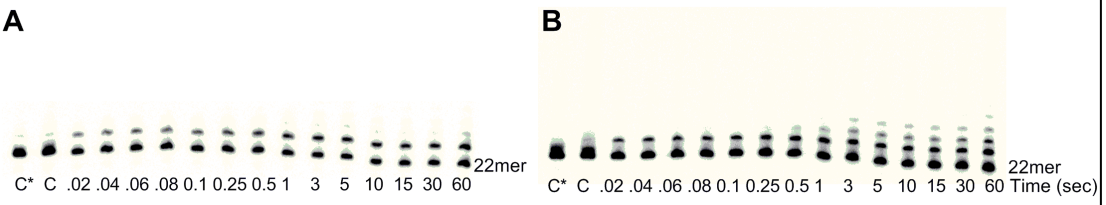

Figure 4.6. Autoradiogram revealing multinucleotide incorporation by pol β on (A) mixed and (B) repeat constructs with a downstream 77mer present in the presence of a 5-fold excess of DNA trap. Experimental conditions were 50 nM DNA construct, 50 nM active pol β, 100 μM each dNTP, 2.5 mg/mL CT DNA (trap) in 50 mM Tris-HCl, 50 mM NaCl, 0.1 mM Na_2EDTA, 5 mM $MgCl_2$, 100 μg/mL BSA, 10% glycerol, and 5 mM DTT at pH 7.6. Reactions were performed at 37 °C using an RQF instrument and quenched with 100 mM EDTA. Control lane (C) represents DNA with pol β in buffer, lacking dNTPs. Control lane (C*) represents incubation of dNTPs, pol β and trap CT DNA, followed by addition of radiolabeled construct DNA for 60 s, to confirm the ability of CT DNA to trap the enzyme.

incorporation by the polymerase is drastically reduced when the calf thymus DNA trap is present. For the mixed-sequence construct, at the longest incubation time point (60 s), we see incorporation of only 2 nucleotides (Figure 4.6A), with the major product resulting from the incorporation of a single nucleotide; for the repeat construct, we see the

incorporation of 4 nucleotides at the longest incubation time (Figure 4.6B). Here, in the presence of the calf thymus DNA trap, we do not observe any incorporation pattern.

To address whether the downstream 77mer is prohibiting the processive ability of pol β, we performed the above processivity assay on 100mer constructs lacking this

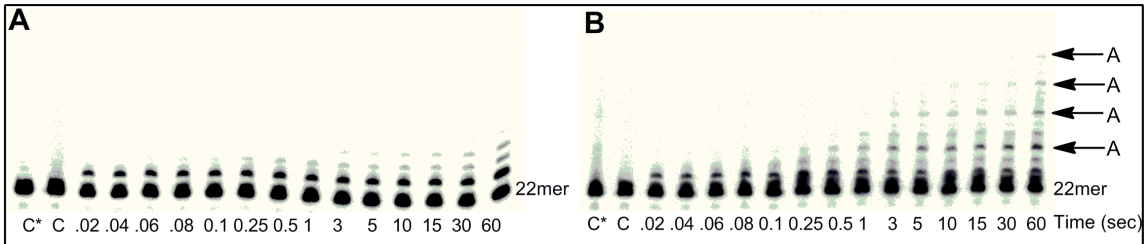

Figure 4.7. Autoradiogram revealing multinucleotide incorporation by pol β on (A) mixed and (B) repeat constructs lacking the downstream 77mer, in the presence of a 5-fold excess of DNA trap. Experimental conditions were 50 nM DNA construct, 50 nM active pol β, 100 μM each dNTP, 2.5 mg/mL CT DNA (trap) in 50 mM Tris-HCl, 50 mM NaCl, 0.1 mM Na_2EDTA, 5 mM $MgCl_2$, 100 μg/mL BSA, 10% glycerol, and 5 mM DTT at pH 7.6. Reactions were performed at 37 °C using an RQF instrument and quenched with 100 mM EDTA. Control lane (C) represents DNA with pol β in buffer, lacking dNTPs. Control lane (C*) represents incubation of dNTPs, pol β and trap CT DNA, followed by addition of radiolabeled construct DNA for 60 s, to confirm the ability of CT DNA to trap the enzyme.

strand. We preincubated our radiolabeled construct (lacking the 77mer) with pol β, followed by mixing with all four dNTPs in the presence of an excess of calf thymus DNA trap. We observe the disappearance of the 22mer substrate, and appearance of the 23mer product, followed by the appearance of higher-order DNA products over time (Figure 4.7A,B). Here, without the presence of the 77mer, but in the presence of the calf thymus DNA trap, we see incorporation of ~3 nucleotides to the mixed-sequence construct and incorporation of ~12 nucleotides to the CAG repeat construct. The intense banding pattern at each A, as denoted by arrows, is present for the repeat construct; we do not see any intense banding for the mixed construct, as the polymerase has only incorporated 3 nucleotides.

4.5 Discussion

4.5.1 Comparison of Single-Nucleotide Incorporation Kinetics for Mixed and CAG Repeat Constructs

During SP-BER initiated by the removal of an 8oxoG lesion, pol β incorporates a single guanine nucleotide opposite a cytosine at the gap site. Here, we examine both transient-state and steady-state kinetics associated with single guanine nucleotide incorporation across a cytosine in mixed and CAG repeat constructs, to understand the kinetic parameters associated with SP-BER. Transient-state kinetics reveal that incorporation of the guanine on both mixed and repeat constructs is the same within error, 4.9 ± 0.3 s^{-1} and 5.5 ± 0.4 s^{-1}, respectively (Table 4.2); therefore, we can conclude that the downstream sequence context does not affect k_{pol} for the incorporation of a single guanine. Steady-state kinetics experiments reveal that pol β releases the mixed-sequence construct slightly at the same rate as the CAG repeat construct, with k_{off} rates of 2.5 ± 0.3 s^{-1} for the mixed construct and 1.8 ± 0.4 s^{-1} for the CAG repeat construct (Table 4.2). Therefore, pol β is just as likely to release to the CAG repeat construct compared to the mixed-sequence construct. Thus, we can conclude that in the presence of just the deoxyguanosine triphosphate, pol β processes mixed-sequence constructs the same as CAG repeat sequence construct. Importantly, *in vivo* SP-BER occurs in the presence of all four dNTPs along with several other enzymes known to coordinate to pol β during the repair, including APE1, FEN1, PCNA, and Lig1, therefore it is possible that in the context of *in vivo* SP-BER, other factors may influence the single-nucleotide incorporation activity of pol β (*10,16,23,34,35*). These data suggest that a disruption in single guanine incorporation or a disruption in the ability for pol β to release the CAG construct is likely not responsible for the multinucleotide incorporation seen within the

context of CAG repeats. Other factors, such as the availability of all four dNTPs or the presence of coordinating BER enzymes must be contributing to the multinucleotide incorporation seen in the context of CAG repeat tracts.

4.5.2. Multinucleotide Incorporation and Processivity of Pol β on Mixed and Repeat Constructs

In order to explore the ability for pol β to incorporate multiple nucleotides at gap sites within mixed and repeat DNA constructs, we performed several multinucleotide incorporation assays in which all four dNTPs were available to the polymerase. In the incorporation assays with DNA constructs containing a 3'-OH and 5'-phosphate present at the gap site, we saw the incorporation of multiple nucleotides for both mixed and repeat constructs (Figure 4.5A,B). Such evidence suggests that pol β has the ability to incorporate multiple nucleotides at gap sites contained within both mixed and repeat DNA sequences, even in the presence of an unmodified 5' group. This may be due to the equal molar concentration of DNA to pol β, and the lack of downstream enzymes, notably, FEN1 and Lig1, in these incorporation assays. Importantly, previous work has shown that the levels of pol β, FEN1 and Lig1 present during the repair event can affect the ability of pol β to undergo multinucleotide incorporation; if FEN1 and Lig1 levels are low, increased multinucleotide incorporation by pol β is observed (*36*, *37*). Although, we do see multinucleotide incorporation for mixed and repeat constructs, we observe longer DNA products in assays with CAG repeat DNA, suggesting pol β performs multinucleotide incorporation more readily on repeat sequence constructs.

To investigate whether the multinucleotide incorporation seen for pol β on the mixed and repeat constructs occurs during a single DNA•pol β binding event, we performed similar multinucleotide incorporation assays described above, except in the presence of a large excess of CT DNA trap. For these experiments, the radiolabeled DNA construct of interest was preincubated with pol β, prior to the addition of all four dNTPS in the presence of the CT DNA trap. The CT-DNA trap has previously been shown successfully bind dissociated pol β (*33*). Upon mixing of the DNA•pol β complex with the dNTPs/CT-DNA trap solution, we expect the incorporation of a single guanine nucleotide followed by either pol β dissociation or processive DNA synthesis. Dissociated pol β would reassociate with the large excess of trap DNA, not the labeled construct; however, bound pol β should incorporate multiple nucleotides to the construct. Therefore, the observation of more than one nucleotide incorporated to our 22mer labeled substrate would be the result of processive DNA synthesis. In the presence of the CT-DNA trap, the ability for pol β to undergo multinucleotide incorporation was drastically reduced (Figure 4.6A,B) compared to multinucleotide incorporation lacking the trap (Figure 4.5A,B), suggesting the longer multinucleotide incorporation products seen in Figure 4.5 were the consequence of many dissociation and reassociation events by pol β. For the mixed-sequence construct, pol β dissociates after the incorporation of a single guanine nucleotide, suggesting that the ability for pol β to undergo processive DNA synthesis was minimal in the allowed time frame (Figure 4.6A). Conversely, pol β was able to incorporate up to four nucleotides on the repetitive DNA sequence, suggesting that the polymerase is slightly more processive on CAG repeat tracts (Figure 4.6B).

4.5.3. Examining the Strand Displacement Activity of Pol β

The drastic differences observed for multinucleotide incorporation with (Figure 4.6) and without the trap (Figure 4.5), prompted us to explore the strand displacement activity of pol β. In the above multinucleotide incorporation assays, pol β must displace the initial base pairs between the 77mer strand and the 100mer complement to incorporate more than a single nucleotide. To investigate whether the presence of the 77mer was impeding pol β processive polymerization, we performed processive, multinucleotide incorporation assays on constructs lacking the 77mer and in the presence of the CT DNA trap. Under these conditions the polymerase incorporated up to 3 nucleotides on the mixed construct and up to 12 nucleotides on the repeat construct, again suggesting pol β is more processive on repeat constructs than mixed sequence. Furthermore, such results imply that the downstream strand is impeding the processivity of pol β, as we saw less processivity when the 77mer strand was present (Figure 4.6A,B). It is important to highlight, that pol β has extremely poor processivity on the mixed-sequence constructs, regardless of whether it must perform strand displacement; at best, we saw the processive incorporation of 3 nucleotides. Furthermore, although the k_{off} of pol β after the incorporation of a single guanine was the same for mixed and CAG repeat constructs, our processivity assays suggest there is an increase in dissociation of pol β from the mixed-sequence constructs or alternatively, a decrease in dissociation of pol β from the repeat constructs during processive polymerization.

4.5.4. Pause Sites by Pol β

During multinucleotide incorporation assays, we observed a distinct pattern in lanes that displayed discernible amounts of multinucleotide incorporation products (Figure 4.5A,B and 4.7B, arrows). Previous experimental evidence on a wide-variety of DNA polymerases revealed random intense banding patterns, and attributed them to polymerase pausing followed by polymerase dissociation. Pausing is typically thought to occur when the polymerase approaches regions of the DNA that are impeding DNA synthesis, such as non-B DNA hairpin conformation or regions of rich GC content (*26*, *27*). For the mixed-sequence construct this pause pattern was random and was only observed when the trap was not present. We attribute this minor pausing pattern to differences in nucleotide incorporation rates, along with the requirement of pol β to perform strand displacement synthesis; as discussed above, pol β has poor strand displacement activity on mixed-sequence constructs that likely leads to polymerase pausing and dissociation. Interestingly, pol β paused at the adenine within each CAG repeat in the repeat construct. Due to the ability of repeat sequences to adopt intramolecular secondary structures, it is possible that such structures are present within the $(CAG)_{19}/(CTG)_{19}$ region; pol β would likely pause as it encountered these hairpins. Indeed, it is likely that hairpin formation is present in the repeat construct lacking the 77mer; the 100mer-R strand contains a $(CTG)_{19}$ region that can form intramolecular hairpins. Interestingly, although the formation of hairpins is thought to limit the processivity of polymerases and cause dissociation, we see an increase in processivity in these dynamic repeat sequences that can readily adopt such structures; the unique interplay between polymerase processivity, polymerase pausing and formation of non-B conformations within repeat tracts will be an area of future research. Furthermore, the

(CAG)/(CTG) region has a high GC content; the polymerase must break 6 hydrogen bonds to displace two GC bps and only 2 hydrogen bonds to break and displace a single AT bp; the energy required by the polymerase to break two GC base pairs may contribute to the pause at each A. It is likely that the pause pattern observed for the repeat tract is a result of both hairpin formation and high GC content.

4.6 Concluding Remarks

The data presented here further contributes to our working model of CAG repeat expansion by the BER cascade. Single-nucleotide incorporation kinetics reveal that pol β incorporates a single guanine within CAG repeat constructs at the same rate as mixed-sequence constructs; furthermore, pol β dissociates from both constructs at the same rate, suggesting an SP-BER event would occur equally as well on both constructs. Conversely, multinucleotide incorporation assays reveal an increase in pol β processivity and strand displacement activity on repeat constructs compared to mixed-sequence constructs. This increased activity along with probable coordination with BER enzymes implicating in promoting pol β processivity and strand displacement activity, i.e. APE1 and PCNA, are likely contributing factors to the incorporation of multiple nucleotides by pol β in TNR tracts. Future studies examining the ability of APE1 and PCNA to promote processivity and strand displacement of pol β on TNR tracts will solidify these conclusions. Furthermore, we observed a periodic pattern during multinucleotide incorporation of the repeat tract, which suggests pausing by pol β at each A within the repeat; one likely explanation for this pause pattern is the presence of intramolecular hairpins within the TNR region. Future structural characterizations of the repeat

construct will provide insight into the presence of these structures. Moreover, future studies examining pol β multinucleotide incorporation on other TNR tracts implicated in the multitude of TNR disorders may provide insight into this pausing pattern and increased processivity seen in these dynamic regions.

4.7 References

(1) Tóth, G., Gáspári, Z., and Jurka, J. Microsatellites in Different Eukaryotic Genomes: Survey and Analysis, *Genome Res.*, **2000**, *10*, 967.

(2) Levinson, G., and Gutman, G. A. Slipped-Strand Mispairing: A Major Mechanism for DNA Sequence Evolution., *Mol. Biol. Evol.*, **1987**, *4*, 203-221.

(3) I.V. Kovtun, Y. Liu, M. Bjoras, A. Klungland, S.H. Wilson, and C.T. McMurray, OGG1 Initiates Age-Dependent CAG Trinucleotide Expansion in Somatic Cells, *Nature*, **2007**, *447,* 447-452.

(4) McMurray, C., DNA Seconday Structure: A Common Causative Factor for Expansion in Human Disease, *Proc. Natl. Acad. Sci. USA*, **1999**, *96*, 1823-1825.

(5) Wells, R., Molecular Basis of Genetic Instability of Triplet Repeats. *J. Biol. Chem.*, **1996**, *271*, 2875-2878.

(6) Gatchel, J., and Zoghibi, H. Diseases of Unstable Repeat Expansion: Mechanism and Common Principles, *Nat. Rev. Genet.*, **2005**, *6*, 743-755

(7) David, S., O'Shea, V., and Kundu, S., Base-excision Repair of Oxidative DNA Damage, *Nature*, **2007**, *447*, 941-950.

(8) Sung, J-S., DeMott, M., and Demple, B. Long-Patch Base Excision DNA Repair of 2-Deoxyribonolactone Prevents the Formation of DNA-Protein Cross-links with DNA Polymerase Beta. *J. Biol. Chem.* **2005**, *280*, 39095–39103.

(9) Horton, J.K., Prasad, R., Hou, E., and Wilson, S.H. Protection Against Methylation-Induced Cytotoxicity by DNA Polymerase β-Dependent Long Patch Base Excision Repair. *J. Bio. Chem.* **2000**, *275*, 2211-2218.

(10) Liu, Y., Prasad, R., Beard, W. A., Hou, E. W., Horton, J. K., McMurray, C. T., and Wilson, S. H. Coordination Between Polymerase Beta and FEN1 can Modulate CAG Repeat Expansion. *J. Biol. Chem.* **2009**, *284*, 28352–28366.

(11) Jarem, D. A., Wilson, N. R., and Delaney, S. Structure-dependent DNA Damage and Repair in a Trinucleotide Repeat Sequence. *Biochemistry* **2009**, *48*, 6655–6663.

(12) Jarem, D. A., Wilson, N. R., Schermerhorn, K. M., and Delaney, S. Incidence and Persistence of 8-oxo-7,8-dihydroguanine within a Hairpin Intermediate Exacerbates a Toxic Oxidation Cycle Associated with Trinucleotide Repeat Expansion. *DNA Repair (Amst.)* **2011**, *10*, 887–896.

(13) Kumar, A., Widen, S. G., Williams, K. R., Kedar, P., Karpek, R. L., and Wilson, S. H. Studies of the Domain Structure of Mammalian DNA Polymerase β. *J. Biol. Chem.* **1990**, *265*, 2124-2131.

(14) Prasad, R., Beard, W. A., Strauss, P. R., and Wilson, S. H. Human DNA Polymerase Beta Deoxyribose Phosphate Lyase. Substrate Specificity and Catalytic Mechanism. *J. Biol. Chem.*, **1998**, *12*, 15263-15270.

(15) Chagovetz, A. M., Sweasy, J. B., and Preston, B. D., Increased Activity and Fidelity of DNA Polymerase β on Single-Nucleotide Gapped DNA. *J. Biol. Chem.*, **1997**, *272*, 27501-27504.

(16) Sukhanova, M. V., Khodyreva, S. N., Lebedeva, N. A., Prasad, R., Wilson, S. H., and Lavrik, O. I. Human Base Excision Repair Enzymes Apurinic/apyrimidinic Endonuclease1 (APE1), DNA Polymerase β and Poly(ADP-ribose)

Polymerase 1: Interplay Between Strand-Displacement DNA Synthesis and Proofreading Exonuclease Activity. *Nucleic Acids Res.* **2005**, *33*, 1222-1229.

(17) Beard, W. A., and Wilson, S. H. Structure and Mechanism of DNA Polymerase β. *Chem. Rev.* **2006**, *106*, 361-382.

(18) Ahn, J., Craynov. V. S., Zhong. X., Werneburg, B. G., and Tsai, M-D. DNA Polymerase β: Effects of Gapped DNA Substrates on dNTP Specificity, Fidelity and Processivity and Conformational Changes. *Biochem. J.,* **1998**, *331*, 79-87.

(19) Brown, J. A., Pack, L. R., Sanman, L.E., and Suo, Z. Efficiency and Fidelity of Human DNA Polymerase λ and β During Gap-Filling DNA Synthesis. *DNA Repair Amst.* **2011**, *10*, 24-33.

(20) Rothwell, P. J., Mitaksov, V., and Waksman, G., Motions of Fingers Subdomain of Klentaq1 Are Fast and Not Rate Limiting: Implications for the Molecular Bases of Fidelity in DNA Polymerases. *Mol. Cell.* **2005**, *19*, 345-355.

(21) Langston, L.D., and O'Donnell, M., DNA Polymerase Delta is Highly Processive with Proliferating Cell Nuclear Antigen and Undergoes Collision Release Upon Completing DNA. *J. Biol. Chem.* **2008**, *283*, 29522-29531.

(22) Maga, G., Villana, G., Tillement, V., Stucki, M., Locatelli, G.A., Frouin, I., Spadari, S., and Hubscher, U. Okasaki Fragment Processing: Modulation of the Strand Displacement Activity of DNA Polymerase Delta by the Concerted Action of Replication Protein A, Proliferation Cell Nuclear Antigen, and Flap Endonuclease-1. *Proc. Natl. Acad. Sci.*, **2001***, 98,* 14298-14303.

(23) Moldovan, G.-L., Pfander, B., and Jentsch, S. PCNA, the Maestro of the Replication Fork. *Cell* **2007**, *129*, 665–679.

(24) Harstenstine, M. J., Goodman, M. F., and Petruska, J. Weak Strand Displacement Activity Enables Human Polymerase Beta to Expand CAG/CTG Triplet Repeat at Strand Breaks. *J. Biol. Chem.*, **2002**, *277*, 41379-41389.

(25) Fortini, P., Pascucci, B., Parlanti, E., Sobol, R. W., Wilson, S. H., and Dogliotti, E. Different DNA Polymerases are Involved in the Short- and Long-Patch Base Excision Repair in Mammalian Cells. *Biochemistry*, **1998**, *37*, 3575-3580.

(26) Mytelka, D. S., and Chamberlin, M. J. Analysis and Suppression of DNA Polymerase Pause Associated with a Trinucleotide Consensus. *Nucleic Acids Res.*, **1996**, *24*, 2774-2781.

(27) Challberg, M. D., and Englund, P. T., The Effect of Template Secondary Structure on Vaccinia DNA Polymerase. *J. Biol. Chem.* **1979**, *254*, 7820-7826.

(28) Hacker, K. J., and Alberts, B. M. The Rapid Dissociation of the T4 DNA Polymerase Holoenzyme when Stopped by a DNA Hairpin Helix. A Model for Polymerase Release Following the Terminiation of each Okazaki Fragment. *J. Biol. Chem.* **1994**, *269*, 24221-24228.

(29) Viguera, E., Canceill, D., and Ehrlich, S. D., Replication Slippage Involves DNA Polymerase Pausing and Dissociation. *EMBO J.* **2001**, *20*, 2587- 2595.

(30) Beaucage, S.L., and Caruthers, M. H., Synthetic strategies and parameters involved in the synthesis of oligodeoxyribonucleotides according to the phosphoramidite method, *Curr. Protoc. Nucleic Acid Chem*., **2000**, 3.3.1- 3.3.20.

(31) Warshaw, M. M., and Tinoco I. Jr, Optical properties of sixteen dinucleoside phosphates, *J. Mol. Biol.*, **1966**, *20*, 29-38.

(32) Beard, W. A., and Wilson, S. H., Purification and Domain-Mapping of Mammalian DNA Polymerase Beta. *Methods Enzymol.*, **1995***, 262*, 98-107

(33) Prasad, R., Shock, D., Beard, W. A., and Wilson, S. H. Substrate Channeling in Mammalian Base Excision Repair Pathways: Passing the Baton. *J. Biol. Chem.* **2010**, *285*, 40479–40488.

(34) Bennett, R. A., Wilson, D. M., Wong, D., and Demple, B. Interaction of human apurinic endonuclease and DNA polymerase beta in the base excision repair pathway, *Proc. Natl. Acad. Sci. U.S.A.* **1997**, *94*, 7166–7169.

(35) Praah, R., Singhal, R. K., Srivastava, D. K., Molina, J. T., Tomkinson, A. E., and Wilson, S. H. Specific Interactions of DNA Polymerase β and DNA Ligase I in a Multiprotein Base Excision Repair Complex from Bovine Testis. *J. Biol. Chem*. **1997**, *271*, 16000-16007.

(36) Goula, A-V., Berquist, B. R., Wilson, D. M. Wheller, V. C, Trottier, Y., and Merienne, K. Stoichiometry of Base Excision Repair Proteins Correlates with Increased Somatic CAG Instability in Striatum over Cerebellum in Huntington's Disease Transgenic Mice. *PLoS Genetics*, **2009**, *5*, e1000749.

(37) Goula, A-V., Pearon, C. E., Maria, J. D., Trottier, Y., Tomkinson, A. E., Wilson, D. M., and Merienne, K. The Nucleotide Sequence, DNA Damage Location, and Protein Stoichiometry Influence the Base Excision Repair Outcome at CAG/CTG Repeats. *Biochemistry*, **2012**, *51*, 3919-3932.

Chapter 5: Conclusions and Future Work

5.1 Conclusions and Future Work

In this work, we have examined the kinetics of some of the major players in the DNA base excision repair (BER) pathway, including the DNA glycosylase oxoguanine glycosylase (OGG1), apurinic/apyrimidinic endonuclease (APE1), and polymerase β (pol β). By performing transient-state and steady-state kinetic experiments, we have gained insight into the substrate specificity of each enzyme as well insight into the coordination that occurs between enzymes. Such information is valuable in understanding the diseases and disorders that arise during deficiencies or incorrect processing during the BER cascade.

Our kinetic work on APE1 provided us with vital insight into the processing of the authentic AP site along with commonly used AP site analogs. Notably, we report that the transient-state strand incision activity rate for APE1 processing the authentic AP site in the presence of the biologically relevant Mg^{2+} is $\geq 700\ s^{-1}$; we were limited by the resolution of the rapid quench instrument. This rate makes APE1 chemistry the fastest of any BER enzyme to date, and the development of a faster quenching technique would be needed to obtain a more quantitative rate. Moreover, rapid quench kinetic techniques allowed us to observe differences in the way APE1 processed the tetrahydrofuran (THF) site compared to the authentic and reduced AP sites; the THF site lacks the C1'-OH group and is locked in the ring-closed conformation, while both the authentic AP and reduced AP sites contain the C1'-OH group and have a ring-opened flexible conformation. Notably, THF site containing DNA was used to obtain all current APE1 x-ray crystal structures, and therefore much of our knowledge regarding the amino acids present within the active site pocket, and the amino acids involved in DNA orientation and

stabilization, are gleaned from structures of APE1 bound to the THF site (*1,2*). The differences seen in strand incision activity of APE1 incising the THF site versus the authentic site suggest these sites may be oriented differently within the active site pocket; therefore, many of the amino acids thought to stabilize the THF site may not stabilize the authentic AP site. Moreover, APE1 is currently a chemotherapeutic target, with the aim to inhibit APE1 activity in cancer cells and cause a disruption in AP site processing, leading to cellular apoptosis (*3*, *4*). Therefore, in order to develop optimal APE1 inhibitors, a correct and complete picture of the APE1 active site is needed.

As discussed within the introduction, a vast array of analogs have been used to reveal the mechanism of monofunctional and bifunctional glycosylase enzymes, therefore, while some analogs may not entirely mimic an authentic substrates binding or processing, they can be helpful in understanding which features of a substrate are necessary for enzyme activity (*5*-*7*). In future work, it would be beneficial to further examine the effects of a wide range of AP site analogs on the strand incision activity of APE1. Such structures would contain either a C1'-OH group or a ring-opened conformation, and may help to solidify the features necessary for optimal strand incision activity. For example, we envision the use of an AP site analog with a five-membered carbon ring containing the C1'-OH group; while this structure contains the C1'-OH, it would lack the ring-opened flexible conformation that both the authentic and reduced AP sites afford. Furthermore, we hope to perform kinetic and binding experiments on the various AP site-containing DNA using a variety of APE1 mutants that would help us identify the amino acids that play a role in binding and catalysis. For example, using electrophoretic mobility shift assays (EMSA) and site-directed mutagenesis in which

asparagine 212 within APE1 was mutated to a glutamine, N212 was implicated in stabilizing the authentic AP site (*8*). We envision using the N212Q mutant in both EMSA and kinetic studies on our AP site analogs to gain further insight into the role this specific amino acid plays in binding and catalysis of APE1.

By performing various kinetic studies of OGG1, APE1 and pol β processing their prototypic substrate within a CAG repeat DNA construct, we have gained significant insight into the toxic oxidation cycle (TOC) proposed for the expansion of these repeat tracts (*9*,*10*). This expansion is the molecular mechanism for the neurological disorder Huntington's disease (HD) (*9*). We have shown that OGG1 will excise an 8-oxo-7,8-dihydroguanine (8oxoG) lesion at the same rate, ~ 55 min^{-1}, from both CAG repeat and mixed-sequence duplex constructs, and furthermore observed a coordination with APE1 to stimulate OGG1 product release from both repeat and mixed duplex constructs. Such results imply that BER is initiated equally as well within a CAG repeat compared to within the well-studied mixed sequence context. Furthermore, due to the fact that both OGG1 and APE1 correctly processes CAG repeat DNA, it is unlikely that action of these enzymes are responsible for the altered repair carried out on the repeat constructs by latter BER enzymes; the action of the latter BER enzymes must be contributing to the expansion mechanism.

We continued our kinetic experiments by comparing single-nucleotide and multinucleotide incorporation by pol β on CAG and mixed-sequence constructs. It is important to recall that within the context of BER, pol β can incorporate a single nucleotide in short-patch (SP) BER, or multiple nucleotides in long-patch (LP) BER; importantly, procession down LP-BER by pol β within the context of CAG repeats is

thought to lead to latter expansion of the repeats (*9,11*). Kinetics examining the single-nucleotide incorporation rate of dGTP by pol β also revealed similar processing on CAG repeat and mixed-sequence constructs. Pol β incorporated dGTP at the same rate, ~ 5 s^{-1}, as well as dissociated from both constructs at the same rate, ~ 2.5 s^{-1}. Therefore, we do not observe differences in what would be a SP-BER event for pol β processing mixed and repeat constructs. We further examined multinucleotide incorporation by pol β on mixed and repeat constructs, and notable differences were observed. First, pol β incorporated more nucleotides on repeat tracts compared to mixed-sequence constructs. Second, pol β had increased strand-displacement activity on repeat constructs compared to the mixed constructs. Finally, a periodic pausing pattern at each adenine within the repeat tract was observed during pol β multinucleotide incorporation of the CAG repeat DNA. These results suggest that when all four dNTPs are present, in contrast to the single dGTP present in single-nucleotide assays, pol β treats the CAG repeat tracts differently than mixed-sequence DNA. The work performed here suggests the increased multinucleotide incorporation and increased strand displacement activity of pol β on CAG repeat tracts may likely be the root of progression down LP-BER versus SP-BER in the context of BER on CAG repeat tracts.

As discussed in the previous chapters, *in vivo* BER is a well coordinated event including many players, such as APE1, pol β, Flap Endonuclease 1 (FEN1), DNA Ligase I (Lig1), and proliferating cell nuclear antigen (PCNA) (*11-14*). Future single-nucleotide and multinucleotide incorporation studies with the presence of these various players may reveal other differences in the processing of CAG repeat DNA compared to mixed-sequences by pol β. Furthermore, careful structural characterization of our DNA

sequences will provide insight into the possibility of hairpin formation within the repeat tract. Moreover, we have already synthesized a series of DNA constructs, identical to the 3-strand 22mer:77mer:100mer mixed and CAG repeat constructs used in our pol β experiments, except the 5'-phosphate present on the 77mer has been replaced with a 5'-THF group. The THF site is known to force LP-BER in the context of mixed-sequence DNA (*11*,*15*). We envision performing single-nucleotide and multinucleotide experiments on 5'-THF containing CAG repeat and mixed-sequenced constructs to observe how this structure will affect the processivity and strand displacement activity of pol β. Current work is being done in our lab to obtain the kinetic parameters of FEN1 and Lig1 in processing CAG repeat DNA constructs. Ultimately, we aim to obtain a full kinetic picture of the processing of CAG repeat constructs within the TOC, to pinpoint where the repair is going awry, and consequently leading to the expansion. Such information would be critical to developing therapeutics to prevent the expansion of the DNA.

Importantly, there is currently no cure for HD, and no way to stop to progressive expansion of the repeat tracts within the DNA. HD patients are typically given dopamine blockers, such as amantadine and tetrabenazine, which aim to reduce the jerky movements that result from the neurodegeneration caused by the accumulation of the mutant huntingtin protein (*16*,*17*). More recently, the accumulation of the mutant huntingtin protein has been shown to cause a disregulation in gene transcription, thought to occur by causing a decrease in levels of histone acetyl transferases (HATs), eventually leading to neuronal death (*18*,*19*). HATs are enzymes responsible for acetylating histone proteins; these proteins package and order DNA into chromatin. HATs work in concert

with histone deactyl transferases (HDACs) to modify chromatin and regulate gene transcription. A currently study uses the HDAC inhibitor suberoylanilide hydroxamic acid, SAHA, in an HD mouse model, to prohibit the deacetylation of histone proteins by HDACs to minimize the effects of the disregulation of HATS by the mutant huntingtin protein (*20*,*21)*. Surprisingly, the motor functions of the HD mouse model were significantly improved in the presence of SAHA. The use of HDAC inhibitors is currently a major focus for HD treatment. Unfortunately, such drugs described above treat symptoms of HD, and do not address the prevention of DNA expansion; such a therapeutic would essentially be the holy grail for HD patients.

It is important to emphasis, that within the context of BER occurring in the CAG repeat tract of the huntingin gene, pol β is incorporating multiple nucleotides; the experiments in this work suggest it is the increased strand displacement and multinucleotide incorporation activity of pol β on the repetitive tracts that leads to LP-BER. Therefore, a therapeutic that aims to prevent multinucleotide incorporation by pol β may prevent the expansion. Interestingly, a 2004 study identified a novel role for the tumor suppressor protein, adenomatous polyposis coli (APC), in blocking pol β-dependent LP-BER (*22*). APC is responsible for regulating DNA replication and cell division. A PCNA-like binding motif was identified on APC that was shown to bind pol β. Furthermore, *in vitro* studies incubating a 63 base pair (bp) mixed-sequence duplex DNA construct with a THF site at the 23rd bp, with APE1, pol β, and all four dNTPs, saw the incorporation of 2-7 nucleotides by pol β, confirming multinucleotide incorporation by the polymerase. Interestingly when APC was added to the incubation, only the incorporation of a single nucleotide by pol β was observed, suggesting complete

inhibition of pol β-dependent LP-BER by APC. Furthermore, the presence of FEN1 and Lig1 were unable to remove the block created by APC (*22*). More recent studies revealed the ability of APC to block entry of FEN1 into the nucleus, providing further evidence that APC plays a role in regulating LP-BER (*23*). In future studies, examining the ability of APC to prohibit LP-BER in the case of pol β processing CAG repeat DNA would be exciting. If APC could effectively prevent multinucleotide incorporation by pol β, this could prevent the ligation of excess CAG repeats by Lig1, preventing the expansion of the CAG repeat tract.

Finally, it is worth noting that the experiments performed within this work were done on oligonucleotides in solution to understand how each BER enzyme works alone and in coordination with one another at the most basic level. As presented above, DNA within the cell is packaged along with histone proteins to create chromatin. Performing similar BER kinetic studies on DNA packaged within chromatin may provide another level of understanding of the BER cascade, and the toxic oxidation cycle.

References

(1) Mol, C. D., Izumi, T., Mitra, S., and Tainer, J. A. DNA-bound structures and mutants reveal abasic DNA binding by APE1 and DNA repair coordination, *Nature* **2000**, *403*, 451–456.

(2) Tsutakawa, S. E., Shin, D. S., Mol, C. D., and Izumi, T. Conserved Structural Chemistry for Incision Activity in Structurally Non-homologous Apurinic/Apyrimidinic Endonuclease APE1 and Endonuclease IV DNA repair, *J. Biol. Chem.* **2013***, 288*, 8445-8455

(3) McNeill, D.R., and Wilson III, D.M., A Dominant-Negative Form of the Major Human Abasic Endonuclease Enhances Cellular Sensitivity to Laboratory and Clinical DNA-Damaging Agents. *Mol. Cancer Res.*, **2007**, *5*, 61-70.

(4) Fishel, M. L., and Kelley, M. R., The DNA Base Excision Repair Protein APE1/Ref-1 as a Therapeutic and Chemopreventive target. *Mol. Aspects Med.*, **2007**, *28*, 375-395.

(5) Schärer, O. D., Ortholand, J.-Y., Ganesan, A., Ezaz-Nikpay, K., and Verdine, G. L. Specific Binding of the DNA Repair Enzyme AlkA to a Pyrrolidine-Based Inhibitor. *J. Am. Chem. Soc.* **1995**, *117*, 6623–6624.

(6) Schärer, O. D., Nash, H. M., Jiricny, J., Laval, J., and Verdine, G. L. Specific Binding of a Designed Pyrrolidine Abasic Site Analog to Multiple DNA Glycosylases. *J. Biol. Chem.* **1998**, *273*, 8592–8597.

(7) Chu, A. M., Fettinger, J. C., and David, S. S. Profiling Base Excision Repair Glycosylases with Synthesized Transition State Analogs. *Bioorg. Med. Chem. Lett.* **2011**, *21*, 4969–4972.

(8) Rothwell, D. G., and Hickson, I. D. Asparagine 212 is Essential for Abasic Site Recognitions by the Human DNA Repair Endonuclease HAP1, *Nucleic Acids Res.* **1996**, *24*, 4217-4221.

(9) Kovtun, I. V., Liu, Y., Bjoras, M., Klungland, A., Wilson, S. H., and McMurray, C. T. OGG1 Initiates Age-dependent CAG Trinucleotide Expansion in Somatic Cells. *Nature* **2007**, *447*, 447–452.

(10) Jarem, D. A., Wilson, N. R., and Delaney, S. Structure-dependent DNA Damage and Repair in a Trinucleotide Repeat Sequence. *Biochemistry* **2009**, *48*, 6655–6663.

(11) Liu, Y., Prasad, R., Beard, W. A., Hou, E. W., Horton, J. K., McMurray, C. T., and Wilson, S. H. Coordination Between Polymerase Beta and FEN1 can Modulate CAG Repeat Expansion. *J. Biol. Chem.* **2009**, *284*, 28352–28366.

(12) Bennett, R. A., Wilson, D. M., Wong, D., and Demple, B. Interaction of human apurinic endonuclease and DNA polymerase beta in the base excision repair pathway, *Proc. Natl. Acad. Sci. U.S.A.* **1997**, *94*, 7166–7169.

(13) Moldovan, G.-L., Pfander, B., and Jentsch, S. PCNA, the Maestro of the Replication Fork. *Cell* **2007**, *129*, 665–679.

(14) Praah, R., Singhal, R. K., Srivastava, D. K., Molina, J. T., Tomkinson, A. E., and Wilson, S. H. Specific Interactions of DNA Polymerase β and DNA Ligase I in a Multiprotein Base Excision Repair Complex from Bovine Testis. *J. Biol. Chem.* **1997**, *271*, 16000-16007.

(15) Sukhanova, M. V., Khodyreva, S. N., Lebedeva, N. A., Prasad, R., Wilson, S. H., and Lavrik, O. I. Human Base Excision Repair Enzymes Apurinic/apyrimidinic

Endonuclease1 (APE1), DNA Polymerase β and Poly(ADP-ribose) Polymerase 1: Interplay Between Strand-Displacement DNA Synthesis and Proofreading Exonuclease Activity. *Nucleic Acids Res.* **2005**, *33*, 1222-1229

(16) Swash, M., Roberts, A. H., Zakko, H., and Heathfield, K. W., Treatment of Involuntary Movement Disorders with Tetrabenazine. *J. Neurol. Neurosurg. Psychiatry.*, **1972**, *35*, 186-191.

(17) Huntington Study Group, Tetrabenazine as Antichorea Therapy in Huntington Disease. *Neurology*, **2006**, *66*, 366-372.

(18) Cha, J-H., Kosinski, C. M., Kerner, J. A., Alsdorf, S. A., Mangiarini, L., Davies, S. W., Penney, J. B., Bates, G. P., and Young, A. B., Altered Brain Neurotransmitter Receptors in Transgenic Mice Expressing a Portion of an Abnormal Human Huntington Disease Gene. *PNAS*, **1998**, *95*, 6480-6485.

(19) Carter, R. L., Strand, A., Peters, N. L., Solano, S. M., Hollinsworth, Z. R., Menon, A. S., Frey, A. S., Spektor, B. S., Penney, E. B., Schilling, G., Ross, C. A., Borchelt, D. R., Tapscott, S. J., Young, A. B., and Olsan, J.M, Decreased Expression of Striatal Signaling Genes in a Mouse Model of Huntington's Disease. *Hum. Mol. Genet.*, **2000**, *9*, 1259-1271.

(20) Hockley, E., Richon, V. M., Woodman, B., Smith, D. L., Zhou, X., Rosa, E., Sathasivam, K., Ghazi-Noori, S., Mahal, A., Lowden, P. A., Steffan, J. S., Marsh, J. L., Thompson, L. M., Lewis, C. M., Marks, P. A., and Bates, G. P. Suberoylanilide Hydroxamic Acid, A Histone Deacetylase Inhibitor, Ameliorates Motor Deficits in a Mouse Model of Huntington's Disease. *Proc. Natl. Acad. Sci. USA.*, **2003**, *100*, 2041-2046

(21) Mielcarek, M., Landles, C., Weiss, A., Bradaia, A., Seredenina, T., Inubasi, L., Osbore, G. F., Wadel, K., Touller, C., Butler, R., Roberston, J., Frankin, S. A., Smith, D., L., Park, L., Marks, P. A., Wanker, E. E., Olson, E. N., Luthi-Carter, R., Putten, H., Beamont, V., and Bates, G. P. HDAC4 Reduction: A Novel Therapeutic Strategy to Target Cytoplasmic Huntingtin and Ameliorate Neurodegeneration. *PLoS Biol.*, **2013,** *11*, e1001717.

(22) Narayan, S., Jaiswal, A. S., and Balusu, R., Tumor Suppressor APC Blocks DNA Polymerase β-Dependent Strand Displacement Sythesis During Long Patch but Not Short Patch Base Excision Repair and Increases Sensitivity to Methylmethane Sulfonate. *J. Biol. Chem.*, **2004**, *280*, 6942-6949.

(23) Jaiswal, A. S., Armas, M. L., Izumi, T, Strauss, P. R., and Narayan, S. Adenomatous Polyposis Coli Interacts with Flap Endonuclease 1 to Blocks Its Nuclear Entry and Function. *Neoplasia,* **2012**, *14*, 495-508.